BOND AND CRACKING OF REINFORCED CONCRETE

PhD Thesis by Simon Hang Chi Chan
scehcc@cf.ac.uk
March 2012

Acknowledgements

I have been helped and assisted by many people throughout the PhD course.

I would firstly like to thank my mother and father for all they have done for me over 28 years after bringing me into this world. In particular, I thank my mum for her unconditional love and also her support and understanding throughout my PhD course.

I would like to thank both Cardiff University and the CELSA Group for funding this programme of research and the supply of the reinforcing bar and other testing materials used in experiments. To Cardiff University, I'm grateful for providing me extensive computer facilities and an excellent and friendly environment for the research period.

I would like to thank my supervisors Bob Lark and Tony Jefferson and all their support along this project. I would sincerely like to thank Bob to offer me such a good research opportunity and to thank Tony for his faith in my ability to complete this project.

My thanks also go to all the laboratory technical staff, Carl, Brain, Ian, Des and Len for all their assistance with reinforced concrete experiment work. I would also like to thank Mark for his technical advice and assistance with the use of the DIC system.

I would like to thank my old and new friends within the department in particular Andrea, Ben, Iulia, Michael, Sahand and Simon whom I had good time with in Room W1.32. To all my friends either in Hong Kong or UK and family members, I offer my grateful thanks.

Finally, I would like to thank my girlfriend for her love and support over the last 8 years since we met on my first flight to UK. Without her patient and understand in my tough time and taking care of my life during the PhD course, my thesis would hardly be completed “easily”.

Dedication

To my dearest mum

Summary

Ribbed reinforcement is described as “high bond” in Eurocode 2 (EC2) and within the code serviceability checks make no allowance for variations in either the ductility or bond characteristics of these bars. In this work, this matter is explored, and the crack development and behaviour of concrete beams reinforced with various types of ribbed steel bar are investigated, using both numerical and experimental approaches. The objective of the experimental approach is to undertake a series of experiments to compare the performance of beams made with standard reinforcement with that of beams formed with a new high-ductility bar produced by CELSA UK. The relationship between the bond strength and the rib pattern of reinforcing steel was studied and the behaviour at SLS load levels of RC beams with reinforcement of different rib patterns in flexure is discussed. The cracking of beams was monitored both visually and using a non-destructive Digital Image Correlation system to trace in-plane deformations and strains on the surface of the specimens. The test results showed that specimens with bars which had the highest relative rib area (f_R value) exhibited the smallest crack spacing and crack width. A numerical model was developed to explore the crack development of reinforced concrete beams under flexural loading. The model employed a non-linear material model for concrete and a smeared crack approach. In order to address the well known numerical stability problems, associated with softening models, a non-local gradient method was used. Crack widths cannot be obtained directly from such models, due to the diffuse nature of non- local simulations, therefore a post-processing procedure was developed to allow the crack characteristics to be calculated. Several numerical examples are presented to illustrate the satisfactory performance of the model. In addition, a series of numerical simulations of the

experimental beams tested in the present study were used validate the numerical model and conversely, to provide confidence in the consistency of the experimental results.

Symbols and abbreviations

The following symbols and abbreviations are used in this thesis:

A	Cross-sectional area of beam	[mm^2]
A_c	Cross-sectional concrete area of beam	[mm^2]
A_s	Cross-sectional steel area of beam	[mm²]
$A_{c,eff}$	Effective area	[mm²]
A_n	Nominal Cross-sectional area	[mm²]
a_m	Maximum height of the transverse ribs	[mm]
B	Strain displacement matrix	[-]
b	Breadth of beam	[mm]
c	Spacing between the transverse ribs	[mm]
c	Concrete cover	[mm]
d	Bar Diameter	[mm]
d_{agg}	Maximum course aggregate particle size	[mm]
$\boldsymbol{D}$	Elasticity tensor	[-]
$\boldsymbol{D}_{sec}$	Secant stiffness matrix	[-]
$\boldsymbol{D}_{tan}$	Tangent D matrix	[-]
E	Young’ s modulus	[kN/mm²]
E_{cm}	Young’ s modulus of concrete	[kN/mm²]
E_s	Young’ s modulus of steel bar	[kN/mm²]
e	Width of longitudinal ribs	[mm]
F_a	Total applied force	[kN]
$f_{ct,eff}$	Mean value of the tensile strength of the concrete effective at the time when cracks are first expected to occur	[N/mm²]
f_{cm}	Target value of the strength class	[N/mm²]

f_c	Concrete uniaxial strength	[N/mm²]
f_{cu}	Cube strength (100mm cubes)	[N/mm²]
f_{ct}	Concrete tensile strength	[N/mm²]
f_{cyl}	Cylinder splitting strength	[N/mm²]
f_R	Relative rib area of the bar	[-]
f_t	Tensile strength of material	[N/mm²]
G_f	Specific fracture energy	[N/mm]
h	Height or depth of beam	[mm]
$\boldsymbol{K}$, $\boldsymbol{K_e}$	Element stiffness matrix	[-]
k	Bond characteristic parameter	[-]
k_1	Coefficient for bond properties of reinforcement	[-]
k_2	Nature of strain distribution	[-]
k_t	Factor dependent on the duration of the load	[-]
l	Length of beam	[mm]
l_{ch}	Characteristic length	[mm]
M	Bending moment	[Nmm]
N	Shape functions	[-]
P	Applied tensile force	[N]
r	Damage evolution parameter which controls damage evolution.	[-]
r_m	Damage evolution parameter r corresponding to a uniaxial tensile strain at the end of the tensile softening curve	[-]
r_t	Initial value of damage evolution parameter r	[-]
$\dot{r}$	Rate of change of damage evolution parameter	[-]
S	Crack Spacing	[mm]
S_o	Transfer length	[mm]
S_{rm}	Mean crack Spacing	[mm]

$S_{r,m\ code}$	Design code calculation of mean crack spacing	[mm]
$S_{r,m\ exp}$	Experimental mean crack spacing	[mm]
$S_{r,m\ num}$	Numerical mean crack spacing	[mm]
S_{rmax}	Max crack Spacing	[mm]
$S_{r,max\ code}$	Design code calculation of maximum crack spacing	[mm]
$S_{r,max\ exp}$	Experimental maximum crack spacing	[mm]
$S_{r,max\ num}$	Numerical maximum crack spacing	[mm]
x	Distance from compressive face to the neutral axis for a theoretically fully cracked section	[mm]
α_e	Ratio E_s/E_{cm}	[-]
β	Coefficient of integration	[-]
$\boldsymbol{\varepsilon}$	Local strain tensor	[-]
$\bar{\varepsilon}$	Non-local strain tensor	[-]
ε_{cmc}	FE mean strain	[-]
ε_{eff}	Effective Strain	[-]
ε_{cm}	Average concrete strain between cracks	[-]
ε_{sm}	Average steel strain between cracks	[-]
ρ	Poisson's ratio	[-]
ρ	Reinforcement ratio (A_s / A_c)	[-]
ρ_{eff}	Effective reinforcement ratio ($A_s / A_{s,ceff}$)	[-]
$\boldsymbol{\sigma}$	Stress tensors	[-]
$\boldsymbol{\sigma}_0^+$	Positive part of stress tensor	[-]
$\boldsymbol{\sigma}_e$	Effective stress.	[N/mm²]
σ_{eff}	Effective stress in beam	[N/mm²]
σ_s	Peak steel stress at the position of a crack	[N/mm²]

τ	Bond stress	[N/mm²]
τ_{ε}	Effective stress parameter	[-]
τ_{x}	Shear stress along the tensile force at the surface between steel and concrete	[N/mm²]
$\tau_{\max}$	Ultimate bond strength	[N/mm²]
ϕ	Bar Diameter	[mm]
w	Scalar damage parameter or tensor	[-]
w_k	Crack width	[mm]
w_{max}	Maximum crack width	[mm]
$S_{r,mCEB}$	Design code CEB fib calculation of mean crack width	[mm]
$w_{r,m\ code}$	Design code EC2 calculation of mean crack width	[mm]
$w_{r,m\ exp}$	Experimental mean crack width	[mm]
$w_{r,m\ num}$	Numerical mean crack width	[mm]
$w_{r,max\ code}$	Design code EC2 calculation of maximum crack width	[mm]
$w_{r,max\ exp}$	Experimental maximum crack width	[mm]
$w_{r,max\ num}$	Numerical maximum crack width	[mm]
∇^2	Laplace operator	[-]
DIC	Digital Image Correlation	
DSCM	Digital Speckle Correlation Method	
FE	Finite element	
LVDT	Linear variable differential transformer	
NDT	Non-Destructive Technology	
RILEM	Reunion Internationale des Laboratories d'Essais et de Recherches sur les Materiaux et les Constructions	
XFEM	Extended finite element model	

Content

List of Figures

List of Tables

Chapter 1 – INTRODUCTION

1.1 Background

Concrete is now the most commonly used man-made material on our planet. There are many advantages of building with concrete, such as exceptional durability, flexibility in shape and form, provision of fire and wind resistance and its strength in compression. The compressive strength for traditional concrete varies from about 20MPa to 60MPa, although this can rise to a strength of 200MPa for high performance concrete (Neville and Aitcin, 1998). Nevertheless, concrete is quasi-brittle in nature and it is approximately 10 times weaker in tension than in compression. Due to the low tensile capacity of concrete, reinforcement is added to carry the tensile forces. The reinforcing steel bars usually have ribs on the surface to enhance the bond with the concrete and prevent slip or pullout out from concrete.

1.2 General Introduction

The amount of reinforcing bars necessary to carry the tensile forces at both serviceability and ultimate load levels is insufficient to prevent cracking in most reinforced flexural members and therefore cracking is inevitable.

Concrete structures nowadays are required not only to be safe, but also to fulfil the aesthetic requirements of clients and of the public. Cracking might impair appearance, function, durability, serviceability, or even the total load resistance of a structure if crack widths grow beyond certain levels.

In order for reinforced concrete to be durable, cracks at serviceability load levels must

remain below prescribed widths (e.g. below 0.3mm). It is therefore important for designers and analysts to be able to predict the size and disposition of cracks in reinforced concrete members and to be able to do this the bond mechanisms between the concrete and reinforcement need to be well understood.

Some researchers (Rehm and Eligehausen, 1979; Tholen and Darwin, 1998) suggest that the rib pattern on the surface of steel reinforcing bars is an important factor in the bond mechanism. The relative rib area of the bar (f_R), which in turn is a function of the geometry of the rib pattern, is commonly used as a measurement. In the present work, an experimental study, which compares the performance of beams with standard reinforcement with those of beams formed with a new high-ductility bar produced by CELSA UK, is described. This includes an investigation into the relationship between the bond strength and the rib pattern. Furthermore, the Serviceability Limit State (SLS) behaviour performance of reinforced concrete (RC) beams with reinforcement of different rib patterns in flexure is discussed.

In addition, a numerical model is used to further explore cracking mechanisms in reinforced concrete beams. For this numerical study, an isotropic damage model, based on that used of Oliver et al. (2002), is used to model concrete cracking and a calculation procedure for computing the disposition and width of cracks in local and non-local finite element analyses from numerical strain fields is proposed. The model is validated using the experimental data from the literature as well as the experimental data gathered in the present work.

1.3 Motivation For The Research

1.3.1 Experimental Investigation

Bond strength is one of the paramount parameters which governs the nature of cracking in concrete structures. This bond not only depends on concrete strength but also upon the characteristic of the ribs on the reinforcement. A 'good' rib pattern, from the serviceability view point, would be expected to have the following characteristics:

- Should provide a strong bond between steel and concrete.
- Should limit width of the concrete cracks to specified limits.
- Should allow ductile RC beam behaviour.

1.3.2 Numerical Modelling

The motivation for the development of finite element modelling work for crack development presented in this thesis is to provide an accurate crack width prediction. A good modelling approach should be able to:

- Simulate the mechanical behaviour of steel and concrete, under loading and unloading conditions.
- Predict a realistic crack pattern for given boundary conditions.

1.4 Objectives And Scope Of The Research

The objectives and scope of the research presented in this thesis are as follows:

1. To undertake bond tests in order to investigate and improve understanding of the effects of having different reinforcement rib patterns and relative rib areas (f_R) upon the bond stresses developed in RC members.
2. To undertake flexural beam experiments for concrete beams reinforced with different

types of ribbed steel bar, in order to better understand the development of cracks and the effect on crack pattern of having these different rib patterns.

3. To simulate crack development within reinforced concrete under tensile loading using a non-linear finite element model and a smeared crack approach.
4. To provide validation of the experimental results by comparing them with the numerical results for a model of the experimental set up and to assess the adequacy of this prediction.

1.5 Layout of the Thesis

This thesis is divided into seven chapters and two appendices. Chapter 2 describes the state of the art in the field of experimental investigation of crack development in reinforced concrete beams. Chapter 3 describes the state of the art in the field of numerical modelling of crack development in reinforced concrete beams.

Chapter 4 illustrates the setup and methodology of the flexural beam test and the bond tests, as well as that of the corresponding material tests. The findings of these tests are also presented and discussed.

Chapter 5 presents the theory of the numerical model developed for predicting crack widths and crack spacings in reinforced concrete beams under flexural loading.

Chapter 6 presents and discusses detailed comparisons between the numerical and experimental results.

Finally, some general conclusions and recommendations for further research in this area are presented in Chapter 7.

The two appendices contain the figures, videos and animations respectively showing the evolution and development of cracks throughout the beam tests for all the flexural beam specimens in Batches A, C and M without stirrups in the central 600mm zone.

Chapter 2 – EXPERIMENTAL LITERATURE REVIEW

2.1 Introduction

Failure as a result of tensile cracking is one of the most common modes of failure for reinforced concrete structures and, as a consequence, it is crucial to be able to predict both its presence and severity. Understanding the bond-slip behaviour at the interface between the steel reinforcement and the concrete helps this prediction. The width, spacing and direction of cracks greatly depend on the bond-slip characteristics of the system (American Society of Civil Engineers, 1982).

The composite behaviour of steel and concrete in reinforced concrete structures is dependent on the bond between the two materials. Considering a reinforced concrete beam subject to flexural loading, the load applied is carried by the concrete in compression and the reinforcing steel in tension, which is transmitted to the concrete in which it is embedded by the bond between the two materials. The bond provides a resistance known as the bond stress which can be thought of a shear stress between the reinforcing bar and the concrete surrounding the bar. The bond stress is defined as a force per unit of nominal surface area of the interface between the reinforcing bar and the concrete in which it is embedded (Jain, 1982; Macginley and Choo, 1990; Pillai and Menon, 1999 and Karve and Shah ,1994). Understanding the bond behaviour can help in understanding the failure mechanism of reinforced concrete components during cracking and the nature of localized failures, such as concrete cracks.

2.2 Bond-Slip Mechanisms

2.2.1 Components of Bond-Slip Mechanisms

The bond-slip mechanism comprises three components, i.e. chemical adhesion, friction and mechanical interlock between the bar ribs and the concrete. Chemical adhesion depends on the chemical reaction between the concrete and the reinforcing steel bars, friction depends on the surface roughness and the magnitude of friction is related to the normal force to the movement direction, and mechanical interlock depends on the reinforcement geometry and surface deformation (Hanus et. al., 2000). The first two components play a more important and primary role in the bond of plain bars, even though some mechanical interlocking takes place due to the roughness of the bar surface. For deformed bars, mechanical interlock is thought to be the primarily mechanism with the others only being secondary effects (Cox and Herrmann, 1999). However, in spite of acknowledging the three bond components as individual mechanisms, they are not independent. They interact with each other and can not be analyzed as separated issues. The combined effect of these components leads to different behaviours. The four general types of bond failure are bar failure, bar pullout, concrete pullout and concrete splitting. Many researchers have contributed to the investigation of bond mechanisms. It is generally accepted that there are different stages of the interaction between steel and concrete when a tensile force is applied to a steel reinforced specimen.

According to the *fib* “Bond of reinforcement in concrete” (2000), the bond stress is low at the beginning of the loading process while the concrete remains uncracked and no bar slip is taken place. Chemical adhesion dominates the resistance for very low levels of

bond (up to about 1.5MPa (Lutz and Gergely, 1967 and Gambarova and Karakoc, 1982)) and mainly localised at the tips of the ribs. The strength of the cohesion greatly depends on the concrete and its chemical reaction with the surface layers of the steel reinforcement. At the same time, the micromechanical interaction between the microscopic rough steel surface and concrete surface also contributes to the bond strength, nevertheless it is considered as a minor role comparing to the chemical adhesion.

When the load further increases, slip occurs after the chemical adhesion is broken down and the mechanical interlock, provided by the wedging action of the ribs, is responsible for the resistance to the pulling apart of the two materials (Chinn et al. 1955, Eligehausen et al. 1983). Secondary internal transverse cracks (radial cracks) are firstly developed at the tips of the ribs to allow slip (as shown in Figure 2.1).

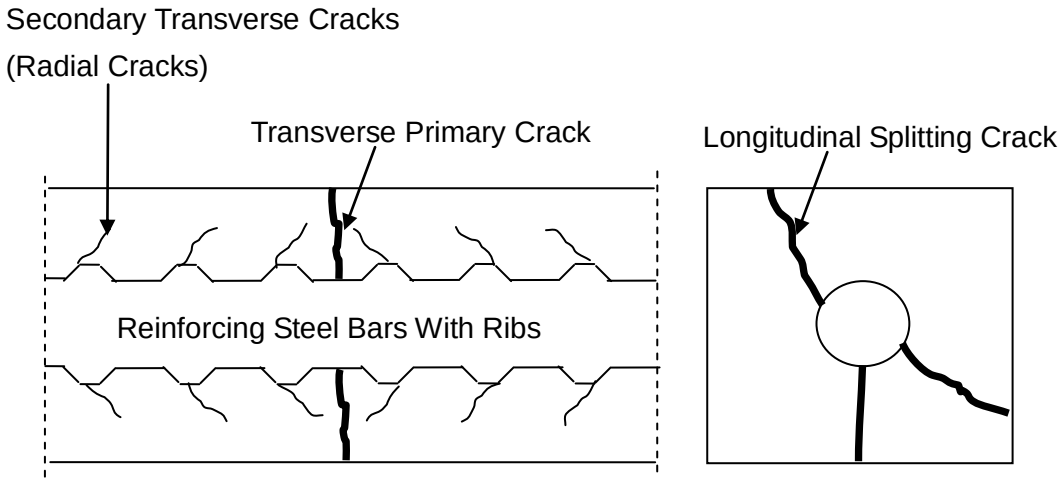

Figure 2.1. Cracks formed in reinforced concrete beams
(Tassios, 1979; CEB Bulletin No. 151, 1982)

Longitudinal cracks (Goto, 1967 and Gerstle and Ingraffea, 1990) are developed and

spread, and when further load is applied, the wedging action is enhanced by crushing of the concrete in front of the ribs. Therefore the component of the wedging action parallel to the reinforcing steel bar depends on the rib pattern of the reinforcement and the outward component depends on the hoop stress provided by the surrounding confinement. According to Tepfers (1979), as long as there is an undamaged outer concrete ring around the reinforcement, the concrete is capable of exerting a hoop stress around the bar, so that bond strength and stiffness are mostly determined by mechanical interlock.

In the case of a low level amount of or even no transverse reinforcement (named as stirrups or links), the specimen would fail in splitting after the splitting cracks propagate through the concrete cover and reach the outer concrete surface. When there is a medium level amount of transverse reinforcement and therefore relatively long bond lengths, pullout failures and splitting failure could be both observed since various stages of bond damage along the bond length are taking place at the same moment. In the case of high level amount of transverse reinforcement or large concrete cover, the splitting cracks are confined around the bar and the splitting is limited to the cracked core around the reinforcement.

In the cases with medium and high level amount of transverse reinforcement, the bar and the bar ribs are essential to ensure that the bond stress can reach what is considered to be an ultimate value of approximately $f_c/3$ (Gambarova and Karakoc, 1982). Splitting failure does not occur but pull-out failure and the bond stress is dominated, instead of rib bearing, by the friction at the interface. Once after most of the

concrete in front of the ribs is sheared off or crushed, the bond stress would be further reduced when the friction interface is smoothened by wearing and compaction.

Due to the non-linear material properties of concrete, it is not surprising that the bond strength contributed by mechanical interlock which is provided by the wedging action of the ribs also increases ascending non-linearly. When enough concrete is crushed in front of the ribs, a wedge with a low incident angle, of about 30 to 40 degrees, exists and produces the inclined transverse cracks, and longitudinal cracks (Malvar, 1992).

2.2.2 Factors Influencing the Bond-Slip Mechanisms

Bond-slip mechanisms are complicated and the factors that influence the bond have already been listed and investigated by many researchers (American Concrete Institute, 1996; Darwin, et. al., 1996; Orangun and Breen, 1975; Orangun and Breen, 1977; Zuo and Darwin, 2000; Abosrra et.al., 2011 and Guizani and Chaallal, 2011). Of these factors the most significant are:

1. *Reinforcement geometry and properties*

   Reinforcement geometry largely contributes to the bond strength. Currently BS EN1992-1 (2004) describes ribbed reinforcement as “high bond bar” and the classification of high bond bar is related to the relative rib area of the bar, f_R, which in turn is a function of the geometry of the rib pattern. Rehm (1961) defined the relative rib area f_R as the ratio between the rib bearing area and the rib shearing area. The coefficient f_R , also called the bond index or relative bond area, provides a specific description or measurement of the size and shape of the reinforcement ribs. It is

defined in BS EN 10080 by:

$$f_R = f(a_m, c, d, e)$$

in which the bar diameter is (d), maximum height of the transverse ribs (a_m), the spacing between the transverse ribs (c) and the width of longitudinal ribs (e) influence the value.

Rehm (1969) used pull-out tests and found a linear relationship between the bond strength and the f_R in which the higher f_R values resulted in higher bond strength.

The influence of steel stress is considered to be negligible in the elastic range as long as the Poisson ratio effect is small and the steel bar ribs transfer the force to concrete. Nevertheless experimental results by Shima et al. (1987), Engstrom (1992) and Bigaj (1995) showed that once the reinforcing steel bars start yielding, a non-linear descending branch in the bond stress to bond slip relationship would result not only from the softening of the surrounding concrete but also from the softening of the yielded steel bar. The steel stress becomes more significant when the friction dominates the bond mechanism because the sudden increase of steel strain due to yielding and the consequent increase of bearing stress in front of the ribs at the yield section cannot be disregarded (Biagaj, 1995). Therefore, in typical tests, the embedded length of the reinforcing bar is relatively short. The reason for this is to make sure that the steel stress and strain are small enough to negate this effect in the test after yielding.

Other properties such as inclination of the ribs might also affect the bond mechanism. Malver (1992) also suggested that the bars with ribs at 90 degrees with the longitudinal axis exhibited a better bond than bars with inclined ribs.

2. *Concrete Properties*

The bond mechanism is actually based on the stress transfer from the steel to the concrete by compression and shear interfacial forces. Therefore the concrete uniaxial strength f_c and concrete tensile strength f_{ct} play an important role in pull-out and splitting failures respectively.

Concrete quality is definitely important for good bond, not only as defined by the concrete strength, modulus of elasticity and Poisson's ratio, but also as a consequence of the technical process of producing and casting the concrete. The compression and tensile strengths, dimensions and texture of the sand and aggregates used in the mix and the mix proportions also have a significant effect such as the variation in strength on the resulting concrete.

The non-linear behaviour of concrete has already been mentioned in the discussion of bond-slip behaviour which depends on the concrete softening around the reinforcing bars. When mechanical interlock dominates the bond mechanism, a wedging action is taking place at the tips of the ribs of the reinforcing bars by the development of radial cracks and then crushing of the concrete in front of these ribs. (Nagatomo, Kaku, 1992) As such, therefore the concrete softening property plays an important role.

3. *Confinement*

Confinement is important to bond efficiency and crack control. Confinement is generally classified as either active or passive. Active confinement (Tepfers, 1973; Eligehausen 1979; Nagatomo and Kaku 1992) is achieved by loads from a direct support or the continuity at a beam/column joint transverse to the bar, whereas passive confinement is provided by the clamping action of a certain level of concrete cover (Plizzari, Schumm and Giuriani, 1987 and Reinhardt and Van der Veen, 1990), transverse reinforcements or stirrups (Tepters, 1973; Eligehausen et al, 1983 and Giuriani and Plizzari, 1985). Active confinement is considered as more effective as it is independent of the actual bond strength compared to passive confinement. (Nagatomo, Kaku, 1992 and Giuriani, Plizzari and Schumm, 1991)

4. *Other factors*

Bond behaviour is a complicated mechanism which involves a lot of influencing factors, including static or cyclic loading (Rehm and Eligehausen 1979), loading time (Frankie, 1976), environmental effects such as bar rusting (Almusallam et al, 1996 and Fang et al, 2004), high/low temperature effects (Schneider et al., 1985 and van der Veen, 1992), etc. However, these are beyond the scope of this investigation and their effect will be limited by adopting a standard loading method and a consistent environment throughout the experimental programme.

In spite of the many factors considered to influence bond, it is believed that the surface condition of the ribs of the steel reinforcement is one of the main factors. Rehm (1969) used pull-out tests and found a linear relationship between the bond strength and f_R

value in which higher f_R values resulted in higher bond strengths. In BS EN1992-1 (2004), it is recommended that the relative rib area f_R should be larger than 0.04 for bars of 6.5mm-12mm diameter and larger than 0.056 for bars with a diameter greater than 12mm. These values are used currently in both the UK and Europe which ensures good bond behaviour at the SLS, but a reduced plastic hinge rotation capacity at ULS.

2.3 Crack Control

In general, cracks are unavoidable in reinforced concrete, no matter whether it is subject to flexural or axial loading. Many researches were done on cracking mechanism (Clark, 1956; Chi and Kirstein 1958; Elfgren and Noghabai, 1998, 2001 and 2002; Mayer, 2002 and Alander, 2002). In design, such as recommended by BS EN1992-1 (2004), such cracks are typically limited to relatively small values of between 0.2 mm and 0.4mm depending on the use and location of the element under consideration. The reasons for limiting these cracks are to:

1. Reduce the risk of steel reinforcement corrosion.
2. Avoid or limit leakage
3. Ensure a smooth and good quality appearance

One of the controlling issues in the economics of design and the provision of reinforced concrete structures at the SLS of durability is the service life. Cracking and both the size and spacing of the reinforcing bars, are significant parameters that are related to the mechanism of bond.

2.3.1 Crack Spacing

Considering a centrally reinforced concrete prism loaded in pure tension, the first crack is developed after the tensile force reaches a certain level. This length is a function of bond strength measured from where the crack developed to where the concrete stress is undisturbed by the crack and is referred to as the "transfer length" S_o. Along the length S_o, the tensile force originally carried by the concrete is transferred to the reinforcement through the bond stress acting at the interface between the two materials, as shown in Figure 2.2.

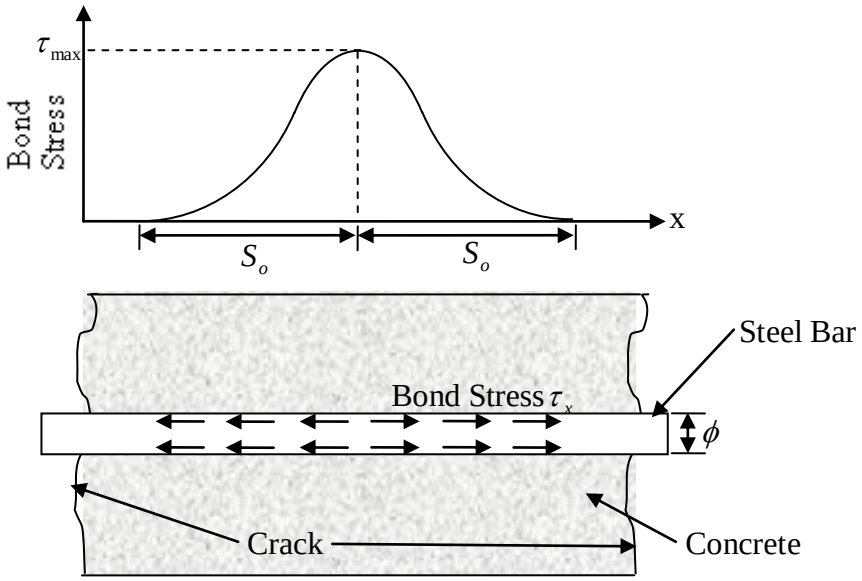

Figure 2.2 Distribution of bond stress between cracks

Therefore,

$$A_c f_{ct} = \pi\phi \int_0^{S_o} \tau_x dx \qquad (1)$$

At the point where the crack is developed, the bond slip is a maximum, decreasing with the distance from the crack until it drops to zero at a length of S_o from the crack. It can be anticipated that the ultimate bond strength $\tau_{\max}$ exists at some point along S_o. Therefore, if β is defined as a coefficient of integration, then equation (1) becomes:

$$A_c f_{ct} = \pi\phi(\beta\tau_{\max} S_o) \tag{2a}$$

Considering ρ as the reinforcement ratio = A_s / A_c and $A_s = \frac{\pi\phi^2}{4}$, equation (2a) can be rearranged as:

$$S_o = \frac{\pi\phi^2 f_{ct}}{4\beta\rho\pi\phi\tau_{\max}} = \frac{1}{4\beta}\left(\frac{f_{ct}}{\tau_{\max}}\right)\left(\frac{\phi}{\rho}\right) \tag{2b}$$

From equation (2b), it can be seen the transfer length S_o is affected by a number of parameters, including the concrete tensile strength f_{ct}, the bar diameter ϕ, the reinforcement ratio ρ and the ultimate bond strength $\tau_{\max}$.

If a first crack has developed, any further loading on the structure could lead to the development of a second crack. It is possible that this is anywhere within the zone of maximum moment but the distance between two cracks can not be less than the transfer length S_o because the concrete stress has been reduced by the presence of the first crack. However, if the second crack is formed at a distance of more than $2S_o$ away from the first crack, there is certain length between the two cracks where the concrete stress remains at a level of f_{ct}. This means at least one crack will form between two

existing cracks if they are at more than a distance of $2S_o$ apart until a stable crack pattern with a crack spacing S is achieved:

$$S_o \leq S \leq 2S_o \tag{3}$$

2.3.2 Crack Width

In the past 40 years, a lot of effort has gone into proving methods of predicting crack width and spacing using the structural concrete design codes. Many formulae have been proposed in different formats to define a satisfactory service performance in relation to the crack width and crack spacing under certain levels and methods of loading. Such formulae have the general form (Beeby, 2004):

$$\omega = k\ \varepsilon \left(\frac{\phi}{\rho}\right) \tag{4}$$

where w is the crack width. From this equation, it can be seen that the key elements which affect the crack width are the bond characteristic parameter k, the bar diameter ϕ, the reinforcement ratio ρ, and the strain ε.

Basically, the maximum crack width $\omega_{\max}$ is actually the result of the extension of the reinforcing steel bar in relation to the surrounding concrete. Therefore this can be written as :

$$\omega_{\max} = 2S_o(\varepsilon_{sm} - \varepsilon_{cm})$$

$$= \frac{1}{2\beta}\left(\frac{f_{ct}}{\tau_{\max}}\right)\left(\frac{\phi}{\rho}\right)(\varepsilon_{sm} - \varepsilon_{cm}) \qquad (5)$$

The similarity of equations (4) and (5) is striking, where $\frac{1}{2\beta}\left(\frac{f_{ct}}{\tau_{\max}}\right)$ is the constant k, assuming that ε_{cm} is so small in comparison to ε_{sm} and that it can be deemed to be negligible.

The general form of crack width equation is generally accepted and used in this form with modification in many modern design codes. In the general form, the concrete cover c is considered as part of the constant, whereas many experimental results (Plizzari, Schumm and Giuriani, 1987 and Reinhardt and Van der Veen, 1990) have shown that concrete cover plays an important role in crack width control. It is generally accepted that the crack width at the concrete surface is larger than the crack width appearing at the bar surface due to the shear deformation of the concrete between the bar surface and the concrete surface.

According to the BS EN1992-1 (2004), the maximum crack width $\omega_{\max}$ is defined as :

$$\omega_{\max} = \left[3.4c + 0.425k_1k_2\left(\frac{\phi}{\rho}\right)\right](\varepsilon_{sm} - \varepsilon_{cm}) \qquad (6)$$

The effect on the crack width due to $\left(\frac{\phi}{\rho}\right)$ varies depending on the type of loading

(tensile or flexural) to which the member under consideration is subjected. In addition to the parameters mentioned above, the presence of secondary reinforcement will also change the crack width as well as the crack spacing.

The other issue of relevance in relation to the experimental work undertaken is that the crack is measured at the surface of the concrete while the above theory relates to the interface of the reinforcement and the concrete. It is anticipated that this will increase the variability of the results and the crack widths that are measured but should not influence crack spacing.

2.3.3 Bond Tests

Crack formation affects the distribution of internal forces, the effective stiffness of the structure, the mode of failure and the corresponding strength (American Society of Civil Engineers, 1982). Therefore understanding the relationship between bond-slip characteristics and the crack formation helps in the development of more accurate prediction models.

In order to investigate the bond-slip mechanism, some simple ways or methods to measure bond stress are essential. Pull-out tests and bond beam tests are frequently used to determine the bond strength between the reinforcing bar and embedded concrete, in which the load in the test is recorded and used to determine the bond strength at various load levels. According to BS EN 10080, ribbed bars should be bonded only over a limited length and plastic sleeves are used elsewhere to avoid the adhesion between the concrete and the bar. These methods are intended for the

determination of the bond strength and provide a basis for the determination of bond performance characteristic of steel bars based on the surface configuration.

The approaches measure the bond strength in a simple way, but do not provide the actual bond stress distribution. When there is no relative displacement at the interface between the concrete and the steel reinforcement, it is regarded as no slip at the interface and therefore the strain in the steel is equal to the strain in the surrounding concrete.

Shima (1987) was aware that many bond-slip relationships have been formulated and published, but they all are different to each other because bond-slip relationships depend on various factors, as mentioned in Section 2.2.1, which vary in different bond experiments (Morita and Fujii 1985). The bond-slip relationship obtained from a short embedded length of steel and concrete, such as in pullout tests, are not the same as that from a long embedded length in another bond tests (Yamao, Chou and Niwa, 1984). The results vary with the locations even along the same specimen in cases of free end slip (Chou et. al., 1983).

In view of the above, some non-destructive evaluation (NDE) methods, such as vibration analysis (Carden and Fanning, 2004 and Farrar, Doebling and Nix, 2001), radar (Concrete Society, 1997 and McCann and Forde, 2001) and acoustic emission (AE) technology (Malhotra, 1976 and Mirmiran and Philip, 2000), are used to investigate and measure the bond of the steel reinforcement. In the experiments reported in this work, specimens were monitored both visually and using a non-destructive Digital

Image Correlation (DIC) Technique, also named as Digital Speckle Correlation Method (DSCM) (Guo et al, 2008). Using a system VIC-2D/VIC-3D adopting the DIC technique, it was possible to produce a complete picture of displacements and strain measurements of the specimens in a 2D/3D contour map and also to trace the three-dimensional displacement and strain changes in three dimensions by monitoring the movement of a speckle pattern painted on the front face of the specimen. More details on this procedure will be given in Chapter 4. However, Cintron (2008) pointed out that the strains measured using VIC-2D are not always accurate because of errors due to the size of the specimens. He also noted that the paint used to create the speckle patterns on the specimens would have different material properties to the specimens themselves and this could again affect the accuracy of the displacement and strain measurements observed.

2.4 SLS And ULS Behaviour

Mayer (1998) highlights the significant dependence of the behaviour of reinforced concrete structures on bond and also emphasises the requirements for bond that must be fulfilled:

- At the serviceability limit state (SLS), the damage and crack width of reinforced concrete structures should be smaller then a certain allowable value. Small crack spacing is therefore expected and stronger bond is required to ensure a small ratio between the mean steel strain and the steel stain at the cracks.

- At the ultimate limit state (ULS), a large rotation capacity at plastic hinges is

required to ensure ductile behaviour of the reinforced concrete. In this case, only weak bond is required so that there is a large ratio between the mean steel strain and the steel strain at the cracks.

- In the area of anchorages and lap splices of reinforcement, high levels of bond strength are required so that the splitting forces are small enough to ensure that short anchorage and lap lengths are sufficient.

This shows that, on one hand, high levels of bond strength are required to ensure appropriate SLS and anchorage behaviour. However, on the other hand, only low levels of bond are required at the ULS to ensure ductile behaviour at plastic hinges. Because of the requirement for two different levels of bond, it is clear that just high bond strength may not be sufficient because of the contradiction between the two requirements. What needs to be identified is the optimal bond strength to satisfy both requirements.

2.5 Conclusion

Bond failure occurs internally within a member, and so understanding of the failure mechanisms is still not without question. A large number of pullout and splitting experiments have been done by previous researchers and many models have been drawn up for bond development. While the recommended models (see BS EN1992-1 (2004)) are generally acceptable, there is still debate as to the significance of the relative rib area f_R and its influence on crack spacing and width (Alander, 2002).

To address this issue a series of tests were undertaken and are reported and discussed

in Chapter 4. Additionally, results obtained using a finite element model of the experimental set-up are presented in Chapter 5. A comparison between the numerical and experimental results is made in Chapter 6.

Chapter 3 – NUMERICAL LITERATURE REVIEW

3.1 Introduction

In most engineering problems, solutions can be obtained explicitly only if regular geometry and simple loads are involved. Numerical methods are therefore required to solve practical problems. Many different numerical techniques have been developed, including finite difference methods, boundary element methods, finite volume methods, spectral methods and meshless methods. Nevertheless, the FEM (Finite Element Method) remains dominant among numerical methods for solving problems in solid mechanics. For the past 40 years, much work has been undertaken on finite element concrete modelling (following either the continuum modelling approach or the discrete modelling approach), however there has been relatively little work undertaken on the prediction of crack widths using the FEM.

This literature review provides an overview of work on finite element approaches for modelling the non-linear behaviour of concrete structures. This provides the background for the work undertaken for this thesis on the finite element modelling of reinforced concrete elements. It addresses both constitutive modelling and computational developments in the field.

3.2 Constitutive Models for Concrete

Plasticity theory is able to simulate many aspects of concrete behaviour and one of the earliest multi-axial plasticity based models for concrete was that developed by Willam and Warnke (1975). In their model, an evolution function was used to govern the growth of the yield surface, under both biaxial and triaxial loading. Frictional hardening

behaviour was included in later developments by Este and Willam (1994), Chen and Chen (1975) also developed a plasticity model for both tension and compression behaviour and then later developed the approach such that the yield surface was able to capture the nonlinearity in hydrostatic compression and simulate frictional hardening (Han and Chen, 1987).

Kochonov introduced the concept of damage mechanics in 1958 to model creep rupture but the term “damage mechanics” was introduced by Hult in 1977. In this approach, concrete fracture is simulated using a damage function which can be expressed in terms of effective stress, strain or other thermodynamic variables. Damage mechanics actually simulates the development of micro-cracking by a degradation of stiffness using damage parameters which govern the degree of the degradation. These parameters may be scalars (Mazars, 1986), vectors (Krajcinovic and Fronseka, 1981) or fourth-order tensors (Chaboche, 1979). Many researchers have worked on models based on damage mechanics. In order to describe the different behaviours of concrete under tension and compression, Mazars (1986) and Mazars and Pijaudier-Cabot (1989) developed a widely used model in which both damage due to tension and compression are included in the formulation. In this model, tensile damage is governed by a tensile evolution function and compressive damage governed by a compression evolution function. Similar isotopic damage models, that also employ two damage functions for tension and compression, have been developed by Faria et. al. (1998), Comi and Perego (2001) and Marfia et. al. (2004). Other examples of effective damage models for concrete are those developed by Oliver et al. (2002) and Comi and Perego (1987).

Concrete is not isotropic once damage has occurred and thus many researchers have explored anisotropic damage formulations. Examples of such anisotropic models include those developed by Simo et al. (1987), Carol et al. (2002) and Desmorat et al. (2007). De Borst and Guitierrez (1999) developed a model which has a unified treatment for both isotropic and anisotropic damage. However, the greater complexity of these anisotropic models, which includes those which use second order tensors (Desmorat et.al, 2007) and even fourth order tensors (Chaboche,1979), leads to convergence problems (Contrafatto and Cuomo, 2006) when they are implemented in finite element codes. As a consequence of this drawback, the isotopic damage model is preferred by many researchers (Jirasek and Zimmermann, 1998; Salari et. at., 2004; Contrafatto and Cuomo, 2006).

3.3 Computational Models for Fracture and Related Issues

Research on non-linear finite element models for concrete began in the 1960s, with the work of Ngo and Scordelis (1967) and Rashid (1968). In both of these investigations, nonlinearity was restricted to tensile cracking. Cracks were modelled as discrete lines by changing the element topology in Ngo's work whereas the cracks were simulated by introducing an orthotropic material with zero strength normal to the cracks in Rashid's work. These two approaches were named 'discrete' and 'smeared' (or 'continuum') respectively according to their characteristics. Not surprisingly, the much greater convenience of the smeared approach with its ease of implementation was more widely adopted.

The discrete approach is attractive in terms of the way it represents discrete cracks, however it suffers from two disadvantages (i) that it requires constant remeshing and (ii) that stress singularities develop at crack tips, which have to be treated with special elements and with fracture mechanics based crack growth criteria if spurious mesh dependency is to be avoided (Tong and Pian, 1973). To overcome these difficulties, Belytschko and coworkers (1999a, 1999b, 2000), developed the 'Extended Finite Element Method' or X-FEM. X-FEM has the advantage that no remeshing is required during crack development. It also resolves the disadvantages of the discrete approach and is able to capture the displacement jumps across the crack and the singular strain and stress field at the tip of crack. X-FEM is classed as a strong discontinuity model and besides X-FEM, there are other, element based, approaches to modelling strong discontinues without remeshing (Simo, Oliver and Armero, 1993; Oliver, 1995; Oliver et. al., 1999; Belytschko and Black, 1999; Moes et al., 1999; Belytschko et al, 2001, Oliver et al., 2002; Oliver et. al., 2004; Oliver and Huespe, 2004a; Oliver and Huespe, 2004b). These element based approaches have proved to be powerful tools for crack simulations, although further research is required to resolve problems such as the simulation of multiple cracks in 3D (Oliver et al., 2004a; Oliver et al., 2004b).

In the continuum approach, a crack is modelled as a zone or a band of degraded material which is locally deformed according the standard continuum mechanism. It means the structure remains a continuum and has no discontinuities, but the mechanical properties are modified to model the evolution of cracks. As a result, remeshing is not necessary in the model. After the first use of this approach by Rashid

(1968), it was gradually noticed that results could be mesh dependent when using this method.

Concrete is a type of quasi-brittle material which has a softening property which means that the load capacity of concrete reduces after the peak load has been reached. According to this property, localization behaviour is observed. Considering a one-dimensional displacement control tensile test of a concrete prism; once the peak load has been exceeded, deformations grow in a few small and limited areas or sections of the specimen, and the rest of the material unloads. This continues until complete failure occurs. If a constant stress-strain softening model is used in a finite element simulation of such a test, a crack localises to a single element and the total dissipation energy is proportional to the area (or volume) of elements in that band. However, this result is obviously impossible from the viewpoint of physics since in the limit of zero element size it implies zero energy for crack propagation. This problem of mesh dependence with strain softening behaviour was recognised by Bazant and Oh (1983) who showed that existing models were mesh dependent. Bazant and Oh provided a solution to this localization problem by introducing the crack band model. The new model was based on the cohesive crack model of Hillerborg et. al. (1976) but was developed on a continuum mechanics basis. In this approach, the strain softening constitutive model is related to the fracture energy of the material and the characteristic length of the elements in which cracks develop. The crack band model has been widely adopted and is successful at reducing mesh dependency. It does not, however, solve the problem of Mesh Bias (Grassl and Jirásek, 2004) nor does it solve the stability

problems which arise with strain softening equations which may lead to bifurcations in the equilibrium path.

3.4 Non-local Approaches

To solve these problems, non-local constitutive models have been proposed. Models in this category include micropolar models (Aifantis, 1984), gradient-enhanced non-local models (de Borst and Mulhaus, 1992; Peerlings et. al., 1996; Peerlings et. al., 1998; de Borst, 2001) and integral non-local models (Pijaudier-Cabot and Bazant, 1987; Bažant and Pijaudier-Cabot, 1988; Bažant and Jirásek, 2002). Peerlings et. al. (2001) reported an interesting finding that the two different non-local approaches were effectively equivalent. Non-local models limit localization by averaging damage over a zone of finite size, the width of which is governed by a length parameter (characteristic length or internal length), which prevents sharp gradients from occurring in the displacement field. A comprehensive review of non-local approaches was presented by Bazant and Jirasek in 2002. Although non-local models successfully overcome the mesh bias and stability problems observed in local models, non-local models are still limited by their computational requirements and by the difficulties of implementing complex constitutive models in non-local computational frameworks (Jefferson, 2010).

A particularly general form of non-local gradient model was presented by Ru and Aifantis (1993) which involves the introduction of higher order strain gradients in the governing constitutive equations. This method can be applied to a range of material models, as illustrated in the later work of Askes and Aifantis (2002).

In gradient and integral nonlocal methods, the element size needs to be smaller than the physical characteristic material length such that a few elements cover a localisation band. If the element size is taken as approximately equal to the coarse aggregate size in concrete, then this requirement would lead to a very fine mesh for a full scale structure and the overall cost of the numerical solution can become prohibitively expensive in terms of solution time. Patzak & Jirasek (2004) developed an adaptive approach to deal with this problem, in which the mesh is refined only where localization regions occur, as shown in Figure 3.1. To do so, the continuum is remeshed and the local solution is remapped onto the new mesh, however Sfantos and Aliabadi (2006) commented that this is rather complicated and interpolation errors will be inevitably introduced.

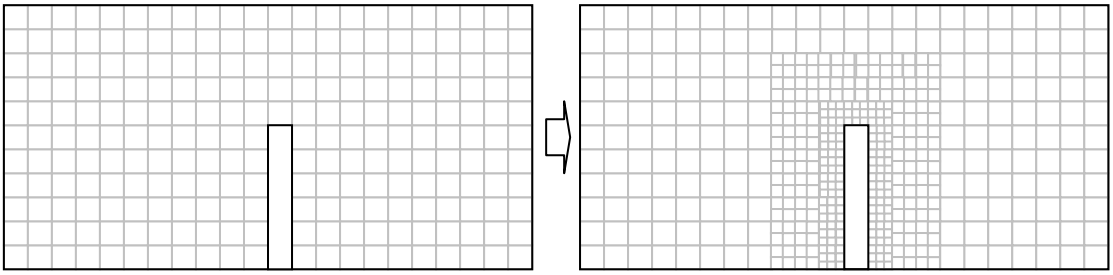

Figure 3.1 Example of continuum remeshing

Much research has been undertaken to justify the size and existence of the characteristic length (Bazant and Pijaudier-Cabot, 1998). Many researchers give the characteristic length as a multiple of the maximum aggregate size (Bažant and Jirásek, 2002; Bazant and Pijaudier-Cabot, 1998; Maier, 2004; Marchner and Vermeer, 2000;

Małecki et.al., 2007), but the factors used in this multiple vary between different materials (Ožbolt 1993).

Another issue, addressed by Pijaudier-Cabot et al. (2004), is that the size of the localisation band should develop along with the degree of localization. Pijaudier-Cabot et al. (2004) deals with this by proposing an evolving characteristic length. Other workers have also adopted this notion and relate an evolution equation for the characteristic length parameter to the initial undamaged material microstructure and to the deformation mechanism under the damage process (Ferrara and di Prisco, 2002; Geers et.al., 1999; Mosalam and Paulino 1997; Pamin, 1994; van Mier, 2004). There are two reasons to support their proposal. Firstly, the microstructure in a material governs the properties of material and the structural behaviour under deformation. The whole process is a complex situation which should not be described by one single constant parameter. Secondly, during the crack development, the nonlocal continuum model transforms from a continuum to a discontinuous body (Ferrara and di Prisco, 2001; Simone et.al., 2003). Furthermore, it proves difficult to experimentally determine the characteristic length in relation to any measurable microscopic material property. Therefore, it is more common to estimate the characteristic length by matching the numerical response with the measured response from structural experiments (Geers et.al., 1999; Carmeliet, 1999; Le Bellego et.al., 2003; Mahnken and Kuhl 1999), even although the choice of experiment does affect the characteristic length calculated. Although the physical meaning of the characteristic length remains unclear it is nevertheless a very useful concept and the author does not agree with the view of some

researchers that the characteristic length is just a 'mathematical trick' (de Borst and Pamin, 1996; Pamin, 1994).

One of the other important aspects of fracture behaviour is size effect (Carmeliet 1999; Le Bellego et.al., 2003). This is relevant to the present work because fracture parameters which control the predicted size effect can be strongly affected by the details of the experiments used to measure them. This is because the stress redistribution in the structures after macro or micro cracks are formed is dependent on the boundary and loading conditions applied in the experiment. Furthermore, different stiffnesses of specimens occur due to hydration, drying or other environmental factors, since larger specimens have smaller surface to volume ratio which might result in uneven properties in the specimens. It should be mentioned that size effect has both an energetic component (Bazant, 1984) and a statistical component. Models for the latter are generally based upon Weibull's weakest link theory (1939) and Carpinteri multi fractal scaling law (1994).

3.5 Conclusion

It is concluded that a relatively simple damage model based on smeared damage principles is appropriate for the present work. This will avoid some of the complex numerical issues discussed above whilst giving acceptable accuracy when modelling damage, or cracking. The model chosen is an isotropic damage model, based on that of Oliver et al. (2002). A smeared damage approach is adopted for cracking and both local and non-local implementations are considered. The theoretical details of the model are presented in Chapter 4.

CHAPTER 4 – EXPERIMENTAL STUDY

Currently BS EN1992-1 (2004) gives serviceability limit state (SLS) design guidelines for crack control of various structures at different stress levels. Ribbed reinforcement is described as “high bond bar” and the classification of high bond bar is related to the relative rib area of the bar, f_R , which in turn is a function of the geometry of the rib pattern. However the significance of these high bond bars at the SLS is not well understood. In this chapter, an experimental investigation of the relationship between the bond strength and the rib pattern of reinforcing steel is described. Furthermore, the flexural SLS behaviour of reinforced concrete (RC) beams with reinforcement of different rib patterns is explored. The cracking of the flexural beams was monitored both visually and using a non-destructive Digital Image Correlation (DIC) system. Using the DIC it was possible to trace the in-plane deformation and strain of the specimen over the full face by monitoring the movement of a speckle pattern painted on the front face of the specimen. For the steel bars used in these tests, the measured relative rib areas f_R were 0.054, 0.057, 0.064 and 0.071 and from the results, it can be seen that the specimen manufactured with the bar with the highest value of f_R exhibited the smallest size of crack and the smallest crack spacing.

4.1 Introduction

4.1.1 General

One of the controlling issues in the design and provision of RC structures is the serviceability limit state (SLS) of durability and hence service life. Cracking, both size and spacing, is a significant parameter in this context, and is related to the mechanism of bond (Jain, 1982; Macginley and Choo, 1990; Pillai and Menon, 1999; Karve and

Shah ,1994 and American Society of Civil Engineers, 1982).

Typically bond failure occurs internally within a member, and so the failure mechanisms remain obscure. Nevertheless, a large number of pullout and splitting experiments have been carried out by previous researchers and many models have been developed that describe the development of bond and its mechanisms. While the commonly used models (CEB-*fib*, 1993) are generally acceptable, there is still debate as to the significance of the relative rib area f_R (defined as the ratio of the area of projection of all ribs on a plane perpendicular to the longitudinal axis of the bar to the rib spacing and the nominal circumference of the bar) (Alander, 2002) and in particular its influence on the SLS parameters of crack spacing and width.

To investigate this issue further, a series of 42 medium scale beam tests were undertaken using bars with various rib patterns. The beams were tested in bending to failure and crack development was measured. In parallel, tests were carried out to BS EN 10080 to measure the bond strength of the different rib patterns.

Results are reported highlighting where potential relationships between the parameters may be significant and a comparison is made to other work in this area.

4.1.2 Background and Previous Research

When a reinforced concrete structure is loaded in flexure or tension, a tensile force occurs in the reinforcing steel bar. The bond mechanism between the steel reinforcement and the concrete allows the longitudinal force to be transferred from the

steel to concrete, and so the forces in both the steel bar and the surrounding concrete vary along the length. In the case of perfect bond, the strain of the reinforcing bar and the strain of the surrounding concrete are the same at the same location due to compatibility. When the bond capacity of the bar is exceeded, the steel strain differs from that in the surrounding concrete and a relative displacement occurs between them. As a result, cracks are formed due to the localized strain of the concrete.

The mechanisms of bond have been investigated and analysed by many previous researchers. Contributions by Lutz and Gergely (1967) and Ferguson (1966) are highlighted.

There are three main mechanisms contributing to the bond, which are chemical adhesion, friction and mechanical interlock. The first two components play a primary role in the bond of plain bars, even though some mechanical interlocking takes place due to the roughness of the bar surface. However, for deformed bars, mechanical interlock is the dominant feature (Cox and Herrmann, 1999). As a consequence of the above mechanisms, reinforcing bar and concrete interact differently with various arrangements of reinforcement and lead to four general types of failure in bond tests: bar failure, concrete splitting, bar pull-out and concrete pull-out.

- In bar failure (Figure 4.1a), the ultimate strength of the bar is comparatively low such that bar failure occurs before either pull-out or splitting failure.
- In concrete splitting failure (Figure 4.1b), longitudinal cracks are formed around the reinforcing bar. The bond can no-longer function and the specimen splits when the

radial cracks reach the outer surface of the concrete surface.

- In bar pull-out failure (Figure 4.1c), the bond fails because there is local failure of the concrete around the reinforcing bar due to the shear imposed by the steel ribs of the bar.

In concrete pull-out failure (Figure 4.1c), the bond between the rebar and concrete is greater than the shear strength of the concrete itself. As such, failure is within the concrete itself and a layer of concrete remains around the rebar when it is pulled out.

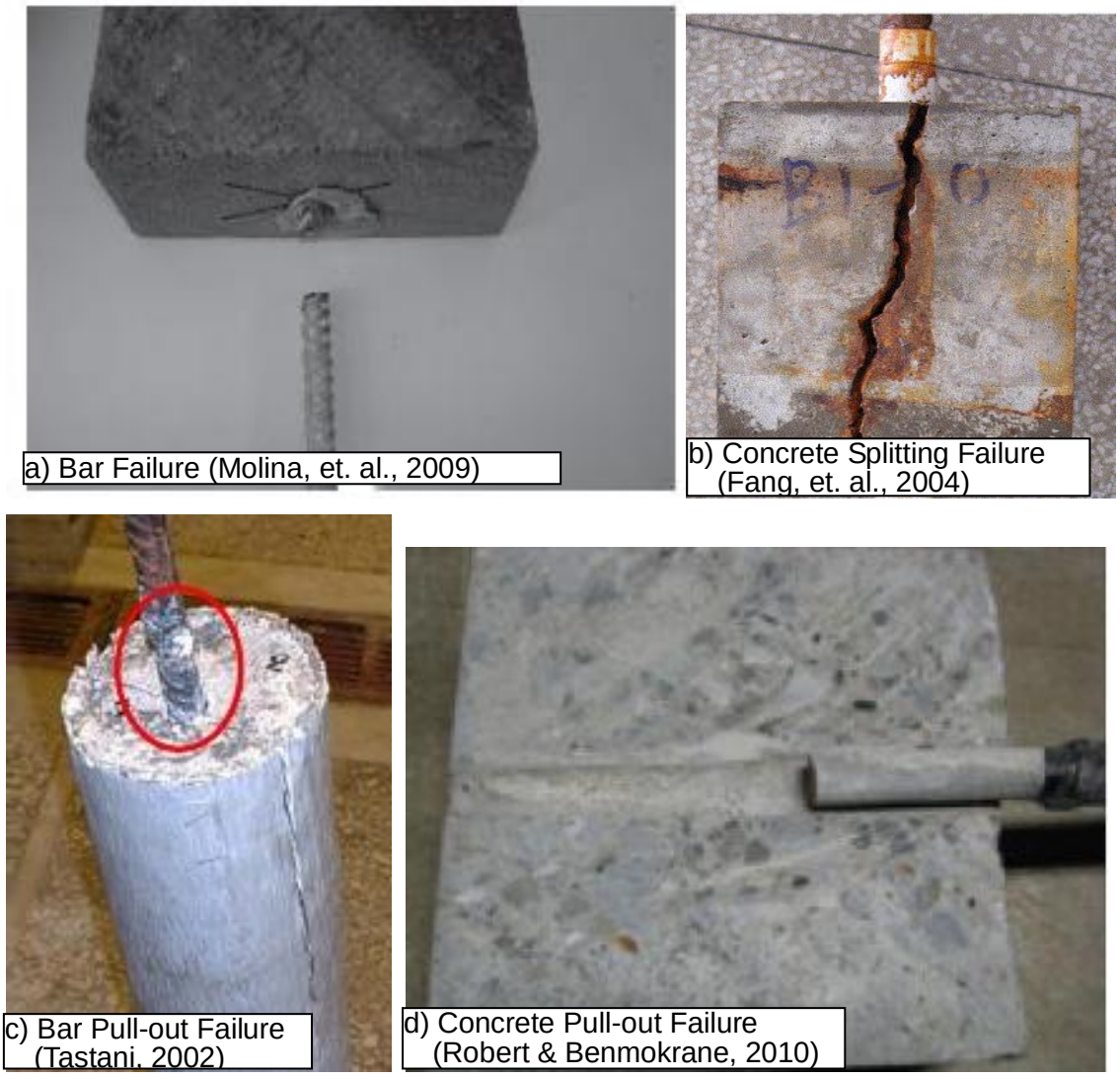

Figure 4.1. Four general types of failure in bond tests

There are many factors affecting the bond between steel and concrete, some of which are listed in the following, although this list is not exhaustive:

- Geometry of the RC structure and the arrangement of the reinforcement, such as, size/diameter (Bazant and Sener, 1988), cover (Tepfers, 1979), bar spacing (Ferguson, 1955), confinement (Harajli, Hamad and Rteil, 2004), and transverse reinforcement (Morita and Kaku, 1979).
- Properties of the concrete and reinforcing steel, such as strength, elastic modulus, yielding and surface rib pattern (Rehm, 1979; Tholen and Darwin, 1998 and McCabe and Pantazopoulou, 1998).
- Environmental effects, such as temperature, bar corrosion (Diederichs, 1981; Cabrera and Godussi, 1992 and Al-Sulaimani et al 1990).
- Load time history, such as short/long term, static/cyclic loading, loading rate and loading level (Edwards and Jannopoulos, 1978).

Baranek (1980) noted that sometimes splitting and pull-out failure occur at the same time, a failure mode that has been called partial splitting. While in some cases the splitting is visible externally, this is not in always the case, depending on whether any of the factors above are significant enough to prevent a complete splitting.

It is by virtue of the bond that exists between the steel bars and the concrete that the composite behaviour of the two materials enables reinforced concrete structures to develop sufficient strength at the ultimate limit state and to have adequate ductility in service. However, according to the findings of Mayer (1998), the requirement for a low level of bond to ensure the strength and safety of the structure is contrary to that required

for ductility, which is associated with the small, closely spaced flexural cracks that occur when the bond strength is high.

4.2. Material Properties

4.2.1 Mixing, Casting and Curing Procedure

A concrete mix with a target strength of 45MPa at 28 days was used, the mix proportion of which are shown in Table 4.1a. The cement was ordinary Portland cement of class 52.5N CEM I complying with the requirements of BS EN 197-1. The fine aggregate was 0/4mm natural sea dredged sand and the coarse aggregate was 4/10mm crushed limestone which both conformed to requirements of BS EN 12620:2008. The water used in the mix complied with the requirements of BS EN 1008:2002 and the slump ranged from 60mm to 80mm.

Table 4.1a. Mix proportions of concrete

Material	Detail	Weight (kg/m^3)
Cement	Ordinary Portland cement	133.3
Fine Aggregate	0-4mm sea dredged sand	293.3
Course Aggregate	4-10mm crushed limestone	506.7
Water	Tap water at about 20℃	66.7

A Belle 200 XT Premier Concrete Mixer with maximum capacity of 300kg mix was used for mixing the concrete. All dry materials were mixed in the drum for about 3 minutes before adding most of the water. Workability of the mix was measured using a concrete slump test (BS EN 12350-2:2009), which also helped determine the consistency between individual batches. More water was added into the mix to adjust the slump and the adjusted water content recorded as necessary and shown in Table 4.1b.

Table 4.1b. Adjusted water content of concrete mix

Concrete Mix	Adjusted Water Content ($0.001m^3$)	Concrete Mix	Adjusted Water Content ($0.001m^3$)	Concrete Mix	Adjusted Water Content ($0.001m^3$)
Bond Test A1	-0.2	Bond Test B1	+0.1	Bond Test C1	+0.2
Beam A1/A2	-0.3	Beam B1/B2	0	Beam C1/C2	0
Beam A3/A4	-0.3	Beam B3/B4	0	Beam C3/C4	+0.1
Beam A5/A6	-0.3	Beam B5/B6	-0.1	Beam C5/C6	0
Beam A7/A8	0	Beam B7/B8	+0.1	Beam C7/C8	+0.1
Beam A9/A10	-0.1	Beam B9/B10	0	Beam C9/C10	-0.1
Beam A11/A12	-0.1	Beam B11/B12	-0.1	Beam C11/C12	0
Bond Test A2	-0.2	Bond Test B2	-0.3	Bond Test C2	0
Bond Test M1	+0.1	Beam M3/M4	0	Bond Test M2	-0.1
Beam M1/M2	0	Beam M5/M6	+0.2		

The pullout specimens were cast in two 200mm cube timber forms. The bond beams were cast in a 100 x 180 x 800mm steel form and the 2m long beams were cast in 150 x 200 x 2000mm timber forms. Concrete samples were cast as controls to monitor the concrete properties of each mix. This included six standard 100mm concrete cubes with each flexural test specimen and four standard 100 x 100 x 500mm concrete prisms, four standard 100 x 200mm concrete cylinders and nine standard 100mm concrete cubes with each of the bond beam and pull-out specimen. A summary is shown in Table 4.2.

Table 4.2. Summary of concrete specimen and curing details

Curing Details	Flexural Beam Specimen	Bond Beam / Pull-out Cube Specimen
28 days in a water tank at 20°C	6 x 100mm cubes	2 pullout cubes 4 x 500mm prisms 4 x 200mm cylinders 6 x 100mm cubes
28 days wrapped with wet hessian and cling film	1 flexural beam	1 bond beam 3 x 100mm cubes

All specimens, apart from the flexural beams were compacted on a vibrating steel table. The flexural beams were compacted using a vibrating poker due to their size.

Specimens were kept in the moulds for 24 hours before de-moulding. They were then either put in a water tank or wrapped with wet hessian and cling film to cure for 28 days. Cling film was used to prevent the wet hessian from drying out too quickly. 3 cubes in each batch were also wrapped in wet hessian to test on the same day as the other cubes for comparison. See the detail in Table 4.2. On the day of testing, the specimens were taken out from the water tank or from the wet hessian and left to air dry for 2-3 hours before testing.

4.2.2 Concrete Properties

Concrete cubes and cylinders were tested to determine the concrete compressive cube strength and splitting strength respectively. Three cubes from each mix were tested at an age of 3 days and 28 days. According the specification of BS EN 12390-3:2000, they are subject to a uni-axial force at a rate of 180kN/min until failure. Four cylinders from each mix were tested at the age of 28 days. According the specification of BS EN

12390-6:2000, cylinders were loaded on their sides with a uni-axial force at a rate of 60kN/min until failure.

The prism specimens were tested in 4-point bending to determine the flexural strength. Three specimens from each mix were tested at an age of 28 days. According to the specification of BS EN 12390-5:2000, the specimens were loaded at a total rate of 7kN/min over a span of 400mm.

Test results are summarized and shown in Table 4.3.

Table 4.3. Concrete properties at an age of 28 days

		Mix A	Mix B	Mix C	Mix M
Sample Size		14	14	14	8
Cube Strength (N/mm^2)	Average	49.06	47.06	49.71	47.41
	Standard Deviation	1.67	3.98	2.45	2.03
Cylinder Splitting Strength (N/mm^2)	Average	5.1	5.2	4.9	5.1
	Standard Deviation	0.35	0.34	0.46	0.35
Prism Flexural Strength (N/mm^2)	Average	4.4	5.5	4.9	5.2
	Standard Deviation	0.43	0.31	0.22	0.47
Slump (mm)	Average	80	70	70	65
	Standard Deviation	12.43	7.93	9.82	11.33

Because of the size of the concrete mixer, there were 8 mixes (in Batch M) and 14 mixes in Batches A, B and C in each batch. More were required for the latter because they were also used to investigate the effect on crack spacing of the presence of stirrups in the middle zone of the beam. The mixes in each batch were completed over a relatively short period of time (10 days) under generally consistent conditions (temperature and humidity) and therefore it was assumed that the properties of the

concrete in the different mixes of the same batch would be similar. The cube strengths of each batch are shown in Figure 4.2. In the figure, the x-direction represents four different concrete mixes: Mix A, Mix B and Mix C (14 specimens each) and Mix M (8 specimens) and the y-direction gives the maximum, minimum and mean concrete strength of each mix, from which it can be seen that the concrete strengths of all batches were similar. It is also seen that the mean values are slightly lower than the median value, which highlights that most of the concrete strength results in each batch tend to be at the lower end of the range of the results.

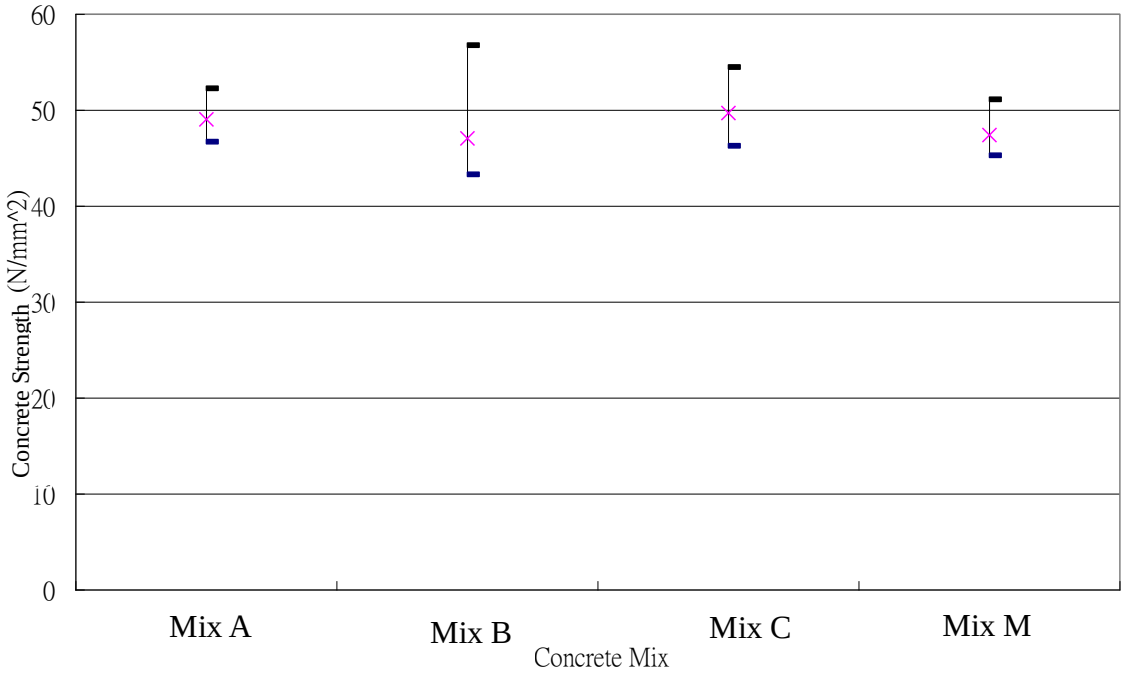

Figure 4.2. Concrete cube strength of specimens

A summary of the consistency of the concrete cube strengths is presented in Table 4.4.

Table 4.4. Detailed summary of concrete cube strengths

	Batch A	Batch B	Batch C	Batch M
Number of Mixes	14	14	14	8
Minimum Strength (N/mm^2)	46.7	43.3	46.3	45.3
Maximum Strength (N/mm^2)	52.3	56.8	54.5	51.1
Average Strength (N/mm^2)	49.1	47.1	49.7	47.4
Standard Deviation (N/mm^2)	1.67	3.98	2.45	2.03

4.2.3 Reinforcement Properties

Four different grades of steel reinforcing bar were used to provide a range of relative rib areas. They all had different rib patterns as shown in Figure 4.3, and the detail descriptions are as follows:

Bar A – Grade A with two longitudinal ribs and a row of parallel inclined transverse ribs between the longitudinal ribs on both sides of the ribs.

Bar B – Grade B with two longitudinal ribs and two rows of parallel inclined transverse ribs between the longitudinal ribs on both sides of the ribs.

Bar C – Grade C with two longitudinal ribs and a row of alternately inclined transverse ribs between the longitudinal ribs on both sides of the ribs.

Bar M – Celsa Max Grade C with two longitudinal ribs and the transverse rib pattern of Bar A between the longitudinal ribs on one side and the transverse rib pattern of Bar C between the longitudinal ribs on the other side.

Figure 4.3. Rib pattern on reinforcing steel bars

The tensile properties of three specimens of each bar type were tested and a summary of the results is presented in Table 4.5.

Table 4.5. Steel reinforcement properties

	Steel grade	Nominal Area* mm^2	0.2% Proof.		Ultimate.		Elongation.		Elastic
			Load kN	Stress N/mm^2	Load kN	Stress N/mm^2	Mm	%	Modulus kN/mm^2
Bar A	A	47.78	27.83	554	29.49	587	5.23	10.5	185
Bar B	B	51.53	26.18	521	29.99	597	10.00	20.0	199
Bar C	C	50.27	27.00	537	33.60	668	12.87	25.7	200
Bar M	C	55.42	26.35	524	32.78	652	11.27	22.5	205

* Area is determined by $\pi d^2 / 4$.

In order to determine the f_R values of the four specimens of steel bar, the bar diameter (d), maximum height of the transverse ribs (a_m), the spacing between the transverse ribs (c) and the width of longitudinal ribs (e) were measured:

- The diameter of the bars (d) was measured using vernier callipers and the result was taken to be the mean of 5 measurements taken on each bar.

- The maximum rib heights (a_m) of the bars was measured after enlargement by projecting a silhouette image onto a white board. These results were quite variable because of damage to the steel surface, the tolerances in the rolling process and observational errors. As this is a critical parameter in the calculation of the f_R value, the value quoted was determined as the mean of 8-10 measurements taken consecutively on each bar.
- The spacing of the two transverse ribs (c) was determined from the average spacing of 10 ribs, measured from the centre of one rib to the centre of another in a straight line parallel to the longitudinal ribs, so that the error in measuring this parameter was minimised. In general, 3 measurements were taken on each bar.
- The width of the longitudinal ribs of the bar specimens (e) was measured using vernier callipers and the result was generally determined as the mean of 3 measurements taken on each bar.

The relative rib area f_R was calculated using the parabola formula given in section 11.3.3 of BS EN ISO 15630-1, as shown:

$$f_R = \frac{2a_m}{3\pi dc}(\pi d - \sum e_i) \tag{4.1}$$

The results are summarised in Table 4.6.

Table 4.6. Summary of f_R values for steel reinforcing bars

Steel bar	Minimum f_R	Average f_R	Maximum f_R	Standard deviation
A	0.054	0.057	0.063	0.003
B	0.058	0.065	0.068	0.004
C	0.051	0.054	0.061	0.004
M	0.061	0.071	0.077	0.0055

The standard deviation of the f_R values for the four batches of steel bar ranged from 5.3% to 7.7% of the mean f_R which is consistent with that expected from normal manufacturing practices.

4.3. Test Specimens

Test specimens were designed and cast to investigate the relationship between bond strength and the distribution and size of the cracks formed in flexural specimen. For this, 42 No., two-metre long flexural beam specimens were cast together with bond specimens comprising 16 pull-out cubes and 8 bond beams. The details of these specimens are described in the following sections.

4.3.1 Flexural Beam Test

The flexural beams tested were 150mm deep, 200mm wide and 2000mm long. Two reinforcing steel bars were cast in each beam as shown in Figure 4.4a and 4.4b. Four types of bar, all of which were 8mm in diameter, with different rib patterns were tested. Six or twelve beams were cast and tested for each batch of steel, the schedule for which is summarized in Table 4.7. The steel orientation is the angle between the longitudinal ribs and the horizontal plane. Where stirrups were used they were 6mm in diameter. Figures 4.4a and 4.4b illustrate the beams and the arrangement of the reinforcing bars

and stirrups. Six of the beams in each of the batches A, B and C had no stirrups in the central, 600mm zone, as shown in Figure 4.4b, and the other six beams had stirrups all along the length, as shown in Figure 4.4a. To ensure 25mm concrete cover, eight 25mm concrete spacers were used to support the rebar cages.

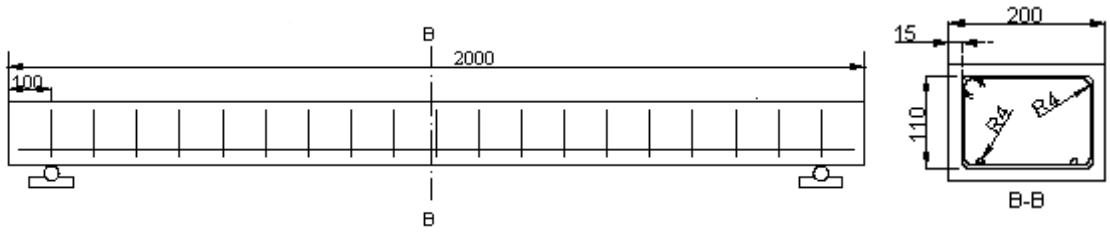

Figure 4.4a. Geometry of the specimens with stirrups all along the length

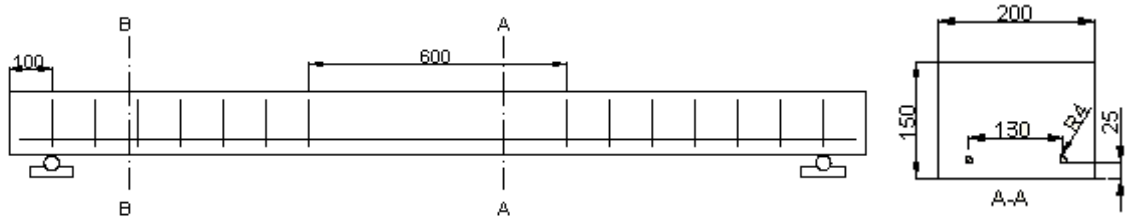

Figure 4.4b. Geometry of the specimens with no stirrups in the central zone of 600mm

Table 4.7. The flexural beam reinforcement schedule

Beam no.	Steel Bar	Steel Orientation	Middle zone of the beam	Concrete Mix
A1-A3	Bar A	0°	With links	Batch A
A4-A6		90°		
A7-A9		0°	Without links	
A10-A12		90°		
B1-B6	Bar B		With links	Batch B
B7-B12			Without links	
C1-C3	Bar C	0°	With links	Batch C
C4-C6		90°		
C7-C9		0°	Without links	
C10-C12		90°		
M1-M6	Bar M		Without links	Batch M

4.3.2 Bond Tests

There are many different types of test that can be used to measure the bond between concrete and the reinforcing steel bars. Detailed descriptions of these tests and their advantages and disadvantages are presented and discussed in the works of Sutton, Orteu and Schreier (2009), Oliver et.al. (2002), Edwards and Jannopoulos (1978) and Ferguson et.al. (1955). The most common of these tests are the pullout test and the bond beam test.

The bond beam test has the advantages that it most closely reflects the influence of flexure. As such, it has the potential to capture the real bonding mechanism and de-bonding behaviour of the RC specimens under loading due to its similarity to a RC beam subject to bending. The pull-out test is the most traditional bond test in which the bar is pulled out directly from the bonded concrete specimen. It has the advantages of simplicity and ease of implementation.

The measurement of the bond properties of the reinforcement used in the flexural beam tests was investigated using both pullout and bond beam tests in accordance with BS EN 10080:2005. Details of the test methods and their set-up are described in the following sections.

4.3.2.1 Pull-out Test

The pull-out specimens were prepared in accordance with BS EN 10080:2005. Each concrete cube specimen contained a single, centrally placed ribbed bar with a standard bond length as shown in Figure 4.5. A bond length of five diameters, i.e. 40mm, was

adopted with the ribs of the bar being protected by a 1mm thick plastic sleeve over the rest of its length. The four different rib patterns were tested using 8mm diameter bars. The schedule of the tests is shown in Table 4.8.

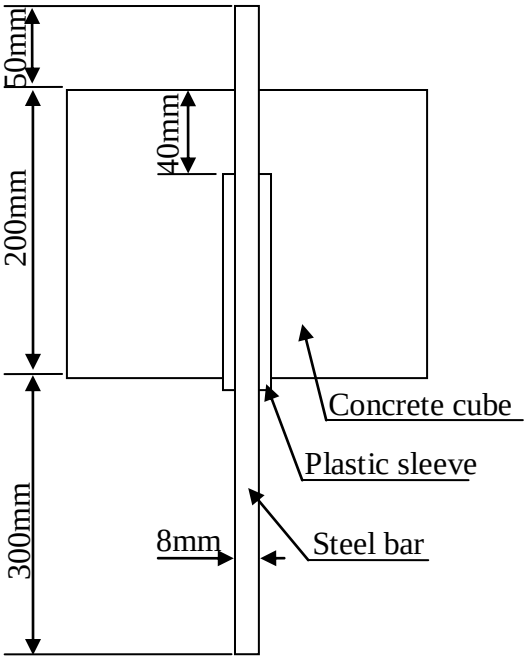

Figure 4.5. Pull-out test specimen

Table 4.8. Pull-out cube schedule

Pullout specimen no.	Steel Bar	Concrete Mix
P1-P4	Bar A	Batch A
P5-P8	Bar B	Batch B
P9-P12	Bar C	Batch C
P13-P16	Bar M	Batch M

4.3.2.2 Bond Beam Test

The bond beam specimens were prepared according to the specification given in BS EN 10080. The ribbed bar had a bonded length of 10 diameters in each half of the beam. Again, 1mm thick plastic sleeves ensured that the bar was de-bonded elsewhere (see Figure 4.6). The four types of steel bar were again tested using 8mm diameter bars (see Table 4.9).

Table 4.9. Bond beam schedule

Beam no.	Steel Bar	Concrete Mix
BB1-BB2	Bar A	Batch A
BB3-BB4	Bar B	Batch B
BB5-BB6	Bar C	Batch C
BB7-BB8	Bar M	Batch M

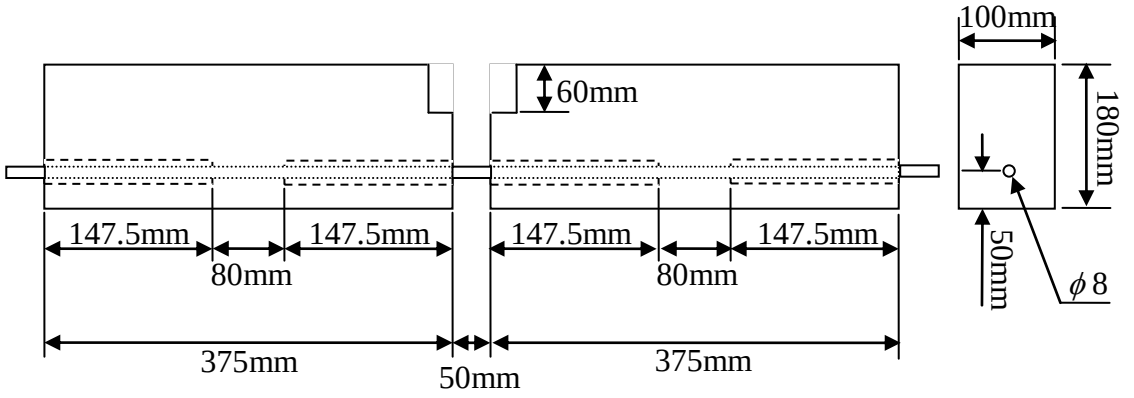

Figure 4.6. Beam specimen for bond test

4.4. Experimental Procedures

4.4.1 Bond Tests

4.4.1.1 Pull-out Test

The pullout tests were carried out in accordance with the specification and test method in BS EN 10080. The setup of the test is shown in Figure 4.7. The specimens were tested using an “Avery-Dennison type 7152” servo-hydraulic universal testing machine with a maximum capacity of 60kN. The cube was placed on a 300mm square steel plate supported by the stationary head. A rubber sheet was placed between the cube and the plate to ensure that a uniform stress distribution was applied to the face of the cube. The tension force *P* was applied to the longer end of the reinforcing bar gripped by the moving head of the test machine through the 50mm diameter central hole in the plate.

Two LVDT (Linear Variable Differential Transformer) transducers with a gauge length of 10mm and an accuracy of 0.5%, (i.e. 50μm) were used for measuring the slip. They were mounted on a cross yoke attached to the reinforcing steel bar as shown in Figure 4.7. The load, measured to an accuracy of +/- 10N was applied continuously under stroke control throughout the test, starting at a rate of 0.002mm/sec and increasing to 0.01mm/sec until bond failure occurred. The slip of the bar was recorded from the beginning until the end at pre-defined increments of loading. The average reading of both the transducers was taken as the slip of bar in the test.

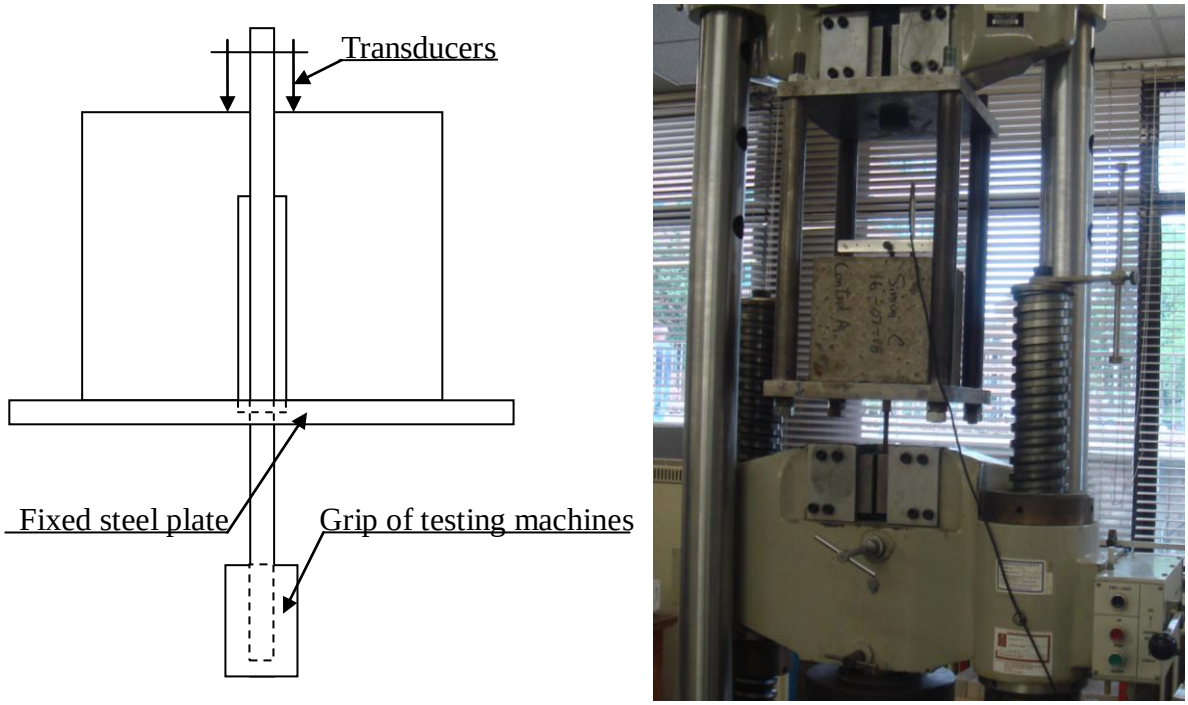

Figure 4.7. Set up of pull-out tests

4.4.1.2 Bond Beam Test

The bond beam tests were undertaken according to the specification and the test

method in BS EN 10080:2005. The setup of the test is shown in Figure 4.8. The specimens were tested in a four-column hydraulic universal testing machine with a maximum capacity of 250kN. The beam was placed on roller supports on top of the stationary head to avoid any arching effect. A hinge formed from two pieces of steel in a T shape of the same width as the beam itself was placed in the compression zone of the beam at mid span, as shown in Figures 4.8a and 4.8b. The load measured to an accuracy of +/- 10N was applied continuously under stroke control throughout the test, starting at a rate of 0.002mm/sec and increasing to 0.01mm/sec until bond failure occurred. Two LVDT transducers having an accuracy of 0.5% (50μm) were used for measuring the slip. They were mounted on a cross yoke attached to the reinforcing steel bar on each side as shown in Figures 4.8a-b. The test was paused when the bond on one side failed. A clamp was then introduced to stop the steel slipping any further on the side that had failed. The test then continued until bond failure occurred at the other side. As a result, two sets of results were obtained from each test and a total of 4 results for each type of bar tested were obtained.

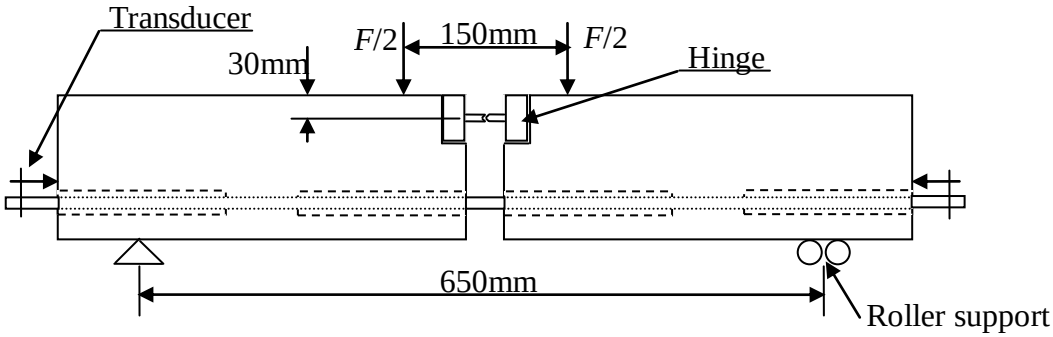

Figure 4.8a. Set up of bond beam experiment

Figure 4.8b. Photo of bond beam experiment

4.4.2 Beam Test

4.4.2.1 Flexural Beam Test

The beams were tested in 4-point bending over a simply supported span of 1800mm loaded at the ⅓ points. This ensured that in the central zone of 600mm where the beam was inspected for cracks there was no shear and it was subject only to bending. One LVDT transducer having an accuracy of 0.1% (0.1mm) was used for measuring the central deflection. The specimens were tested in a rig with a maximum capacity of 60kN. The setup of the test is shown in Figures 4.9a-b. The load was applied continuously under stroke control throughout the test, starting at a rate of 0.002mm/sec and increasing to 0.01mm/sec after a stabilised crack pattern with no more newly developed cracks had been established. This gave enough time for the crack pattern to be

monitored by eye and for the Digital Image Correlation (DIC) System to capture the necessary images to track the change in displacements and strains on the surface of the test specimens.

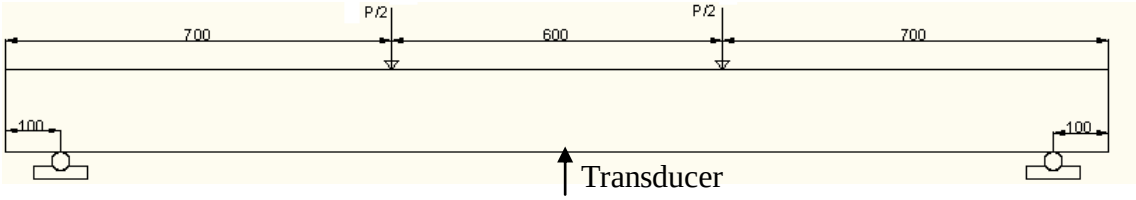

Figure 4.9a. Set up of flexural beam experiment

Figure 4.9b. Photo of flexural beam experiment

4.4.2.2 Digital Image Correlation

A new non-destructive technology that has been introduced over the last two decades and which has become more popular with the advances in digital cameras and improved computer technologies is Digital Image Correlation (DIC). Tests undertaken to verify the accuracy and efficiency of this new technology were reported by Guo et al. (2008) and Carden (2004).

The DIC employs two cameras to monitor the 2D or 3D in-plane deformation of the specimen stereoscopically. To use this optical system, a speckle pattern painted on surface of specimen has to be first calibrated by taking 20 – 30 photos of a calibration grid board (Figure 4.10).

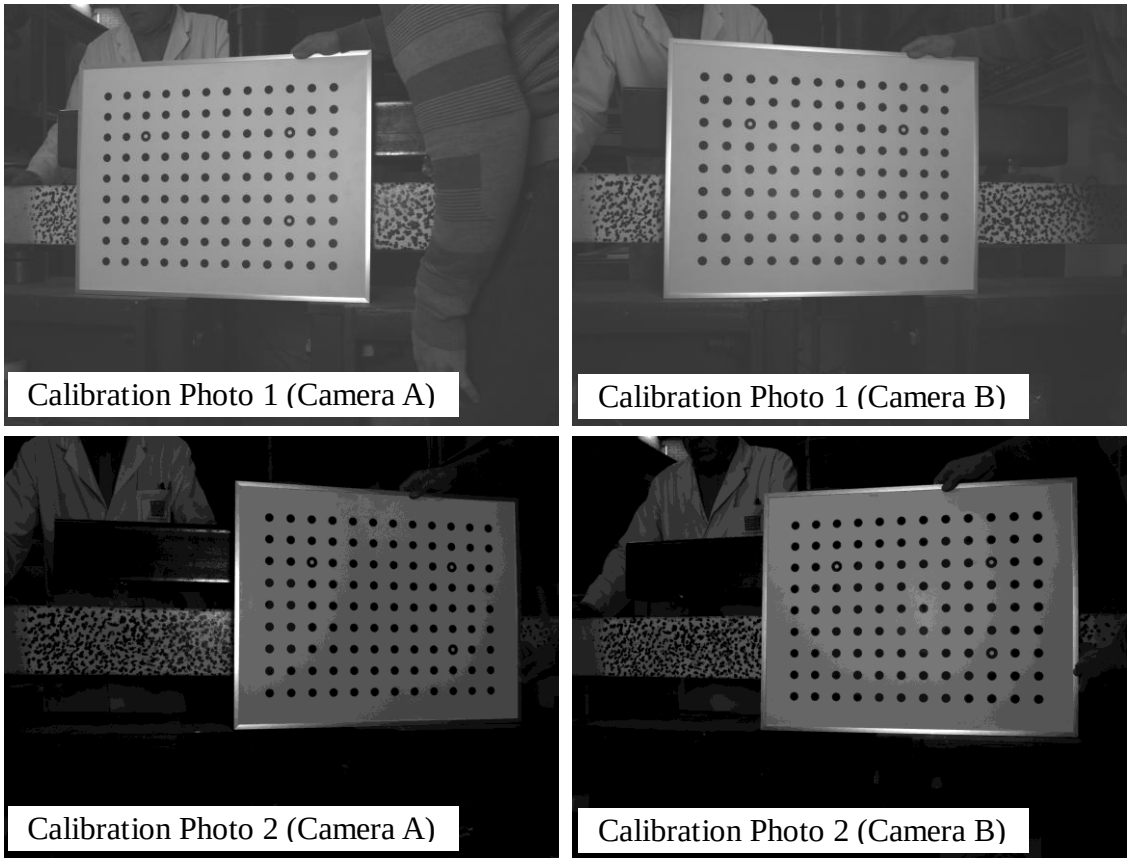

Figure 4.10. Calibration of DIC system with Calibration Grid Board

A series of images are then taken by the two cameras simultaneously at prescribed time intervals throughout the testing. The movement and deformation of the specimen are tracked by analysing the relative displacement of the speckle pattern painted on the surface of specimen.

The general advantages of using DIC include the portability and ease of implementation of the system which requires only a laptop and two cameras. To investigate different sizes of specimens it is simply a matter of changing the lenses of the cameras. It has the capability to monitor complex structures in both 2D and 3D, under long term or short term loading and also has no limitations on curved surfaces. The post-processing software enables strain to be calculated from the measured deformations and allows strain distributions as well as strain contours over the specimen surface to be plotted. It provides deformations in all three directions over the whole specimen area and can also be resolved into a single direction of interest, e.g. x-x direction, out of plane direction, etc. The distribution of any kind of deformations, e.g. displacement or strain, etc, over a long section specified by the user can be extracted, as shown in Figure 4.11a. Therefore, crack widths can be obtained by measuring the strain across the crack in x-x direction using the post-processing software and in this way cracks that are not even visible can easily be located, as shown in Figure 4.11b.

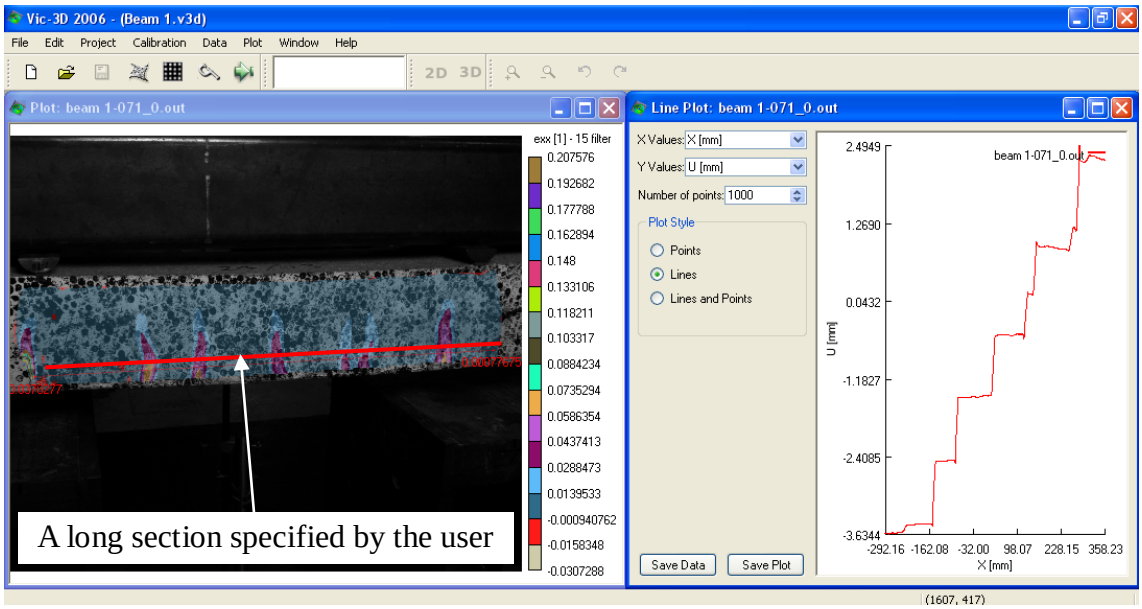

Figure 4.11a. Distribution of deformation and crack width measurements as obtained from DIC post-processing software

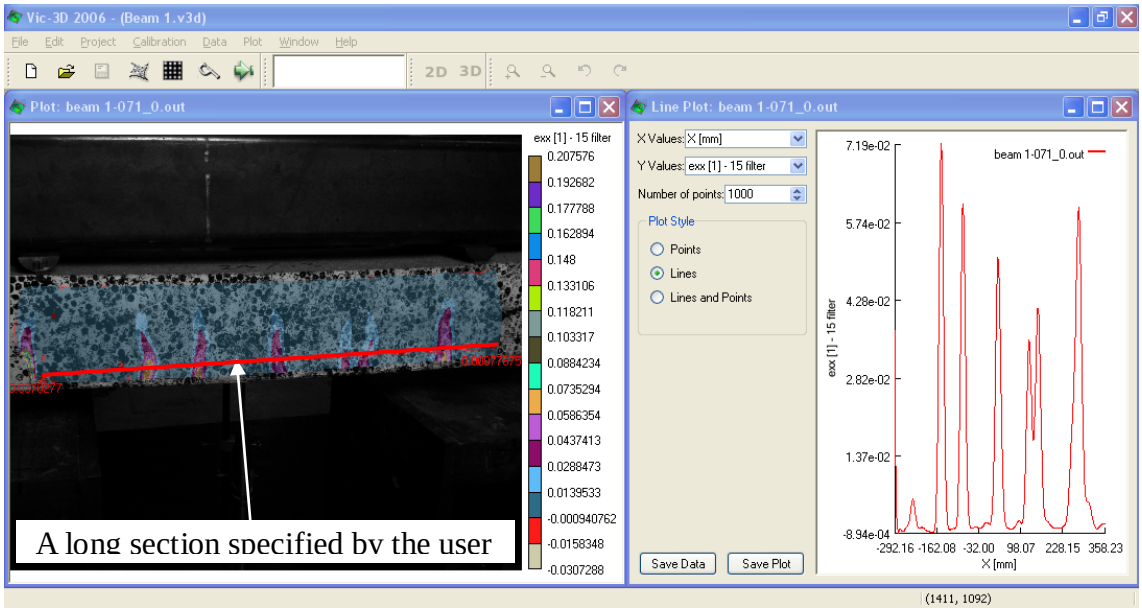

Figure 4.11b. Crack location and spacing determined by DIC post-processing software

Figure 4.11c. Specimen being monitored by DIC camera system

In this programme of work, the DIC system was employed in the flexural beam testing as shown in Figure 4.11c. Speckle patterns were painted on one side of each beam in advance. Two cameras were used to monitor the damage process of the specimen to produce 3-D displacement and strain plots, even though the plots of the out-of-plane displacements were not of any particular interest in this experiment. However, they did confirm that the specimens were loaded vertically with no out-of-plane deformations. The software VIC 3D® was employed to post-process the data collected from the experiment and to transform and present it as 3D displacements and a strain field across the specimen surface. Crack widths were then determined by comparing the change in distance between the speckle patterns on either side of the crack before and after the test.

4.5. Experimental Results and Discussion

4.5.1 Bond Tests

In all 8 bond beam tests and 16 pull-out tests only pull-out failures and bar tensile failures were observed; none of them failed by splitting of the concrete.

In the bond tests, the applied tensile force P (for the pullout test) or the total applied force on test beam F_a (for the bond beam test) were recorded and used to calculate the bond stress τ. The following equations from EN 10080:2005 were applied to determine the corresponding bond stress:

For the pull-out tests : $P = \tau \cdot L \cdot (\pi d) \cdot \frac{f_c}{f_{cm}}$

$$\tau = \frac{1}{5\pi} \cdot \frac{P}{d^2} \cdot \frac{f_{cm}}{f_c} \qquad (2a)$$

where f_{cm} is the target value of the strength class (i.e. 45 MPa in this set of tests), L is the bond length of $5d$ and f_c is the average concrete strength of the test specimens.

For the bond beam tests : $\tau = \frac{\sigma_s}{40}$ (2b)

where $\sigma_s = \frac{1.25F_a}{A_n}$ for a bar diameter d which is less than 16mm.

A summary of the bond stress results at various slip levels for the bond beam tests is given in Table 4.10a. No slips were recorded in bond beam tests B1 and B2 because of a malfunction of the recording equipment. It can be seen that in many tests a slip of 1mm was not achieved and therefore the corresponding bond stress could not be computed.

Table 4.10a. Summary of bond stress results at various slip levels for bond beam tests

	Bond Stress		
	Slip = 0.01mm	Slip = 0.1mm	Slip = 1.0mm
Bond Beam A1	3.11	8.37	
Bond Beam A2	3.93	10.11	
Bond Beam A3	4.31	10.27	19.02
Bond Beam A4	7.83	14.80	
Bond Beam B1			
Bond Beam B2			
Bond Beam B3	2.73	7.18	20.46
Bond Beam B4	6.52	12.70	
Bond Beam C1	7.76	14.60	
Bond Beam C2	7.92	11.18	
Bond Beam C3	6.34	11.34	
Bond Beam C4	6.90	12.26	
Bond Beam M1	10.98	16.23	
Bond Beam M2	13.39		
Bond Beam M3	9.47	16.15	
Bond Beam M4	11.31	16.53	

A Summary of the bond stress results at various slip levels for the pull-out tests is given in Table 4.10b. No slip was recorded in pullout test B3 because of a malfunction of the recording equipment and therefore the corresponding bond stress could not be computed.

Table 4.10b. Summary of bond stress result at various slip levels for pull-out tests

	Bond Stress		
	Slip=0.01mm	Slip =0.1mm	Slip=0.01mm
Pullout A1	0.66	3.97	21.53
Pullout A2	0.84	6.51	24.57
Pullout A3	0.67	3.39	21.94
Pullout A4	4.02	11.82	22.82
Pullout B1	8.33	16.63	15.39
Pullout B2	1.40	6.19	16.91
Pullout B3			
Pullout B4	6.15	11.85	17.27
Pullout C1	5.46	11.00	10.16
Pullout C2	4.74	7.43	21.63
Pullout C3	0.80	6.18	20.40
Pullout C4	7.31	13.23	23.60
Pullout M1	1.58	7.24	18.12
Pullout M2	1.60	9.09	22.02
Pullout M3	4.50	10.17	24.58
Pullout M4	5.75	13.25	27.19

In Figures 4.12a and 4.12b, the average relationship between the bond strength and corresponding slip value of each batch of specimen for the bond beam tests and pull-out tests are plotted respectively. The relationship is shown with respect to a slip up to a value of 0.1mm.

It can be seen that the bars from Batch M generally have the highest bond strength, followed by the bars from Batches A, B and C, in both bond beam tests and pull-out tests as illustrated in Figure 4.12a and 4.12b.

It can be seen that the bond stresses measured from the pullout tests are lower than those from the bond beam tests, even thought the ranking of the four batches are the same in both sets of results.

Furthermore, it is also noted that the rate of initial bond-slip development is more gradual in the bond beam tests compared to the rapid increase in bond at an early stage in the pullout tests. It is believed that this is due to the different testing methods and specimen arrangements such as the specimen sizes and the presence of transverse reinforcement providing confinement in the bond beam test.

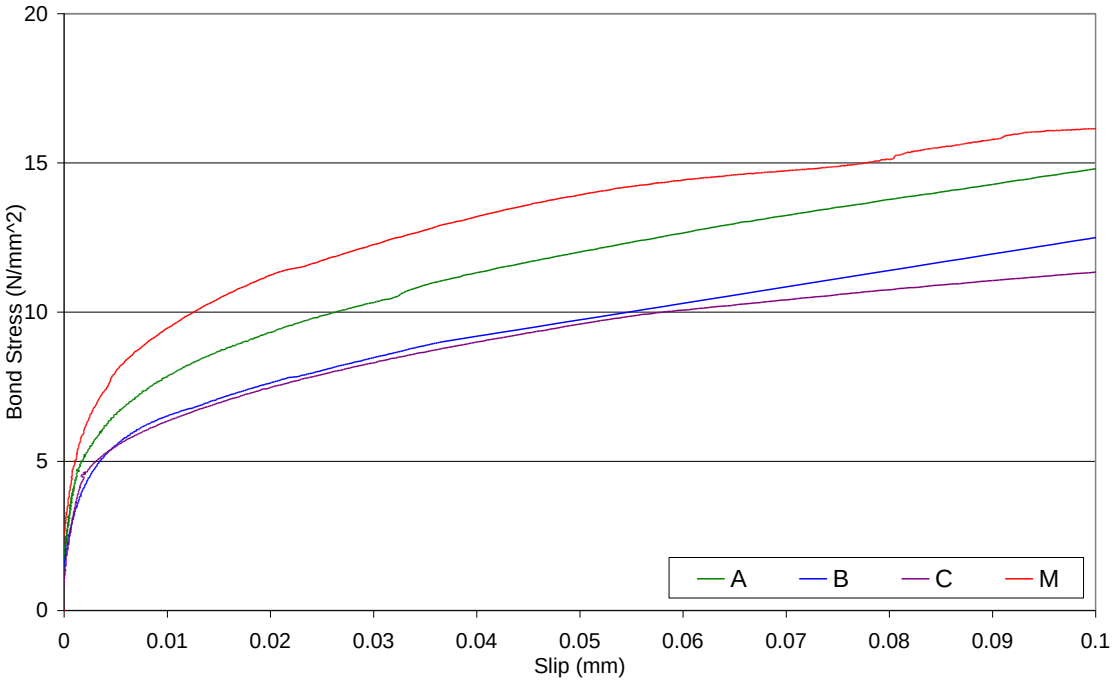

Figure 4.12a. Plot of bond stress against slip for bond beam tests

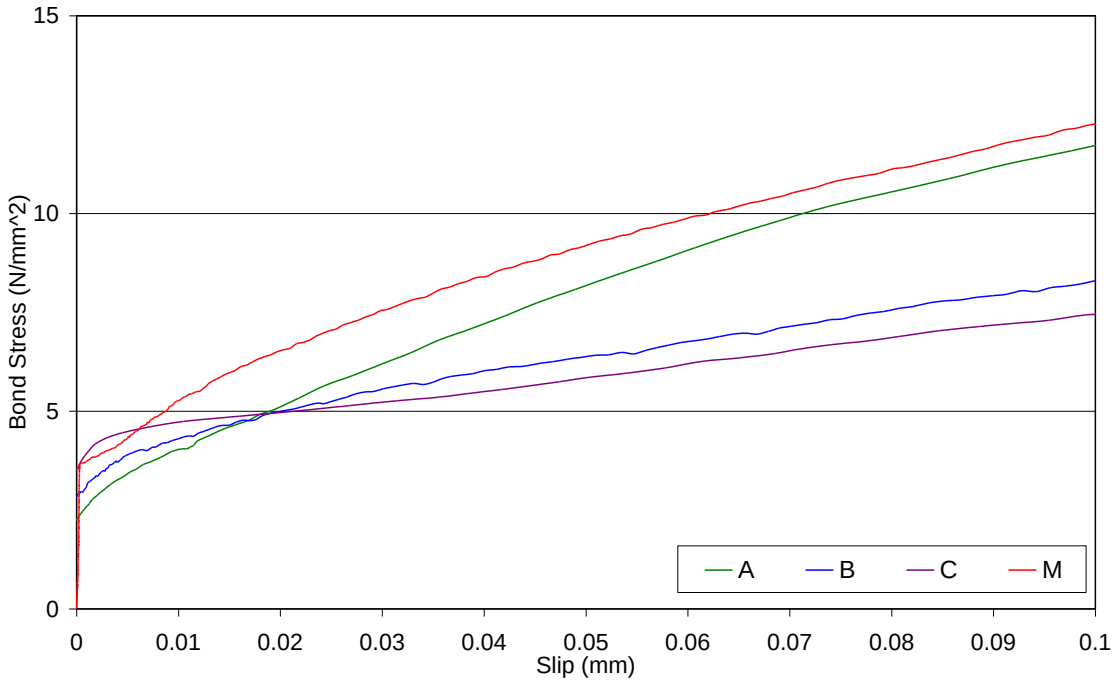

Figure 4.12b. Plot of bond stress against slip for pull-out tests

In Figures 4.12c to e, the relationships between the bond strengths and f_R values are plotted. Figure 4.12c shows a plot of bond stress against f_R having combined the results from both the bond beam tests and pull-out tests. The relationship is shown with respect to the three critical slip values of 0.01mm, 0.1mm and 1.0mm at which bond is usually considered to be a function of chemical adhesion, friction and mechanical interlock respectively.

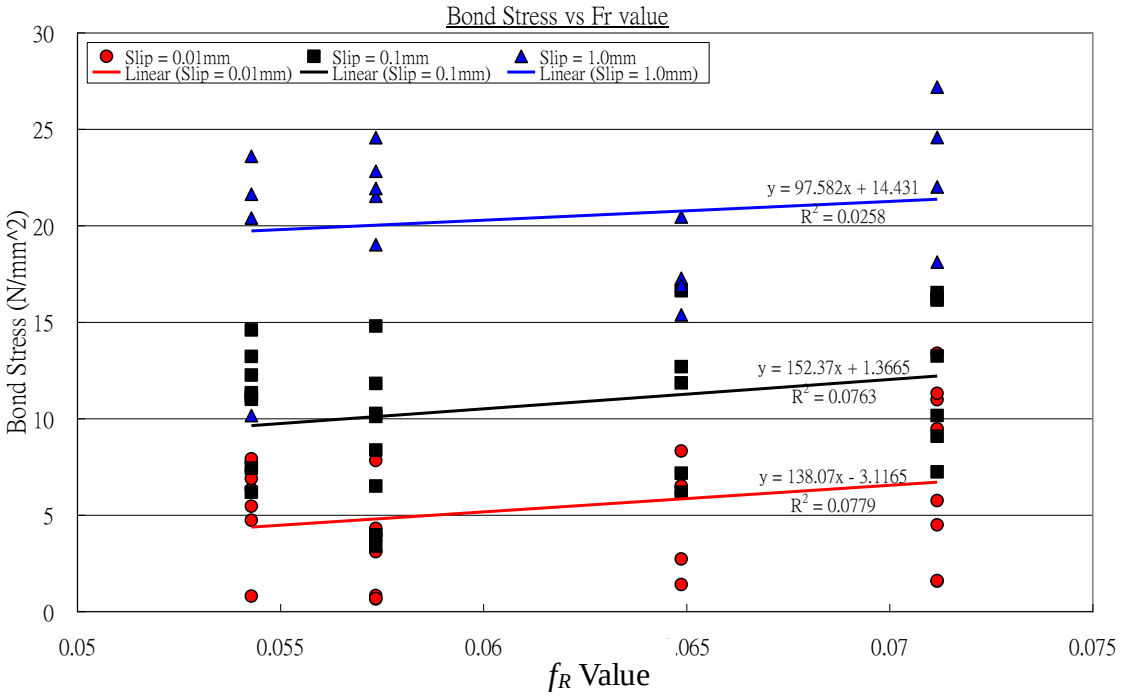

Figure 4.12c. Plot of bond stress against f_R having combined the results from both the pull-out and bond beam tests

It can be seen that bars with higher f_R values generally have a higher bond stress, i.e. stronger bond, at all slip levels. However, bond strength is affected by many other parameters, as discussed above. Therefore, while many variables, such as concrete cover, transverse reinforcement, testing methods and arrangement, were made as consistent as possible for all the specimens that were tested, it can be seen that there is still a significant variation in the results. It is believed that one reason for this scatter is the variability of the concrete strength which, although within an acceptable range (Figure 4.2) does have a significant impact on the results.

Figures 4.12d and 4.12e give plots of bond stress against f_R value for the bond beam test and pull-out test respectively.

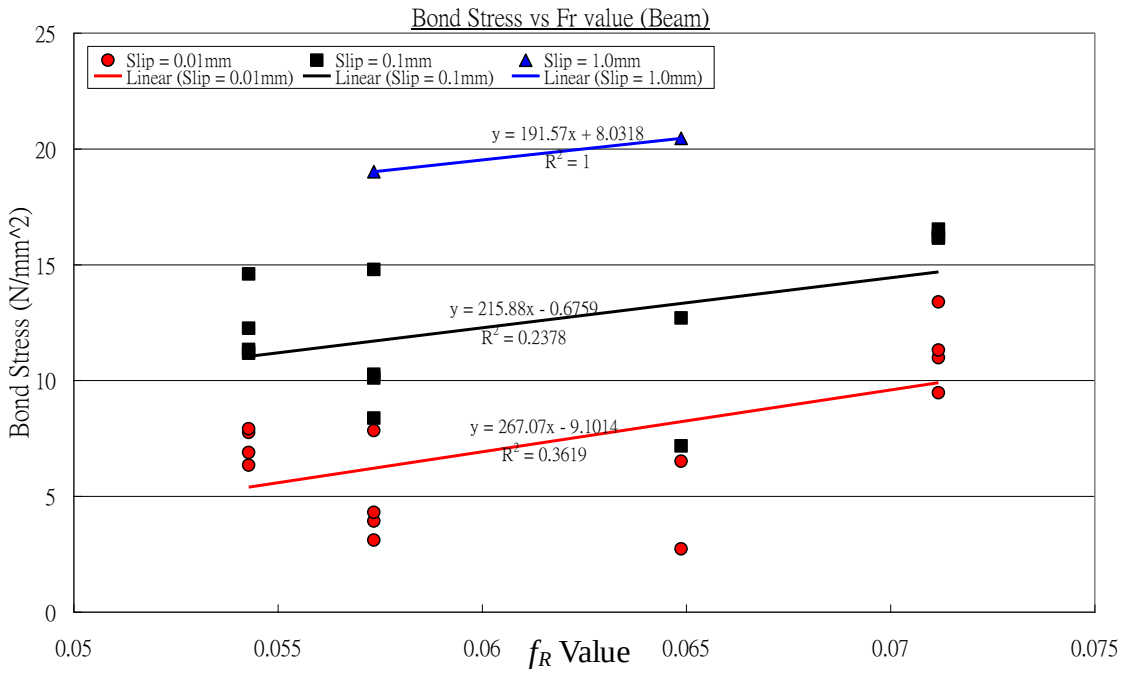

Figure 4.12d. Plot of bond stress against f_R for bond beam tests

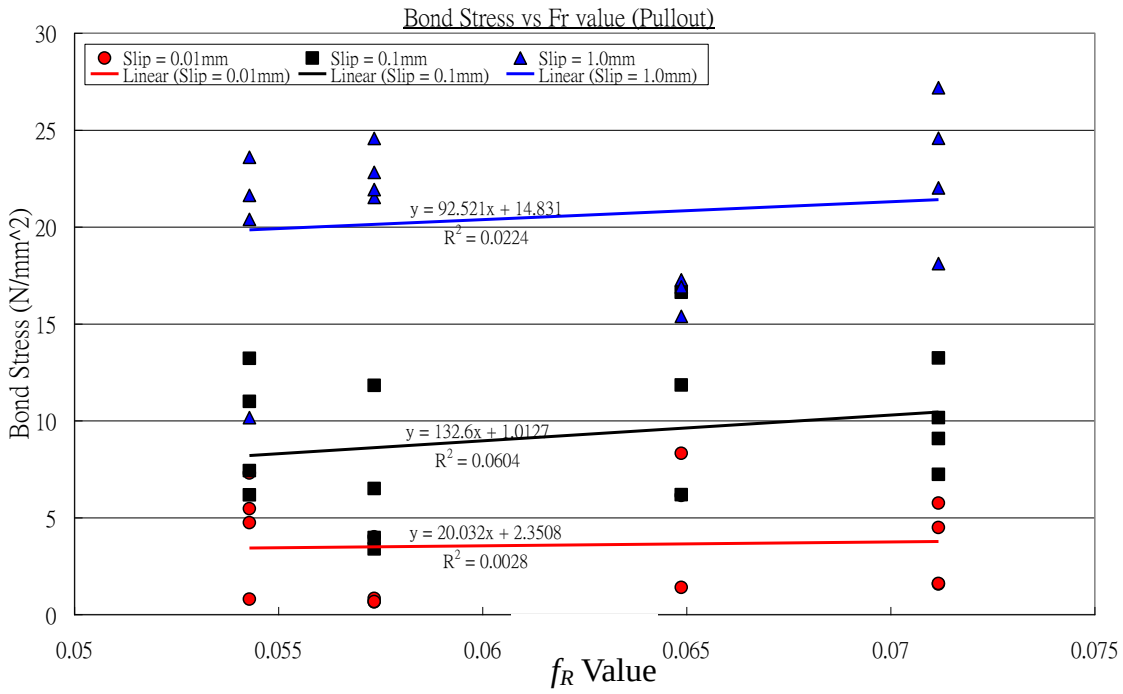

Figure 4.12e. Plot of bond stress against f_R for pull-out tests

As might be expected, the general trend of bars with higher f_R values exhibiting a higher bond strength, i.e. stronger bond, at all slip levels can be seen. However, it is noted that the slope of the bond stress versus f_R value plots for all slip levels is steeper for the bond beam tests than it is for the pull-out tests. In the bond beam tests, the beam was reinforced with steel cages which provide significant confinement of the concrete around the steel bar compared to that in the pull-out tests. It is possible that because of this high confinement in the bond beam tests, the increase in bond strength with steel bars of higher f_R value is not as significant as in the pull-out tests, nevertheless the general trends in both tests are consistent as evident from the combined results shown in Figure 4.12c.

It must also be noted that the reliability of the plotted trend line at the slip level of 1.0mm is suspect because, as shown in Table 4.10a, for the bond beam tests, a slip of this magnitude was only achieved only on two occasions.

In Figure 4.12f, a plot of bond strength at a slip of 0.1mm against f_R value obtained by Rehm (1969) is presented. It shows a similar trend to the current study, i.e. the higher the f_R value, the higher the bond strength.

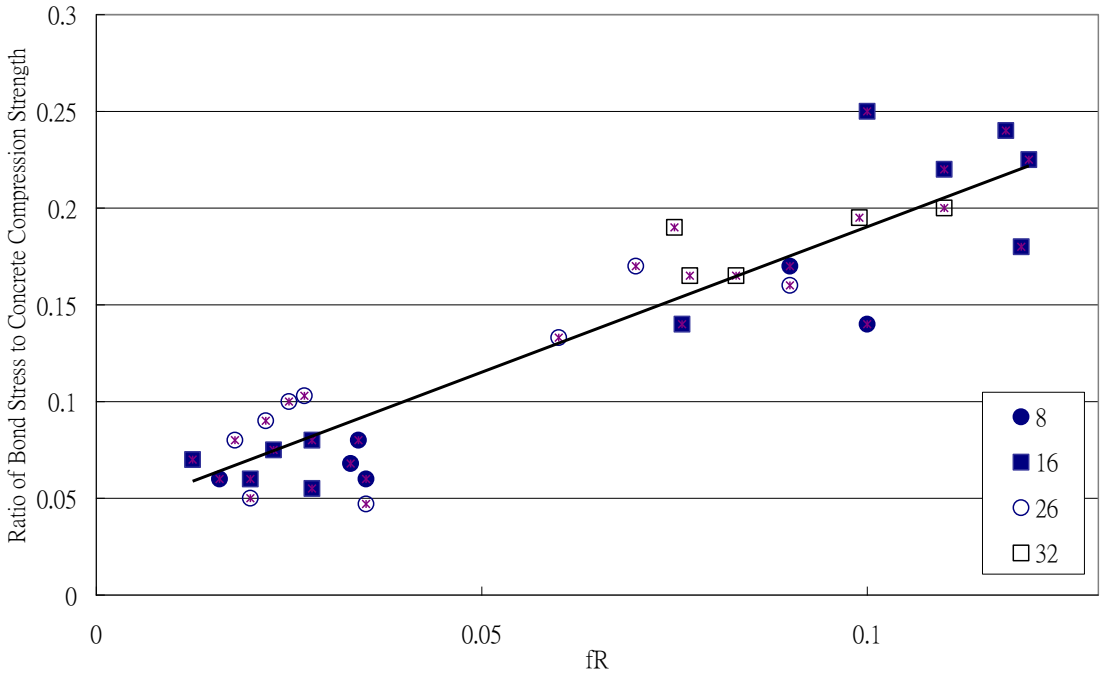

Figure 4.12f. Plot of bond strength against f_R by Rehm (1969)

If the results of this study are plotted together with Rehm's results the curves given in Figure 4.12g are obtained.

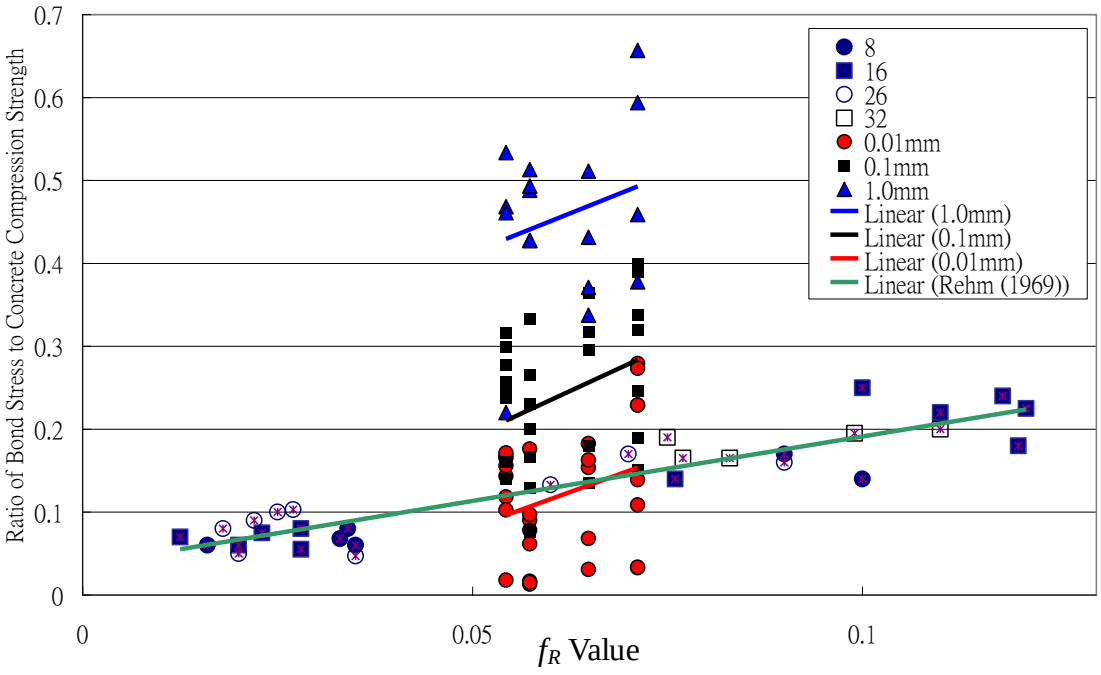

Figure 4.12g. Variation of Bond Stress with f_R from the current study and that reported by Rehm (1969)

From this figure it can be seen that the trend of bond stress is the same in both studies, i.e. the higher the f_R value, the higher the bond stress and although not identical, the slopes of the four curves are very similar. As such it can be concluded that the results of this study are consistent with those reported by Rehm (1969) which gives confidence in the results of the current study.

4.5.2 Flexural Beam Test

6 specimens were tested in Batch M and 12 specimens (in Batches A, B and C) using the flexural beam test. These tests were performed under stroke control and therefore, as a newly formed crack in the beam resulted in a reduction of stiffness of the specimen, a drop in load was an indication of the formation of a crack. The first significant drop in

load during the testing of each specimen was therefore taken as the initial cracking load. Results for the initial cracking load and ultimate load from the experimental data are shown in Table 4.11a and summarized in 4.11b.

Table 4.11a. Initial cracking load capacity and ultimate load capacity of beam specimens

Beam Specimen	A1	A2	A3	A4	A5	A6	A7	A8	A9	A10	A11	A12
Initial Cracking Load (kN)	8.2	8.2	7.5	8.8	8.6	9.3	9.1	9.0	8.6	9.5	8.8	8.9
Ultimate Load (kN)	24.3	22.7	23.1	22.4	23.5	24.3	23.4	24.1	23.4	24.4	23.6	23.8
Beam Specimen	B1	B2	B3	B4	B5	B6	B7	B8	B9	B10	B11	B12
Initial Cracking Load (kN)	6.8	7.0	7.7	7.3	7.1	6.9	7.9	8.2	9.5	8.3	8.6	8.4
Ultimate Load (kN)	19.7	19.1	22.0	20.6	24.4	21.1	21.3	21.1	22.2	22.0	21.2	20.3
Beam Specimen	C1	C2	C3	C4	C5	C6	C7	C8	C9	C10	C11	C12
Initial Cracking Load (kN)	11.1	10.0	8.3	9.1	9.9	7.6	9.1	9.5	9.8	9.6	8.6	9.1
Ultimate Load (kN)	29.4	28.2	27.8	27.5	23.4	23.0	23.0	22.9	22.6	23.5	22.7	23.0
Beam Specimen	-	-	-	-	-	-	M1	M2	M3	M4	M5	M6
Initial Cracking Load (kN)	-	-	-	-	-	-	10.6	7.2	9.0	9.2	9.3	10.1
Ultimate Load (kN)	-	-	-	-	-	-	27.0	26.7	26.0	26.5	27.6	26.7

Table 4.11b. Summary of initial cracking load capacity and ultimate load capacity of beam specimens

Beam Specimen		Minimum	Average	Maximum	Standard Derivation
Batch A :	Initial Cracking Load (kN)	7.5	8.7	9.5	0.5
	Ultimate Load (kN)	22.4	23.6	24.4	0.6
Batch B :	Initial Cracking Load (kN)	7.9	8.5	9.5	0.5
	Ultimate Load (kN)	20.3	21.4	22.2	0.7
Batch C :	Initial Cracking Load (kN)	8.6	9.3	9.8	0.4
	Ultimate Load (kN)	22.6	23.0	23.5	0.3
Batch M :	Initial Cracking Load (kN)	7.2	9.3	10.6	1.2
	Ultimate Load(kN)	26.0	26.8	27.6	0.5

In Figure 4.10a and Table 4.11b, it can also be observed that there is little difference between the elastic performances for Batch A, Batch B, Batch C and Batch M and the initial cracking loads are about at the same level. In the nonlinear range, their performances are still similar, but Batch M has a noticeably higher ultimate load. It is believed that both the initial cracking loads and ultimate loads tend to increase with bond strength, however the degree of increase for the initial cracking load capacity is small in comparison to that for the ultimate load capacity.

In Figures 4.13a and 4.13b, typical load-deflection curves for the mid-point of each batch of flexural beam specimens in the linear and non-linear ranges are shown.

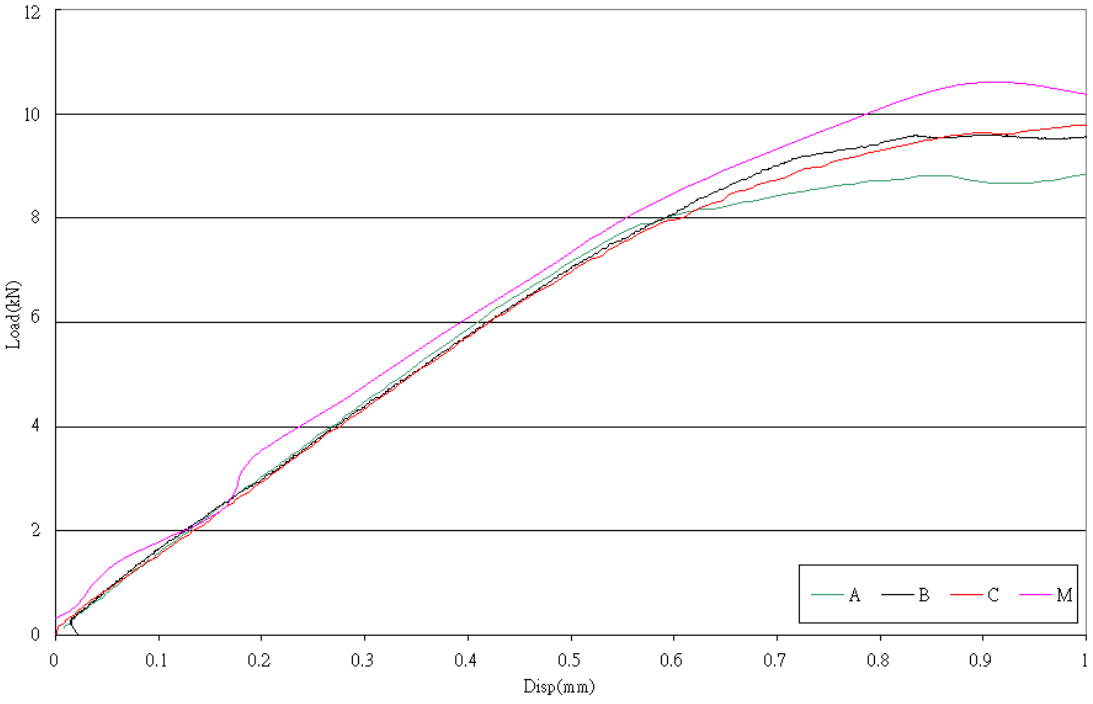

Figure 4.13a. Typical load-deflection curves for the mid-point of each batch of flexural beam specimen in the linear and early non-linear range

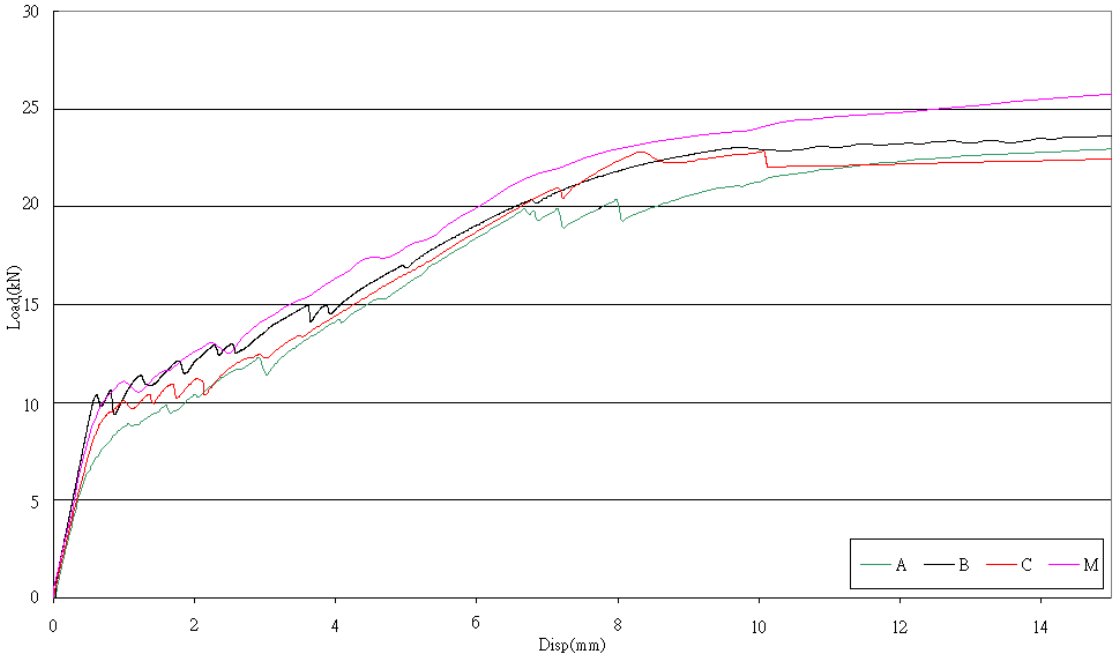

Figure 4.13b. Typical load-deflection curves for the the mid-point of each batch of flexural beam specimens in the non-linear range

Figures 4.14a to c give typical plots of the development of cracks for samples A8, C9 and M1 obtained using the data files from DIC system. They show the evolution of the cracks during the flexural beam tests as monitored by DIC System. Crack spacings and crack widths were measured directly from these plots. Similar plots for all other beam specimens are given in Appendix I and animations and videos of the evolution and development of the cracks are given in Appendix II. A summary of the crack spacings and crack widths are presented and discussed in Section 4.5.2.3.

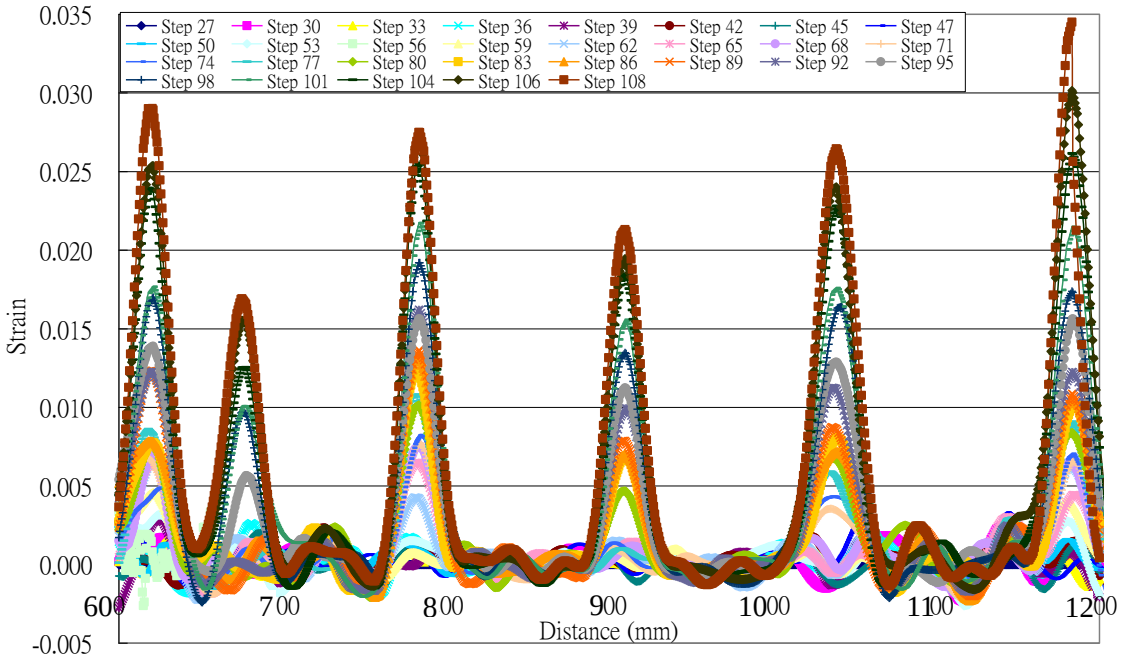

Figure 4.14a. The evolution and development of cracks in Beam specimen A8

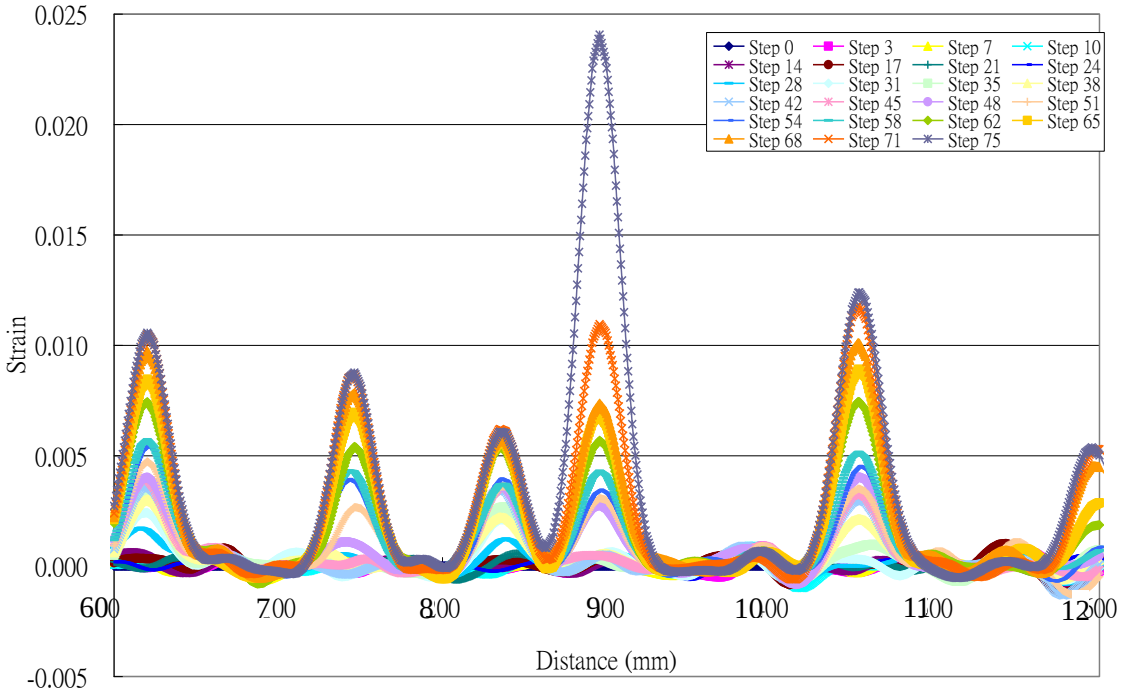

Figure 4.14b. The evolution and development of cracks in Beam specimen C9

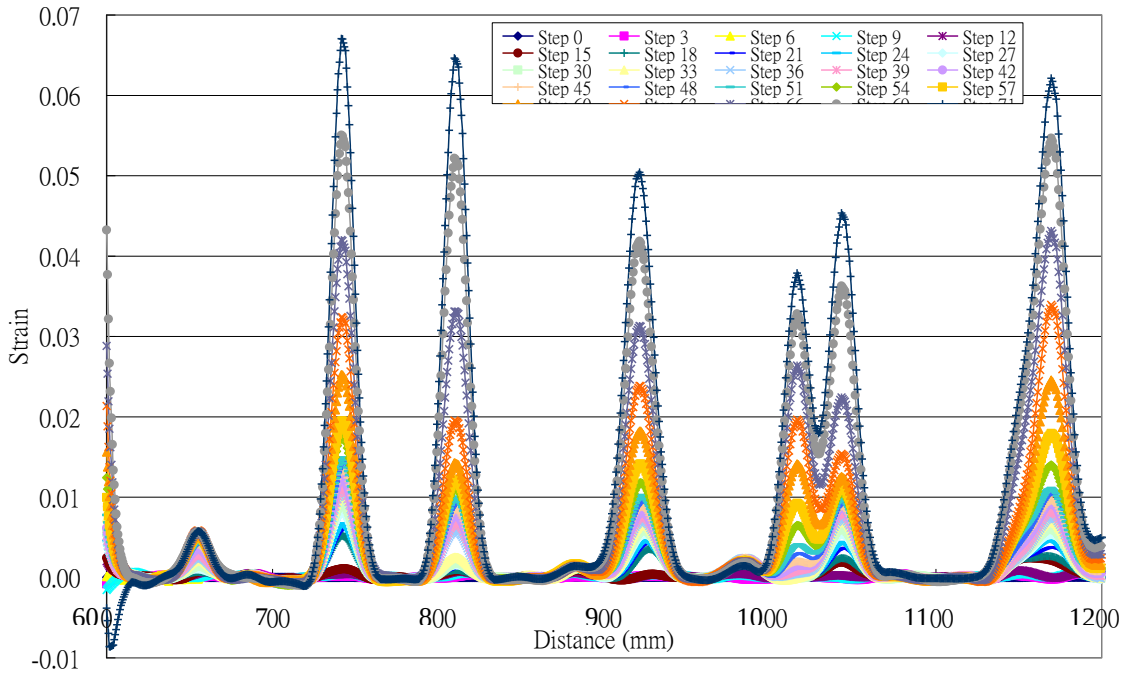

Figure 4.14c. The evolution and development of cracks in Beam specimen M1

4.5.2.1 Parameter Test – Effect of Orientation of Reinforcing Bars

During the design of the flexural beam test, it was recognized that the orientation of the reinforcing bars may have an effect on the bond strength and cracking behaviour. As a result, six beams in each of two batches, Batch A and C, of the beam specimens had the reinforcing steel bars with their longitudinal ribs facing upward (Orientation 90^{o}), and another six beams in each of the two batches had them aligned horizontally (Orientation 0^{o}). A summary of the comparison between the performance of two sets of specimens and that of the whole batch is shown in Table 4.12.

Table 4.12. Variation of crack spacing and crack width with reinforcing bar orientation

Batch	Orientation*	Crack Spacing (mm)		Crack Width (mm)	
		Average crack spacing with central stirrups	Average crack spacing without central stirrups	Average crack width with central stirrups	Average crack width without central stirrups
A	90°	103.34	119.74	0.328	0.388
	Overall (Whole Batch)	108.98	128.40	0.337	0.402
	0°	114.02	133.48	0.343	0.415
	Max. Variation	5.04	5.08	0.006	0.013
		4.9%	4.0%	1.8%	3.2%
C	90°	104.17	120.81	0.259	0.299
	Overall (Whole Batch)	102.23	118.24	0.275	0.292
	0°	100.29	115.66	0.291	0.286
	Max. Variation	1.94	2.58	0.016	0.006
		1.9%	2.2%	5.8%	2.1%

* Steel orientation is the angle between the longitudinal ribs and the horizontal plane.

As can be seen, the average crack spacings and crack widths of these RC beams seem to be independent of the orientation of the reinforcing bars, with the maximum variation only being small. This suggests that the orientation of the bars is not a key factor in this type of testing and note that the discussion regarding the cracks in the following sections will ignore the orientation of the bars. As this finding was during the testing of Batch A and Batch C, no attempt to make to pre-set the orientation of the bars in the remaining batches, i.e. Batch B and Batch M.

4.5.2.2 Parameter Test – Effect of Existing Stirrups in the Central Zone

The aim of the flexural beam test was to investigate the SLS performance of the beam

in a zone of constant moment and zero shear force. As such, shear reinforcement in the form of stirrups was not really necessary. However, in practice some form of shear link, even if only to complete the reinforcement cage, would be necessary. It was therefore decided to explore if the existence of stirrups throughout the central constant moment zone would affect the cracking behaviour observed. As a result, six beams in each of the first three batches of the flexural beam specimens had no stirrups in the constant moment zone, i.e. in the central 600mm of the beams, while stirrups were placed throughout the length of the beam specimens in another six beams in each of the first three batches. The comparison between the two sets of specimens is shown in Table 4.13.

Table 4.13. Variation of crack spacing and crack widths with the presence or otherwise of stirrups in the centre zone

	Batch	Stabilised Crack Spacing (mm)			Cracks Spacing between first 3 cracks (mm)			Crack Width (mm)		
		Min.	Avg.	Max	Min.	Avg.	Max	Min.	Avg.	Max
With stirrups in centre zone	A	49.45	108.98	183.40	140.63	218.58	298.91	0.161	0.337	0.471
	B	60.00	99.00	124.00	90.00	232.83	312.00	0.200	0.307	0.500
	C	77.14	102.23	135.83	115.76	243.67	315.03	0.181	0.275	0.353
Without stirrups in centre zone	A	55.28	128.40	181.36	149.63	232.45	398.51	0.273	0.402	0.658
	B	45.00	114.64	160.00	103.00	252.00	339.00	0.100	0.318	0.500
	C	58.47	118.24	176.41	156.67	274.73	396.93	0.200	0.292	0.391

From these results it can be seen that the average stabilised crack spacing of the RC beams that had stirrups throughout their length in all three batches was 103mm which is very similar to the stirrup spacing, i.e. 100mm. This confirms that the cracks tend to form at the location of the stirrups. For all three batches the range between the minimum and

maximum crack spacing in the RC beams that had stirrups throughout their length was smaller than that of the beams having no stirrups in central zone. As such, it is considered that the SLS behaviour, as characterised by crack spacings and crack widths is influenced by the existence of stirrups. This phenomenon can also be observed in the crack spacing of the first three cracks to be formed.

For the beams that have no stirrups in the middle zone, the average crack spacing was generally more than 100mm. For comparison with the predictions obtained from the numerical modelling described in Chapter 5, it is this behaviour that is considered to be more appropriate. As such, any further analysis and discussion of the crack spacing and crack widths that are presented will focus solely on the beams having no stirrups in the middle zone.

4.5.2.3 The Relationship between f_R Value, Crack Width and Crack Spacing

The crack spacing and crack width results for the four batches of flexural beam tests are summarised in Table 4.14.

Table 4.14. Summary of crack spacing and crack width measurements

Beam	Final crack spacing (mm)			Crack spacings between first 3 Cracks (mm)		Crack width(mm)			
	Min.	Avg.	Max.			Min.	Avg.	Max.	At Steel Stress (N/mm^2)
A7	114.2	154.4	181.36	282.3	322.6	0.32	0.41	0.56	550
A8	60.7	113.7	146.13	164.4	398.5	0.30	0.39	0.45	
A9	107.5	132.0	154.63	153.5	152.2	0.34	0.39	0.47	
A10	87.6	109.1	149.86	210.6	149.4	0.29	0.39	0.66	
A11	57.1	117.9	175.76	230.3	153.0	0.36	0.45	0.55	
A12	55.3	143.3	176.3	230.2	342.8	0.27	0.39	0.50	
B7	67.0	115.0	152.0	103.0	219.0	0.30	0.35	0.40	523
B8	80.0	107.4	160.0	275.0	262.0	0.20	0.31	0.50	
B9	45.0	99.83	148.0	266.0	333.0	0.10	0.26	0.40	
B10	85.0	114.8	160.0	305.0	269.0	0.25	0.35	0.50	
B11	81.0	123.0	143.0	276.0	339.0	0.25	0.29	0.35	
B12	99.0	127.8	149.0	130.0	248.0	0.25	0.35	0.50	
C7	73.5	119.2	158.2	265.6	325.0	0.20	0.29	0.39	537
C8	93.9	124.5	145.4	376.5	247.8	0.27	0.32	0.35	
C9	58.5	122.4	176.4	214.5	396.9	0.21	0.31	0.38	
C10	80.4	106.8	156.7	156.7	214.9	0.20	0.26	0.30	
C11	95.9	122.2	151.8	259.1	217.4	0.24	0.30	0.36	
C12	86.0	113.9	146.5	206.4	250.3	0.20	0.28	0.34	
M1	70.9	116.5	152.7	179.4	152.7	0.19	0.28	0.36	524
M2	86.1	113.0	152.9	301.1	152.9	0.17	0.28	0.35	
M3	43.0	102.8	135.0	233.0	178.0	0.15	0.22	0.29	
M4	70.0	107.4	132.0	317.1	155.6	0.15	0.18	0.21	
M5	76.9	111.7	154.3	262.9	146.9	0.20	0.17	0.40	
M6	82.0	115.6	159.0	299.0	197.0	0.19	0.23	0.32	

A plot of crack spacing against f_R value is shown in Figure 4.15a.

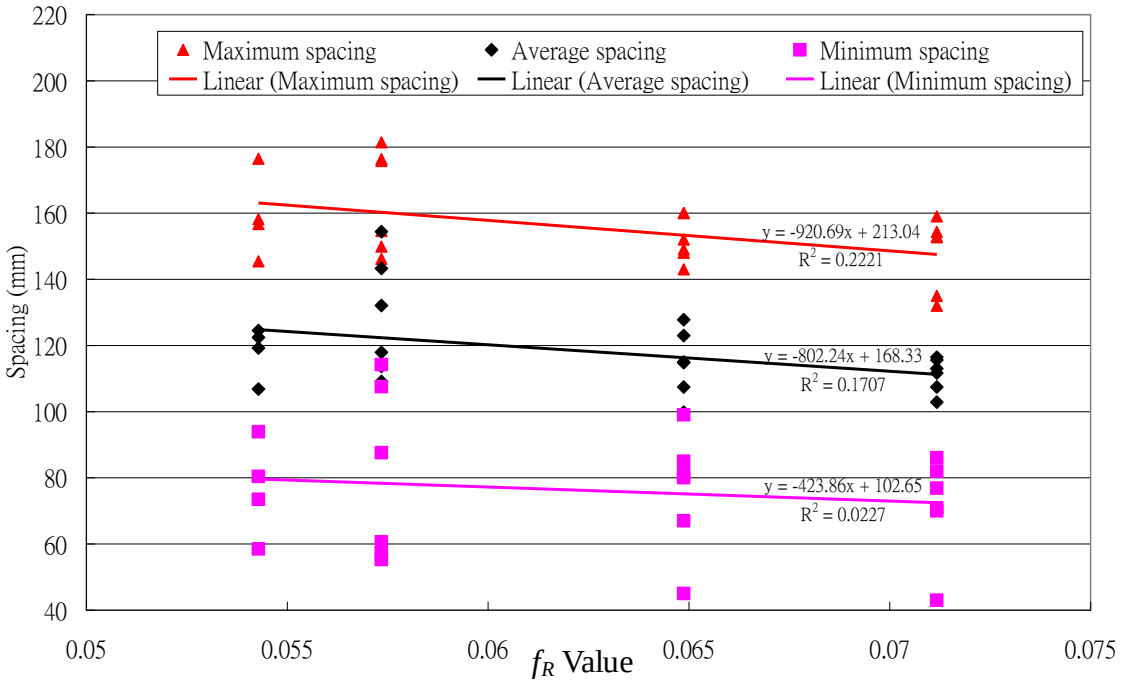

Figure 4.15a. Variation of crack spacing with f_R value close to the ultimate load of 11kN

From the above figure, although the results are scattered, the trend is that the higher the f_R value, the smaller the crack spacing, irrespective of whether it is the minimum, average or maximum crack spacing that is being considered. By comparing the three trend lines, it can be seen that the slope of the maximum crack spacing curve is the steepest and the slope of the minimum crack spacing is the shallowest. This highlights that maximum crack spacing is more sensitive to the f_R value of the bar while on the other hand, the minimum crack spacing is less sensitive to the f_R value of the bar.

A plot of crack width against f_R values is shown in Figure 4.15b.

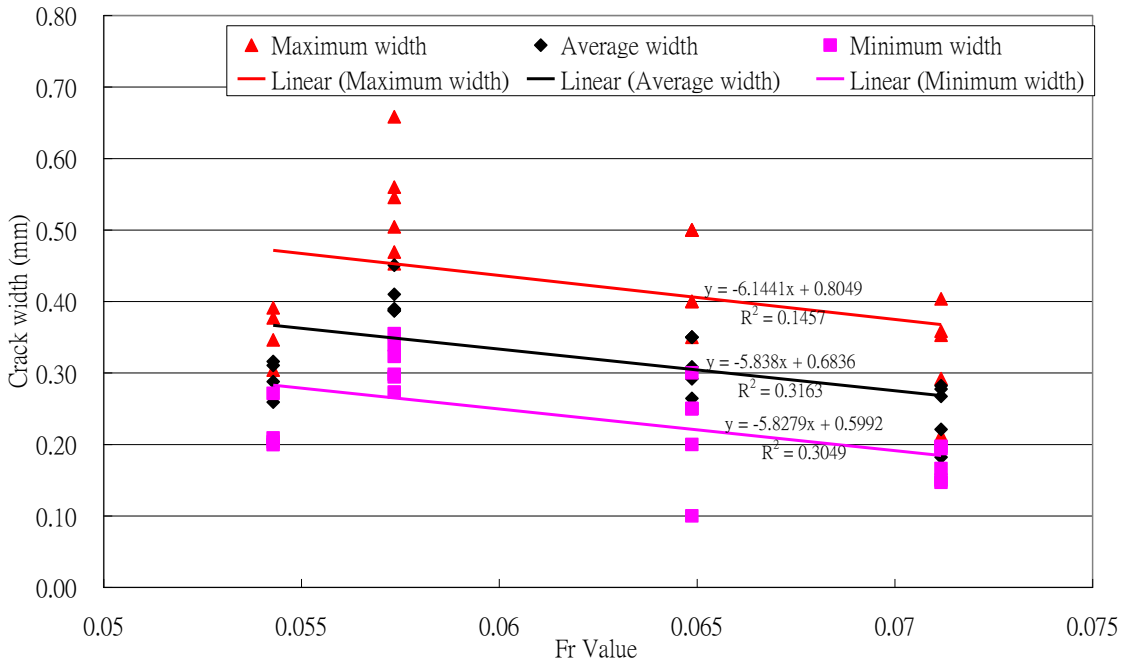

Figure 4.15b. Variation of crack width with f_R value close to the ultimate load of 11kN

From this figure, although the results are again scattered, the trend in this case is that the higher the f_R value, the smaller the crack width, irrespective of whether it is the minimum, average or maximum crack width which is being considered. By comparing the three trend lines it can be seen that the slope of the maximum crack width curve is the steepest and the slope of the minimum crack width curve is the shallowest. This highlights that the maximum crack width is more sensitive to the f_R value of the bar while on the other hand, the minimum crack width is less sensitive to the f_R value of the bar.

In Figures 4.16a and 4.16b, plots of crack width against f_R value obtained by Alander (2002) and Mayer (2002) are presented. They both show a similar trend to the current study, i.e. the higher the f_R value, the lower the crack width, but because of the variability of the experimental techniques that have been used there are significant differences

between the crack width results obtained by Alander and those of the current study.

Of particular note is the fact that the trends observed in this study agree well with those obtained by Mayer, although the maximum crack widths recorded by Mayer are slightly lower than the maximum cracks width measured in the current study. This is attributed to the smaller span-to-depth ratio of 6.0 (1200mm/200mm) with Mayer's specimens compared to that of 12.0 (1800mm/150mm) with specimens in this study.

Compared with Alander's result, the results in the current study appear to be much more sensitive to the f_R value (i.e. a steeper slope when crack width is plotted against f_R value). In addition, it is noticed that the magnitude of the crack widths measured in Alander's experiment are slightly lower than those obtained by Mayer and in the current work. These differences are attributed to the differences in specimen configuration, experimental technique, the definition of crack width and the steel stress at which it was measured. Both sets of results support the crack width findings of the current study.

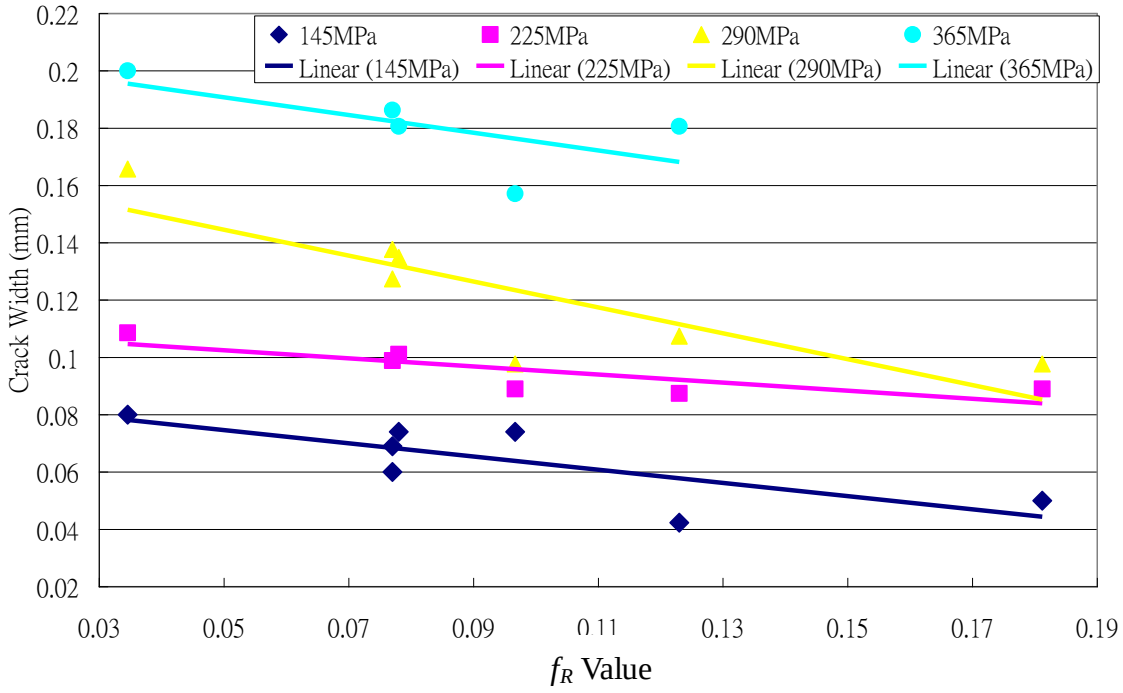

Figure 4.16a. Variation of maximum crack width with f_R by Alander (2002)

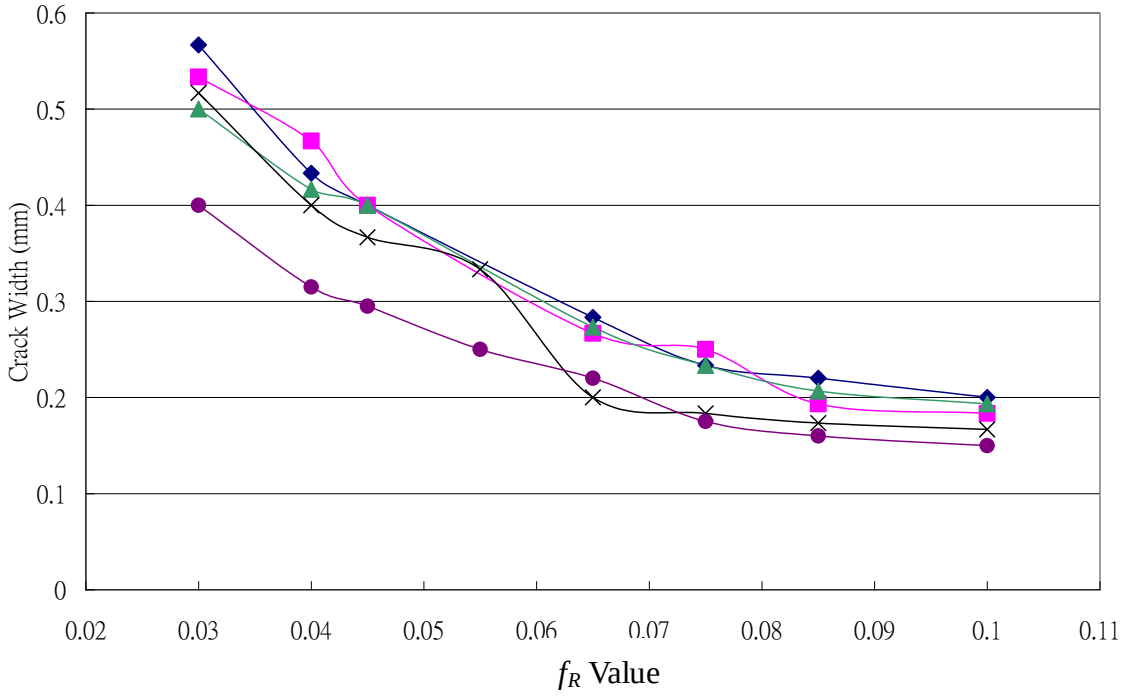

Figure 4.16b. Variation of crack width with f_R by Mayer (2002)

Further to Figure 4.12a, Figure 4.16a and 4.16b, a combined figure, Figure 4.17, containing best fit curves to all the data is presented. Although the experimental set up, the way and the loads at which the cracks were measured and the steel stress at which they were measured are all different, the agreement between the results of the current study and those of Mayer is reasonably good and in all cases the trend is one of the higher the f_R value, the lower the crack width.

As such it is concluded that the results of the current study do adequately describe the relationship between crack widths and the bond characteristics of the bar as defined by the f_R value and can be used to extend the outputs of the numerical analysis to reinforcement with different bond characteristics.

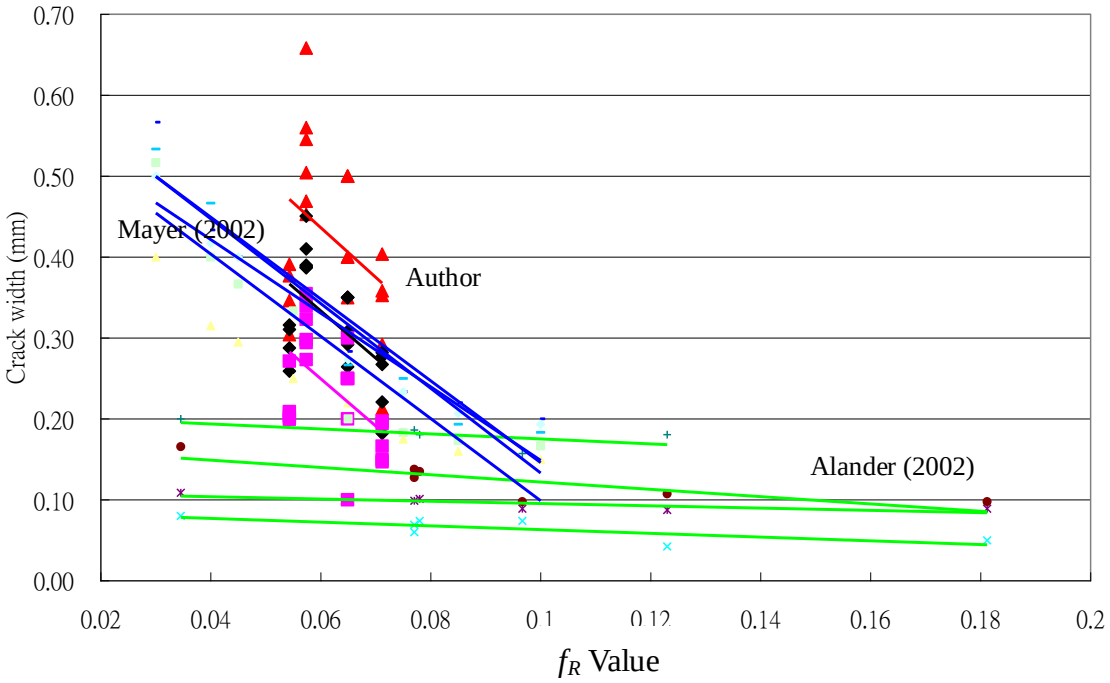

Figure 4.17. Variation of crack width with f_R by the Author, Alander (2002) and Mayer (2002)

4.6. Conclusions

From the plots of bond stress against f_R (Figures 4.12d, 4.12e and 4.12f), it can be seen that the higher the f_R value the greater the bond stress. It is also noted that the maximum crack spacing and crack width decrease with an increasing f_R value. However, care should be exercised when using this data because this variation of bond stress, crack spacing and crack width due to the f_R value is smaller than the scatter of the experimental results.

In Table 4.12, the crack spacings and crack widths of the different orientations of the reinforcing bar are summarized and the crack spacings and crack widths obtained from the overall results are added for comparison. The pattern of the results is somewhat random and therefore it is believed that the orientation of the steel bar does not affect the cracking performance.

In Table 4.13, the behaviour of two sets of flexural beam specimens, with and without stirrups in the central zone, is summarized in terms of crack spacing and crack width. It is observed that the average crack spacing of beams with stirrups in the middle zone is about 100mm, which is the same as the spacing of the stirrups cast in the beam specimen. Also, the average crack spacing of beams with no stirrups in the middle zone is always greater than that when they are present. It is believed that the results for the beams with no stirrups in the middle zone are an appropriate representation of the theoretical cracking behaviour of a simple reinforced concrete beam. However, in practice, such a beam would always have stirrups throughout its length and therefore further work using different stirrup spacings is required to confirm how their presence

effects crack spacings in practical structural elements.

The failure mode of the beams tested was a typical flexural failure and the appearance of regular, vertical cracks reflects what would be anticipated. It is noted from these tests that there were more but smaller cracks formed on the concrete beams which were reinforced with steel bars with a greater f_R value. Crack widths for the beams cast using steel from Batch M were stable and were less than 0.2–0.3 mm at 70% of the ultimate load. However, these cracks develop rapidly when the steel bar starts yielding and then the deflection of the concrete beam increase rapidly. From the plots of crack spacing and crack width against f_R value (Figures 4.15a and 4.15b), it is apparent that crack spacing and crack width are generally smaller the greater the f_R value. It is also noted that maximum crack spacing and crack width are the most sensitive to the f_R value.

The latter concurs with the findings of tests carried out by Mayer (2002) and those carried out at Helsinki University of Technology and the University of Stuttgart as reported by Alander (2002). Plots of crack width against f_R value for their tests are given in Figures 4.16c and 4.16d, in which the bond stress is found to be dependent on the relative rib area f_R and that the crack widths are smaller the greater the f_R value.

On the one hand, bond strength is directly influenced by the f_R value in that bond strengths are greater the larger the f_R value, and on the other hand, crack width and crack spacing are likewise directly influenced by the f_R value in that crack width and crack spacing are smaller the greater the f_R value. As such the stronger the bond and the smaller the cracks when steel bar with a higher f_R value is used, although it should

be recognized that the range of relative rib areas f_R considered was small and therefore further work is still required to give confidence in these results.

4.7. Modelling of Experiments

To complement this experimental work, computational modelling using finite elements and a non-local gradient method is being developed to simulate the SLS behaviour of RC beams. A smeared damage approach based on the equations of the isotropic damage model used by Oliver (2002) is adopted for cracking and both local and non-local implementations were considered and this numerical work is described in Section 5.

Chapter 5 – NUMERICAL METHOD

5.1 Introduction

It is important for designers and analysts to be able to predict the size and disposition of cracks in reinforced concrete elements since satisfaction of code crack width limits is an important design criterion. However, there has been relatively little focus on, or success in, accurate crack width prediction in the vast amount of work undertaken in the finite element modelling of reinforced concrete structures over the past 40 years.

The smeared crack approach, linked to either damage (Mazars and Pijaudier-Cabot 1989) or plasticity (Feenstra and de Borst 1995) constitutive models, is frequently used for modelling cracking in finite element models of concrete structures. However, it is well known that when cracking is simulated with strain softening material models, spurious mesh sensitivity becomes an issue and this leads to non objective results and also can lead to convergence failure of the nonlinear solution process. The term 'regularisation' has been applied to techniques which prevent this spurious mesh sensitivity and the traditional crack-band approach of Bazant and Oh (Bazant and Oh 1983, Bažant and Planas 1998) has been widely used for such regularisation. However, this method does not solve numerical stability problems associated with softening materials. Stability and regularisation are both addressed by non-local approaches, which may be of gradient (de Borst and Miihlhaus 1992, Aifantis 1984 and Peerlings et al 1996) or integral form (Pijaudier-Cabot and Bažant 1987, Bazant and Pijaudier-Cabot, 1988 and Bažant and Jirásek 2002). These non-local approaches are highly effective at both regularising and stabilising finite element solutions but they simulate cracking in a diffuse manner which means that crack widths cannot be obtained directly

from such solutions.

One option for obtaining crack widths is to use a model in which crack openings are computed explicitly. Such models include approaches with embedded cohesive elements (Tijssens et.al. 2000), approaches which model strong discontinuities in meshes (Oliver et.al. 2003) and element free methods (Rabczuk and Belytschko 2007). However, to obtain accurate crack width predictions, meso-level information such as bar spacing, bar bond characteristics and cover (EC2 EN1992-1-1 2008) is required. Finite element models of full scale structures would currently be too expensive if such details were simulated explicitly with single-scale models. Thus, when the aforementioned approaches are applied to full scale structures, the extracted crack widths are likely to be approximate and hence unlikely to be consistent with code of practice predictions required by designers and analysts. Such models also have computational overheads associated with crack tracking procedures which can be particularly demanding when simulating full-scale 3D structures with multiple cracks.

Non-local approaches remain attractive for analysts but there are certain issues over their validity and usefulness for the analysis of large scale RC structures. These issues include the appropriateness of using a non-local approach for naturally non-local reinforced elements, the fineness of mesh required to properly simulate fracture process zones, at scale, and the difficulty of extracting accurate crack widths from non-local solutions. The former two issues are not addressed here but the work in this thesis concentrates on a method for calculating crack widths from non-local and, for comparison, local smeared solutions based on the assumption that it is valid to use a

non-local approach for reinforced concrete elements.

Some work had been undertaken recently on this problem for unreinforced situations by Dufour et al. (2008), who have proposed a method for extracting crack widths from a nonlocal strain field, using an approach in which a non-local effective strain variable is equated to a regularised effective strain derived from an assumed discontinuity.

Małecki et al, 2007, explored the effect of varying the characteristic length in a non-local model on the spacing of localized zones when analyzing reinforced concrete prisms under tensile loading. They concluded that the spacing of these zones (taken as cracks) is 7 to 16 times the characteristic length (l_{ch}) and that l_{ch} values of between 5 and 10 mm give a good match to crack width and spacing values calculated using CEB-FIP model code 90.

At a cracked section of a RC beam, tension forces are carried by the reinforcement. However, the bond between steel and concrete still exists and this bond gradually transfers the force in the reinforcement at a crack position to the uncracked concrete in between two adjacent cracks (See Figure 5,2). This action stiffens the response of RC beams relative to that of a theoretically fully cracked beam (Kaklauskas et. al., 2009) and has therefore been termed ‘tension stiffening’. By contrast, tension softening is a property of plain concrete which describes the gradual loss of stiffness that occurs with increased micro-cracking. This behaviour can be modelled using fracture mechanics (Bazant and Oh, 1983). The issue of tension stiffening has also been recently explored with the aid of a 2D finite element model by Ng et.al. (2010). Other authors have used

detailed finite element models to aid the understanding of cracking behaviour in laboratory scale experiments (Wu and Gilbert, 2009 and Tammo et. al., 2009).

The main purpose of the present contribution is to present a calculation procedure for computing the disposition and width of cracks in local and non-local finite element analyses from numerical strain fields. An isotropic damage model, based on that used of Oliver et al., 2002, is used to model concrete cracking.

5.2 Numerical Model

5.2.1 Nonlocal Implementation

A non-local damage model has been employed for the present work. The non-local implementation uses the gradient formulation due to Ru and Aifantis (1993), see also Askes et al. (2008).

A non-local strain tensor ($\bar{\varepsilon}$) derived from the following differential equation is employed

$$\bar{\boldsymbol{\varepsilon}} - \ell_{\mathbf{ch}}{}^{\mathbf{2}} \cdot \nabla^{\mathbf{2}} \bar{\boldsymbol{\varepsilon}} = \boldsymbol{\varepsilon} \qquad (1)$$

where ℓ_{ch} is a characteristic length, ∇^2 is the Laplace operator, ε and $\bar{\varepsilon}$ are the local and non-local strain tensor respectively.

The discretised form of these equations is as follows,

$$\mathbf{D_f}\,\bar{\boldsymbol{\varepsilon}} = \mathbf{E}\mathbf{u} \tag{2}$$

where

$$D_f = \int_{\Omega}\left(N^T N + \ell_{ch}{}^2 \cdot \nabla N^T \nabla N\right)d\Omega \qquad \text{and} \qquad E = \int_{\Omega} N^T B d\Omega$$

This may also be written

$$\bar{\boldsymbol{\varepsilon}} = \mathbf{W}\mathbf{u} \tag{2a}$$

in which $\mathbf{W} = \mathbf{D_f}^{-1}\mathbf{E}$

Natural boundary conditions are assumed to apply such that Equation (2) is solved without the application of any additional boundary conditions, other than those applied to nodes with prescribed and fixed displacements.

5.2.2 Concrete Constitutive Model

The essential constitutive equations of the isotropic damage model used for this study are based on those of Oliver et al., 2002. Here, only tensile damage is considered since tension cracking is the primary concern of this study.

The total (secant) stress-strain relationship is written (in compact tensorial notation) as follows:

$$\boldsymbol{\sigma} = (1-\omega)\mathbf{D} : \boldsymbol{\varepsilon} \tag{3}$$

where $\boldsymbol{\sigma}$ and $\boldsymbol{\varepsilon}$ are the stress and strain tensors respectively, **D** is the elasticity tensor which is assumed to be isotropic and ω is a scalar damage parameter, and $\boldsymbol{\sigma}_e = \mathbf{D}_e : \boldsymbol{\varepsilon}$ is the effective stress.

The response of undamaged material is linear elastic and the damage parameter ω is set to zero initially. When the material is deformed under loading, micro cracks develop and these reduce the stiffness of the material. The damage parameter starts growing from zero and it represents the loss of integrity of the material. When the damage parameter $\omega = 1.0$, the material is completely damaged and its corresponding stiffness vanishes.

The effective stress parameter is defined as:

$$\tau_{\varepsilon} = \sqrt{\boldsymbol{\sigma}_0^+ : \mathbf{D}^{-1} : \boldsymbol{\sigma}_0^+} \tag{4}$$

The evolution of damage in effective stress space is driven by the following damage loading function:

$$f = \tau_{\varepsilon} - r = \sqrt{\boldsymbol{\sigma}_0^+ : \mathbf{D}^{-1} : \boldsymbol{\sigma}_0^+} - r \tag{5}$$

where $\boldsymbol{\sigma}_0^+$ denotes the positive part of stress tensor i.e. a tensor which contains only the components associated with the positive eigenvalues of the tensor. *r* is a damage evolution parameter which controls damage evolution.

Damage increases only when the current value of *r* exceeds the previous limit, with the initial value being that associated with the elastic limit. Damage evolution can be expressed by the following loading / unloading condition:

$$f \le 0 \qquad \dot{r} \ge 0 \qquad \dot{r} f = 0$$

The damage parameter ω depends upon the damage evolution parameter *r* as follows :

$$\omega = \begin{cases} 0 & if\ r \le r_t \\ 1 - \dfrac{r_t}{r} e^{-5\left(\frac{r - r_t}{r_m - r_t}\right)} & if\ r \ge r_t \end{cases} \tag{6}$$

in which $\omega \in [0,1]$ and $r \in [r_t, \infty]$

where r_m is the damage evolution parameter *r* corresponding to a uniaxial tensile strain at the end of the tensile softening curve, which can be related to the fracture energy. The power constant 5 in equation 6 is a standard value which allows the equation to represent the response of a uniaxial tension test accurately.

The initial value of damage evolution parameter r_t is directly related to the tensile strength, as follows :

$$r_t = \frac{f_t}{\sqrt{E}} \tag{7}$$

where *E* is Young's modulus, f_t is the uniaxial tensile strength.

The tangent D matrix for a local version of the model is as follows:

$$\mathbf{D}_{\tan} = (1-\omega)\mathbf{D} - \frac{d\omega}{dr}\left[\frac{\boldsymbol{\sigma}_0^+ \otimes \boldsymbol{\sigma}_0^+}{r}\right] \tag{8}$$

noting that $d\boldsymbol{\sigma} = D_{tan} : d\varepsilon$

For the non-local version of the model, Equation (3) is rewritten:

$$\boldsymbol{\sigma} = (1 - \omega(\bar{\varepsilon}))\mathbf{D} : \boldsymbol{\varepsilon} \tag{9}$$

The consistent tangent stress-strain law is then as follows:

$$d\sigma = D_{\text{sec}} : d\varepsilon + D_{t2} : d\bar{\varepsilon} \tag{10}$$

where the secant stiffness matrix is defined as $D_{\text{sec}} = (1-\omega)D_e$, $D_{t2} = -\frac{d\omega}{dr}\left[(D_e : \varepsilon) \otimes \left(\frac{\partial r}{\partial \boldsymbol{\sigma}_0^+} \right) \right]$ and $d\bar{\varepsilon}$ is the rate of equivalent strain. The second term D_{t2} disappears if the strain is not on the damage surface.

The fully consistent finite element tangent stiffness matrix for the non-local form of the model is as follows :

$$K = \int_{\Omega} B^T D_{\text{sec}} B d\Omega + \int_{\Omega} B^T D_{t2} N d\Omega \; W \tag{11}$$

where *N* denotes the shape functions. *B* is the strain displacement matrix defined as :

$$\varepsilon = Bu$$

5.2.3 Numerical Details

The use of Newton solutions for non-local models was discussed by Jirásek and Patzák (2002). They presented the comparison of the efficiency of solution strategies using secant or tangent stiffness matrices. The secant stiffness matrix was shown to have a linear convergence rate and the tangent stiffness matrix had a quadratic convergence rate, once the state of damage stabilizes in an increment, thus the latter converges with fewer iterations. Here, a fully consistent tangent stiffness matrix is used.

The finite element program described here was written in MATLAB by the author (from scratch). An overview of this program is given in Figure 5.1.

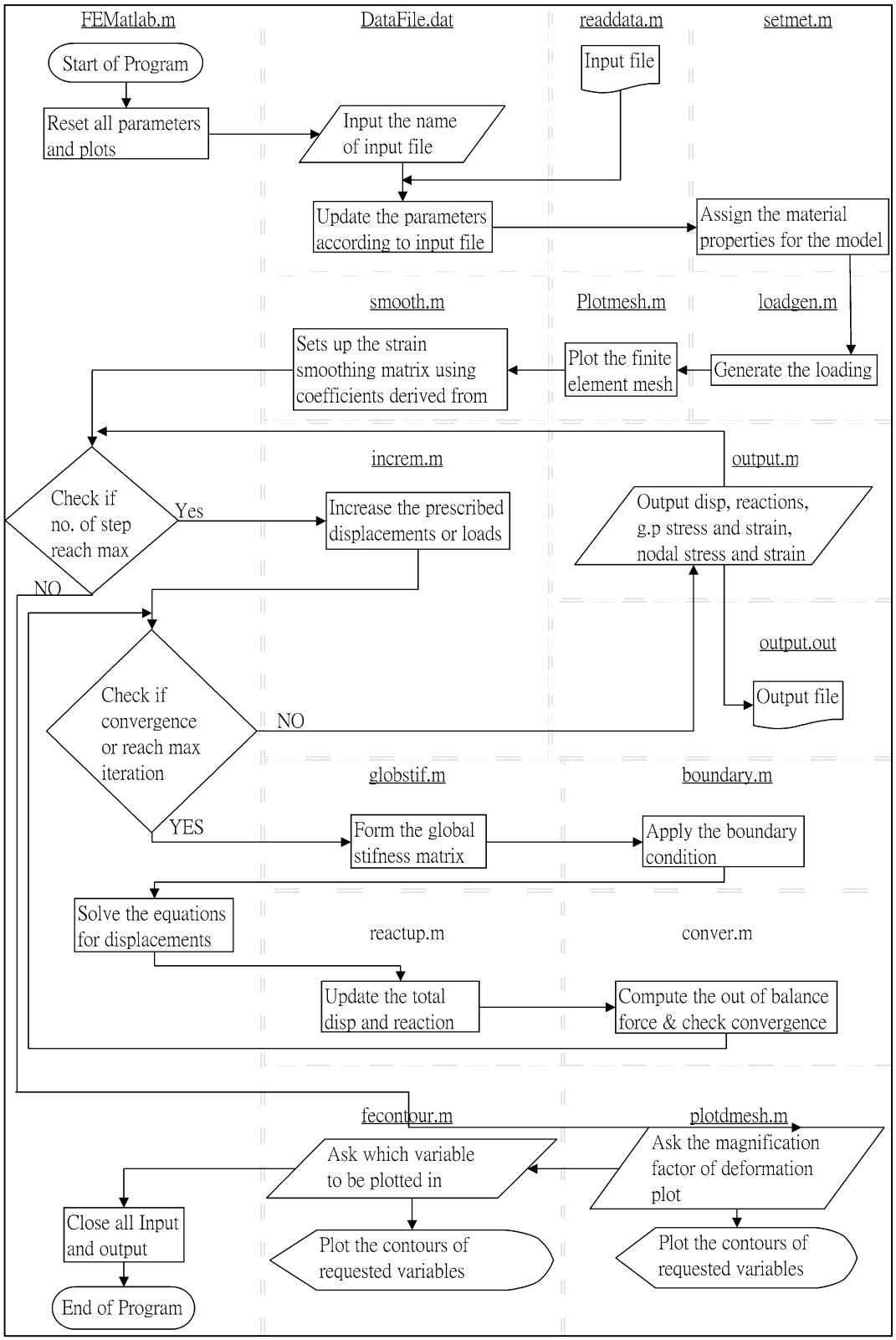

Figure 5.1. Algorithm of the program

5.3 Equations for Crack Width Calculations

A large body of work has been undertaken to derive expressions to predict the spacing (S_{rm}) and width (w_k) of cracks for structural elements with a view to their use in codes of practice. A summary of work undertaken to develop crack width formulae was presented in 2005 by Borosnyoi & Balazs.

The main parameters which affect crack spacings and widths are the main bar size (ϕ), the effective reinforcement ratio (ρ_{ef}), the average steel strain between cracks (ε_{sm}) and peak steel stress at the position of a crack (σ_{s0}). The variation of steel and concrete strains between two adjacent cracks is illustrated in Figure 5.2 which shows that the steel strain reduces from a peak at the crack location to a minimum half way between the cracks whilst the concrete strain which follows a converse pattern. The crack opening is computed as the integral of the difference between the steel and concrete strains over two half crack spacings.

The effective reinforcement ratio for a flexural member is the reinforcement area to effective concrete area ratio, where the effective concrete area is, nominally, that which is equivalent to a member in direct tension. The peak steel stress is generally calculated as the crack from a section in a 'fully cracked state', i.e. the theoretical stress that would exist in a section if concrete had zero tensile strength. Recent work has been undertaken on the effect on crack-widths of varying cover (Tammo, Lundgren and Thelandersson 2009) and of varying the parameter ϕ/ρ_{ef} (Beeby, 2004).

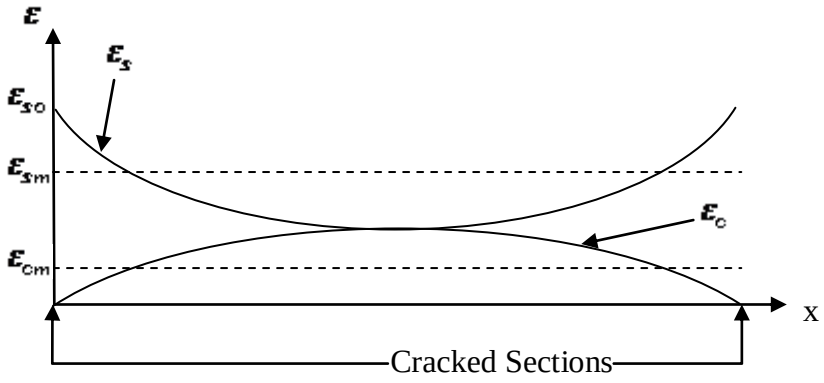

Figure 5.2a. Strain distribution after cracks are formed

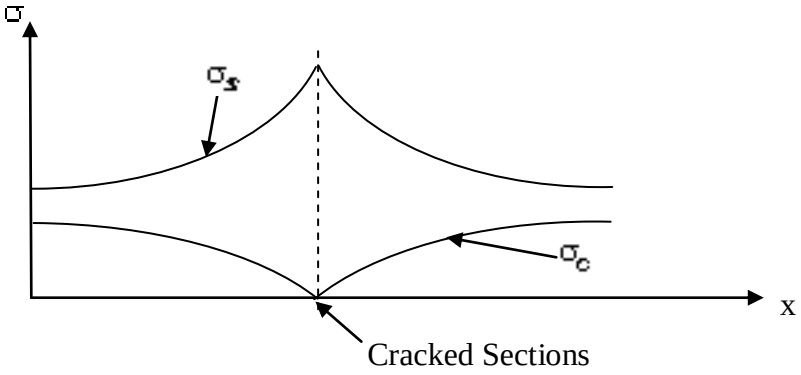

Figure 5.2b. Steel stress at a cracked section

In the present work, the formulae from Eurocode 2 will be used for the main calculations. A full background to the Eurocode equations for cracking is provided in the text of Narayanan and Beeby (2005). Whilst EC2 formulae have been used here, the principles established could be applied to any code calculation formulae. Although standard, the EC2 procedure will be summarised here for completeness.

The mean strain, which is obtained from the fully cracked strain minus the strain component from tension stiffening, is as follows; noting that EC2 notation and constants have been adopted throughout.

$$\left(\varepsilon_{sm}-\varepsilon_{cm}\right)=\frac{\sigma_s-k_t\dfrac{f_{ct,eff}}{\rho_{p,eff}}\left(1+\alpha_e\rho_{p,eff}\right)}{E_s} \tag{12}$$

the characteristic maximum crack spacing is given by,

$$S_{r,\max}=k_3c+k_1k_2k_4\frac{\phi}{\rho_{p,eff}} \tag{13}$$

and the design crack width,

$$w_{k,m,code}=S_{r,\max}\left(\varepsilon_{sm}-\varepsilon_{cm}\right) \tag{14}$$

in which k_1 is a coefficient for bond properties of reinforcement (0.8 for high bond and 1.6 for plain bars), k_2 denotes the nature of strain distribution (1.0 for pure tensile and 0.5 for flexural), k_3 = 3.4 and k_4 = 0.425. k_t is a factor dependent on the duration of the load, which equals 0.6 for short-term loading. α_e is the ratio E_s/E_{cm} and $\rho_{eff}=\dfrac{A_s}{A_{c,eff}}$. $f_{ct,eff}$ is the mean value of the tensile strength of the concrete effective at the time when cracks are first expected to occur. Where the experimental cylinder splitting strength (f_{cyl}) is available, $f_{ct,eff}$ is taken to be 0.9 f_{cyl} , which follows the recommendation of CEB-FIP model code 90 (1990). However, it is acknowledged that van Mier (1997) has cast doubt on the existence of an exact relationship between uniaxial tensile strength and cylinder splitting strength.

For a flexural member, the effective area ($A_{c,eff}$) used in the reinforced beams/slabs is the lesser of 2.5(c+ϕ/2) or (h-x)/3; where c is the cover to main bars, h is the overall section depth and x is distance from compressive face to the neutral axis for a theoretically fully cracked section.

$S_{r,max}$ is the appropriate value to use in design since this gives the maximum calculated crack width and it is the parameter that designers need to limit to a prescribed value (typically 0.3mm, as given in EC 2 for moderate exposure conditions). However, as explained by Narayanan and Beeby (2005), the relationship between the mean crack spacing ($S_{r,m}$) and the characteristic maximum has been found to be $S_{r,max}$=1.7 x $S_{r,m}$ and it is the mean crack spacing that is considered to be the most appropriate value to use when comparing calculated and experimental mean values.

In 2005, Narayanan and Beeby point out that the aspect of crack calculation which varies most between codes of practices is the crack spacing. To allow this to be assessed for the present examples, the mean crack spacing formula from CEB-FIP model code 1990 is also shown below. The chief difference between the CEB-FIP and EC2 formulae is that the latter includes a term which allows for variations in cover, which is reported to be a superior approach (Narayanan and Beeby 2005).

$$S_{r,mCEB} = 0.185\frac{\phi}{\rho_{p,eff}} \qquad (15)$$

5.4 Crack Calculations from Finite Element Results

The basic premise of the proposed procedure is that the non-local strain (or smeared

strain in the local analysis), if considered over the calculated crack spacing, can be considered to be equivalent to the mean strain used in code calculations once tension stiffening has been taken into account. In making this assumption it is acknowledged that the simulation of distributed micro-cracking with strain softening is not the same as tension stiffening which accounts for intact concrete in-between discrete cracks. The truth is that, in reality, the concrete in-between discrete cracks will be micro-cracked and thus experimental derived expressions for tension-stiffening implicitly allow for micro-cracking.

The resulting method developed for calculating crack widths comprises the following steps:

1. Undertake a nonlinear analysis up to the relevant working load level at which crack widths are required.
2. Identify the locations of maximum tensile strain in reinforcing elements.
3. Read in the bar size of primary reinforcement, cover, secondary reinforcement size and k factors appropriate for the location.
4. Compute the maximum crack spacing ($S_{r,max}$) from the code formula Equation (13)
5. Compute the average strain in the reinforcing bar over a distance $S_{r,max}$, centred upon the maximum strain location.
6. Account for the elastic strain in the concrete, assuming that the stress from the crack location varies from 0 to f_{teff} to obtain ε_{cmc} which is then assumed to be equivalent to (ε_{cm} -ε_{sm}) in Equation (14).
7. Compute the mean crack width $w_{k,m,code}$ using Equation (14), with $S_{r,max}$ from

step 4 above and ε_{cmc} in place of $(\varepsilon_{cm} - \varepsilon_{sm})$.

It is emphasised that this is a post-processing procedure and no attempt is made to feed these results back into the analysis.

5.5 Examples

The analyses were undertaken with a MATLAB code written by the author, to which was added the post-processing algorithm described above. The characteristic length (l_{ch}) used in gradient solutions is a micro-scale (or meso-scale) parameter. It is linked to the fundamental particle size, which in the present case is the size of the coarse aggregate particles. In gradient-elasticity, l_{ch} has been taken as the particle size by Askes, Moratab and Aifantis (2008). In their 2002 review of non-local models, Bazant and Jirasek discuss the difficulty of exactly determining the characteristic length whilst recognising its connection to the size of the fracture process zone and the fundamental particle size. Here, the value of l_{ch} is taken as equal to the coarse aggregate particle size (d_{agg}), and it is further noted that the use of $l_{ch} = d_{agg}$, is generally consistent with the findings of Małecki et. al (2007).

Two types of structural element are considered in this chapter (i) axially loaded prisms and (ii) beams loaded in flexure. The axially loaded reinforced prisms were tested by a group of researchers in a round robin testing programme led by Elfgren & Noghabai (1998, 2001 and 2002). This is followed by results from the analysis of the beams tested by Clark (1956) and then of a beam tested by the author. The main purpose of the experimental series tested in Cardiff was to compare the performance of beams

with standard reinforcement with those of beams formed with a new high-ductility bar produced by CELSA UK.

The procedure described in Section 5.4 was used to calculate crack spacings for each example. As explained, $S_{r,max}$ is the spacing appropriate to design whereas the mean value $S_{r,m}$ is considered the best value to use when comparing the numerical and experimental results. Therefore, both the theoretical values for $S_{r,m}$ and $S_{r,max}$ are presented in the results tables. Where available, $S_{r,m,exp}$ and $S_{r,max,exp}$ are given and these are defined as the mean and maximum of the crack spacings measured in the experiment over a section of constant nominal axial load or moment as appropriate. Mean and maximum crack widths are calculated using the associated values of spacing.

In each of the examples, a finite element mesh was designed for the analysis. Before the final finite element mesh was confirmed, the examples were simulated to test the sensitivity of mesh by considering a series of different sizes of trial mesh from coarse to fine. The final finite element mesh was selected when the mesh sensitivity dropped below 1%. In all cases, 8-noded quadratic elements were used to represent the concrete and 3-noded quadratic 'bar' elements to represent the reinforcement. In plots of the damage, the degree of damage varies from 0 (no damage) to 1 (complete damage).

5.5.1 Axially Loaded Tests from Elfgren & Noghabai

The example considers results from a round-robin experimental test series reported by

Elfgren & Noghabai (1998, 2001 and 2002). The geometry of the specimens and testing arrangement are illustrated in Figure 5.3 and the material properties are summarized in Table 5.1. In the experiment, axial loading was applied to the bar and crack details monitored. The finite element mesh used for the analysis is shown in Figure 5.4a and plots showing the scalar damage variable at the same elongation of 1.0mm are shown in Figure 5.4b and 5.4c. The beams have been considered with the local model and with the non-local model using a characteristic length equal to the coarse aggregate particle size.

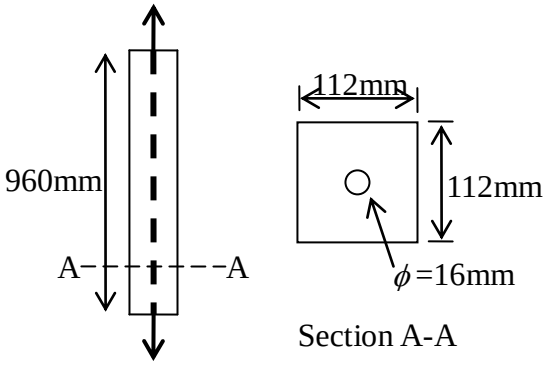

Figure 5.3. Geometry of the specimens

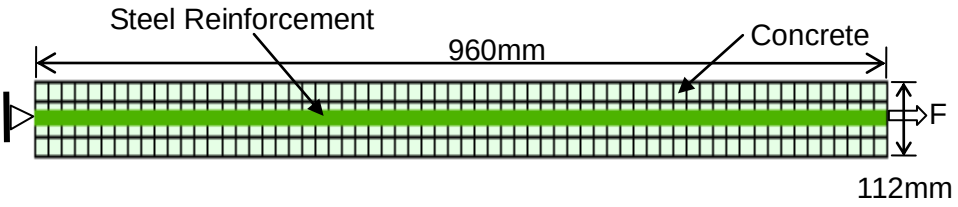

Figure 5.4a. Finite element mesh plot

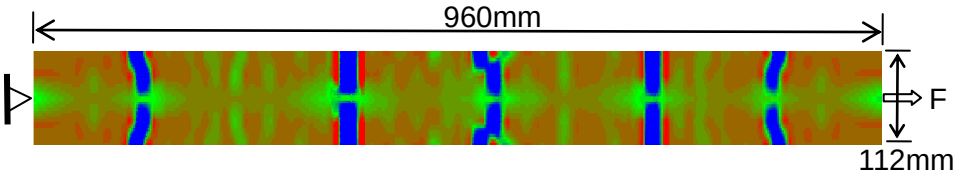

Figure 5.4b. Damage plot at 1.0mm for local model

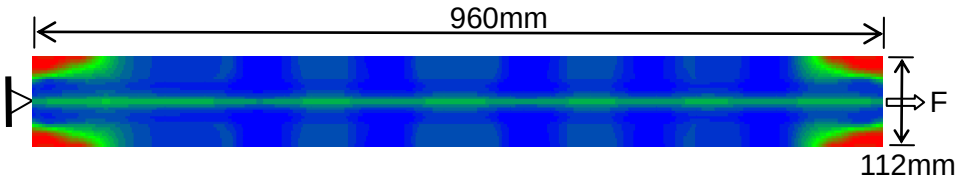

Figure 5.4c. Damage plot at 1.0mm for non-local model using a characteristic length equal to the coarse aggregate particle size

Table 5.1. Material properties of Noghabail's test

Specimen	Concrete				Steel	
	f_c (N/mm^2)	f_{ct} (N/mm^2)	E_c (kN/mm^2)	G_f (N/mm)	E_s (kN/mm^2)	f_{sy} (N/mm^2)
Noghabail	60	3.75	37.2	0.170	180	563

The first observation from the results is that, with the local model, even with initial uniform properties, the damage shows a significant degree of localisation, even at the working displacement level of 1.0mm. This localisation did not occur to any significant degree when using the non-local model.

The numerical and experimental load displacement responses are presented in Figure 5.5. It may be seen that the local model captures the multiple oscillations (load drops) in the early post-cracking region, whilst the non-local model only captures the overall trend of the response. Nevertheless, the overall response achieved for both models is considered reasonable relative to the natural variations observed in such experiments.

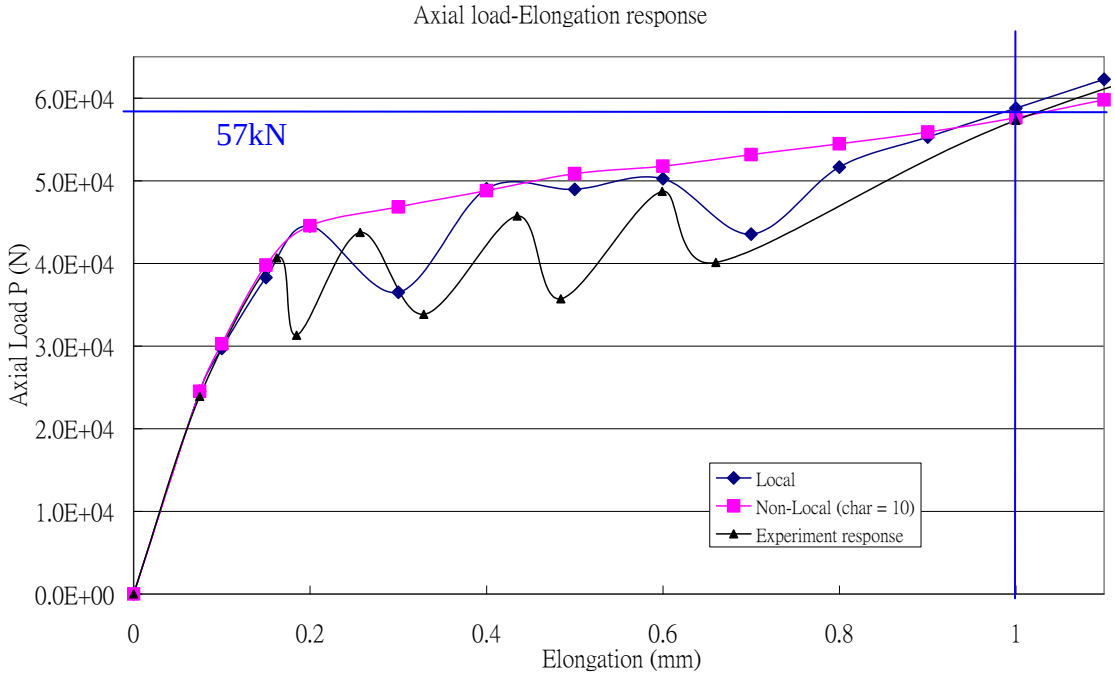

Figure 5.5. Experimental and numerical response

The results have been presented in Table 5.2 for the same end displacements. The displacement chosen is that from the experiment at the chosen working load level. In this case, the results, in terms of predicted crack widths, are considered to be adequately close.

Table 5.2. Results in terms of crack widths and crack spacings for axial loaded test result

Model	Experiment			Numerical	Numerical			Eurocode
	$S_{r,m,\exp}$ $S_{r,m,\exp}$ $S_{r,\max,\exp}$ (mm)	$w_{k,exp}$ $w_{k,m,\exp}$ $w_{k,\max,\exp}$ (mm)	Steel Strain	FE mean strain ε_{cmc} over s_r	$S_{r,m}$ $S_{r,\max}$ (mm)[d]	$w_{k,m}$ $w_{k,\max}$ (mm)	$w_{k,m}$ with exp spacing $S_{rm\exp}$ (mm)	$w_{k,m,code}$ (mm) $(\varepsilon_{sm}-\varepsilon_{cm})$
Non-Local	200[a]	0.15[a]	0.00105[b]	0.00103	296	**0.305**	0.206	0.217
	207[b]	**0.135**[b]			503	0.518	**0.213**	0.000735
	248[c]	0.15[c]					0.255	
Local				0.00104	296	**0.308**	0.208	
					503	0.523	**0.215**	
							0.258	

[a] Noghabail (mean spacing but w_k is a maximum), [b] Round-robin mean, [c] Round-robin max, [d] Spacings computed from Eurocode

There is a significant discrepancy between the mean experimental and mean code crack spacing. Interestingly, crack spacing was also calculated according to the CEB-FIP model code 90 and the code gives a mean crack spacing of 185mm, which is much closer to the mean experimental values from the round-robin tests in this case.

The finite element prediction is very close to the code of practice prediction in this case, which would be an important factor for designers.

It may be seen that if the experimental mean spacing is used the crack widths are closer to the experimental, for both local and non-local analyses, than if the mean code

of practice spacing is used; however the numerical values are still somewhat high.

5.5.2 Beam Tests from Clark

The example presented here uses results from an experimental test series undertaken by Clark in the 1950s, when crack patterns were first being properly investigated. The specimen details and testing arrangement are illustrated in the Figure 5.6 and the steel and concrete properties of Clark's test are summarized in Table 5.3. The finite element mesh used for the analysis is shown in Figure 5.7a and plots showing the scalar damage variable at a deflection of 4mm are shown in Figures 5.7b and 5.7c.

Table 5.3. Steel and concrete properties of Clark's test

Steel			Concrete			
ϕ (mm)	A (mm^2)	E_s (kN/mm^2)	f_c (N/mm^2)	E_c (kN/mm^2)	f_t (N/mm^2)	G_f (N/mm)
22.2	50.27	195	29.3	33	2.9*	0.07*

*Values based on f_c values using CEB-FIP 1990 formulae

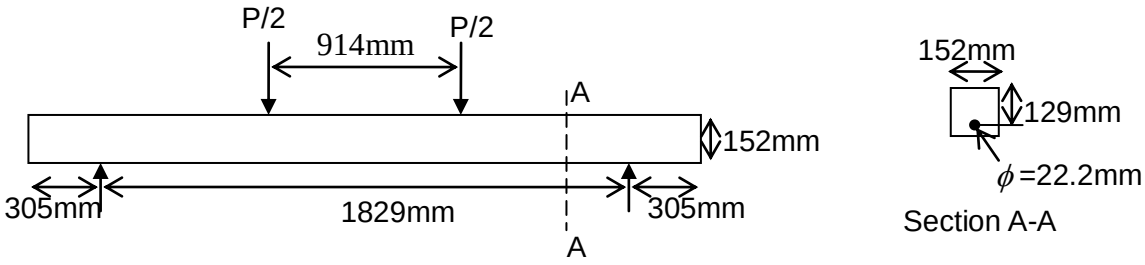

Figure 5.6. Geometry of the specimens

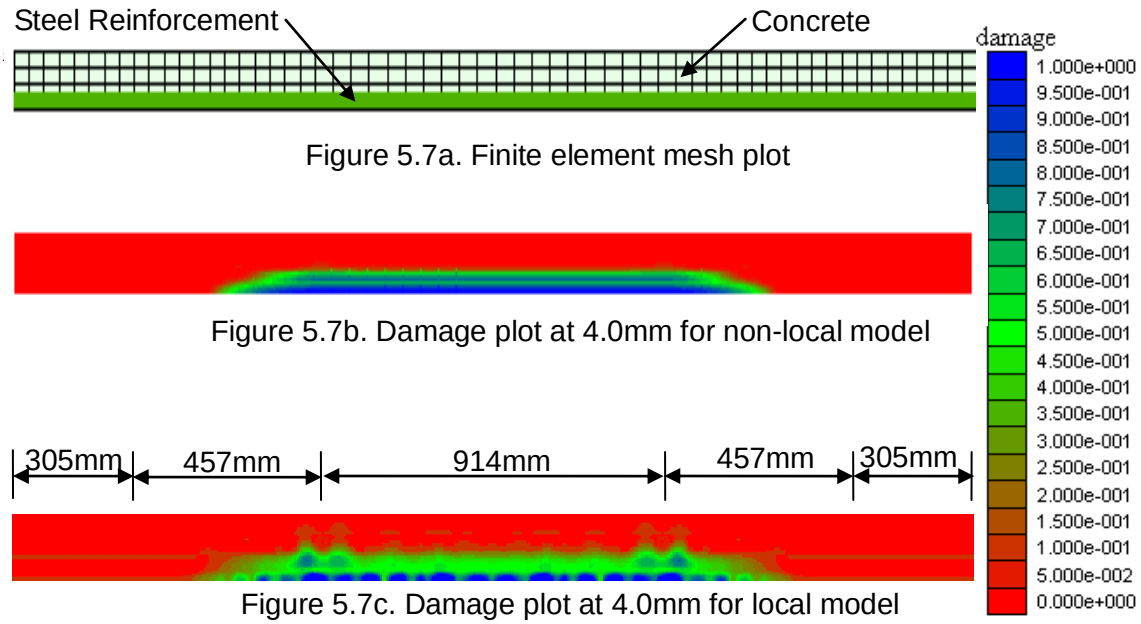

Figure 5.7a. Finite element mesh plot

Figure 5.7b. Damage plot at 4.0mm for non-local model

Figure 5.7c. Damage plot at 4.0mm for local model

A load-deflection plot is shown in Figure 5.8a, in which the loads and displacements of corresponding load stages are indicated. Note that the load-deflection curve from the experiment is not available. Strain profiles from the local and non-local gradient analyses with a characteristic length of 10mm are shown in Figure 5.8b.

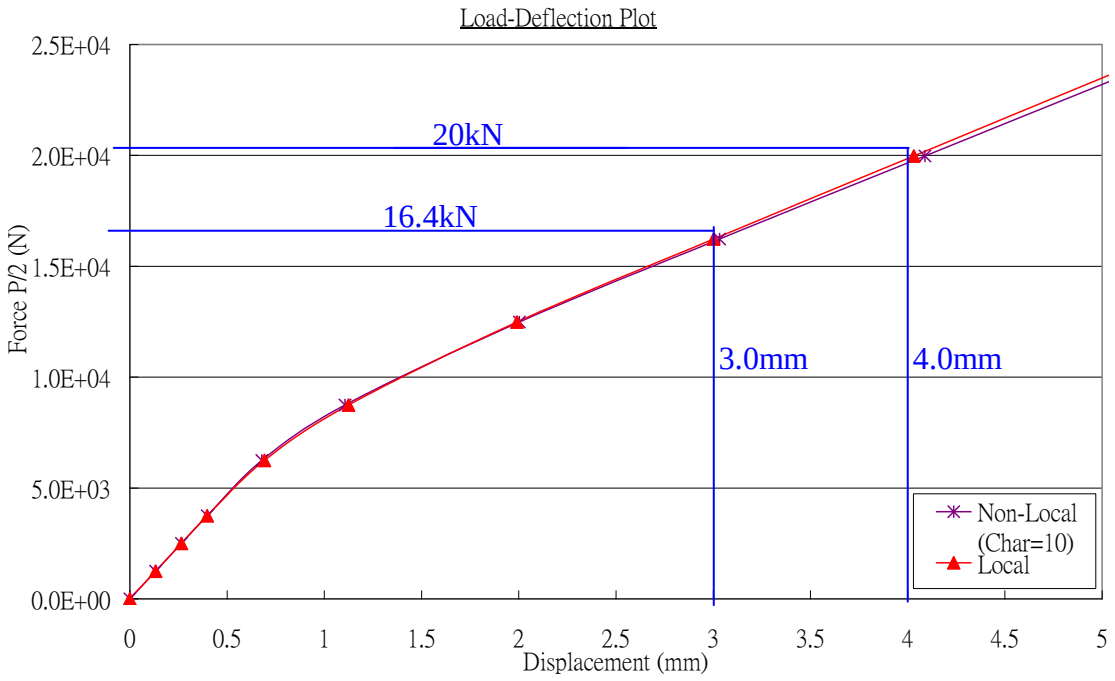

Figure 5.8a. Load – Central deflection response

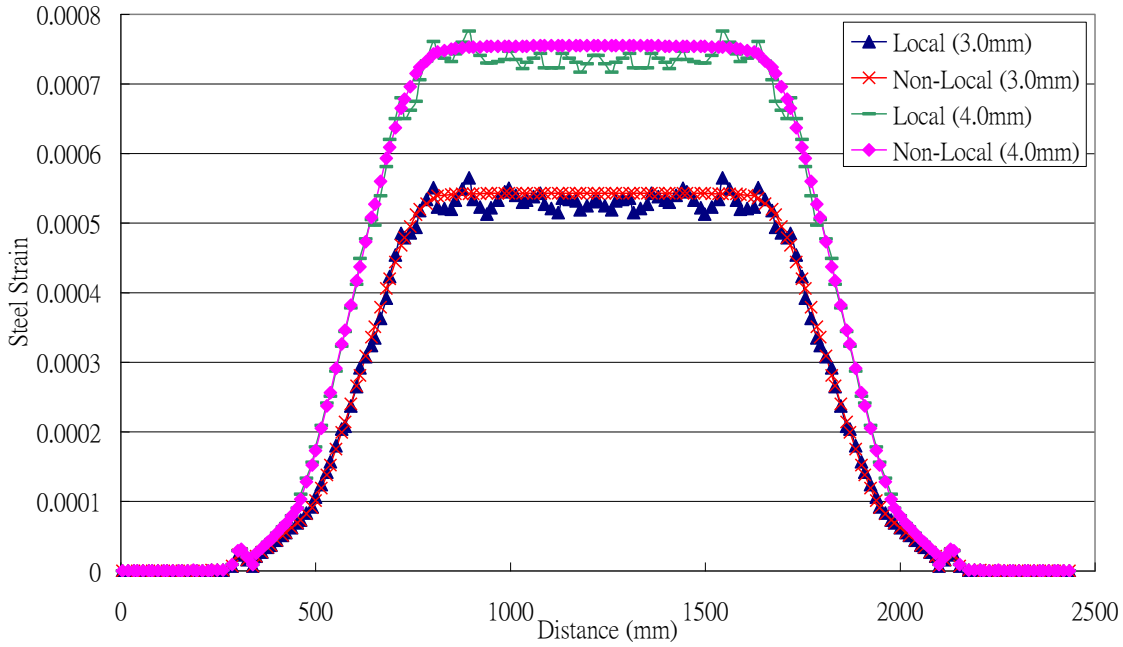

Figure 5.8b. Strain profile at different applied load levels

It may be seen from Figure 5.8a that, in this case, the overall response from the local and non-local analyses are very close to each other. As with the previous example, localisation occurs in the analysis using the local model whereas no significant localisation is exhibited for the non-local model.

The results in terms of crack widths and crack spacing for central deflections of 3.0mm and 4.0mm are presented in Table 5.4.

Table 5.4. Results in terms of crack widths and crack spacings for Clark's test result

Model (working level)	Experiment			Numerical	Numerical			Eurocode
	$S_{r,m\exp}$ $S_{r,\max,\exp}$ (mm)	$w_{k,m,\exp}$ $w_{k,\max,\exp}$ (mm)	Mean steel strain*	ε_{cmc}	$S_{r,m}$ $S_{r,\max}$ (mm)	$w_{k,m}$ $w_{k,\max}$ (mm)	$w_{k,m}$ with experiment spacing $S_{rm\exp}$ (mm)	$w_{k,m,code}$ (mm) $\left(\varepsilon_{sm}-\varepsilon_{cm}\right)$
Non-Local (3.0mm)	104	**0.057** 0.084	0.00053	0.000540	**53.1** 90.2	**0.029** 0.049	0.056	0.039 0.00073
Local (3.0mm)				0.000531	**53.1** 90.2	**0.028** 0.048	0.055	
Non-Local (4.0mm)		**0.090** 0.130	0.00071	0.000750	**53.1** 90.2	**0.040** 0.068	0.078	0.049 0.00092
Local (4.0mm)				0.000734	**53.1** 90.2	**0.039** 0.066	0.076	

*Based on quoted steel stress and assumed E value for steel

For this configuration, the mean crack spacing from CEB-FIP model code 90 = 54mm, which is close to the 53mm predicted by EC2.

The main results in Table 5.4 show an experimental crack width of 0.057mm at 3mm deflection and a corresponding local numerical result of 0.055mm when the experimental crack spacing is used. This suggests that for this example the effective mean strain in the concrete from both the local and non-local analyses are acceptably close to that in the experiment.

5.5.3 Cardiff Celsa Test

This example uses the results from one of the author's experimental beams, which was described in Chapter 4 of this thesis (Section 4.5.2.3). The testing arrangement and specimen geometry are illustrated in Figure 5.9a. The properties of the steel reinforcement and concrete are given in Tables 5.5 and 5.6. The finite element mesh

used for the analysis is shown in Figure 5.9b.

Table 5.5. Steel properties in Cardiff Celsa test

Steel	Grade	A (mm^2)	0.2% Proof. σ (N/mm^2)	Ultimate. σ (N/mm^2)	Elongation. ε (%)	E_s (kN/mm^2)
A	A	47.78	554	587	10.5	185
B	B	51.53	521	597	20	199
C	C	50.27	537	668	25.7	200
Max	C	55.42	524	652	22.5	205

Table 5.6. Concrete properties in Cardiff Celsa test

Concrete	E_c (kN/mm^2)	f_c (N/mm^2)	f_{cyl} (N/mm^2)	G_f (N/mm)
A	39.5	49	5.1	0.105
B	39.6	47	5.2	
C	39.2	49	4.9	
Max	39.0	47	5.1	

Figure 5.10 shows a photograph of cracked Celsa beam in which the cracks have been highlighted and damage plots at a deflection of 2.6mm are shown in Figures 11a-h.

The cracks in the specimen were monitored in two ways during the tests (i) by visual observation and pencil tracing and (ii) using a Digital Image Correlation system (DIC). The same surface observations were made with both methods, with crack disposition and spacing measurements being in close agreement. Crack widths were monitored visually by using a magnifier but were also obtained, with greater accuracy, using the DIC images. It is data from the latter that are presented in the results tables.

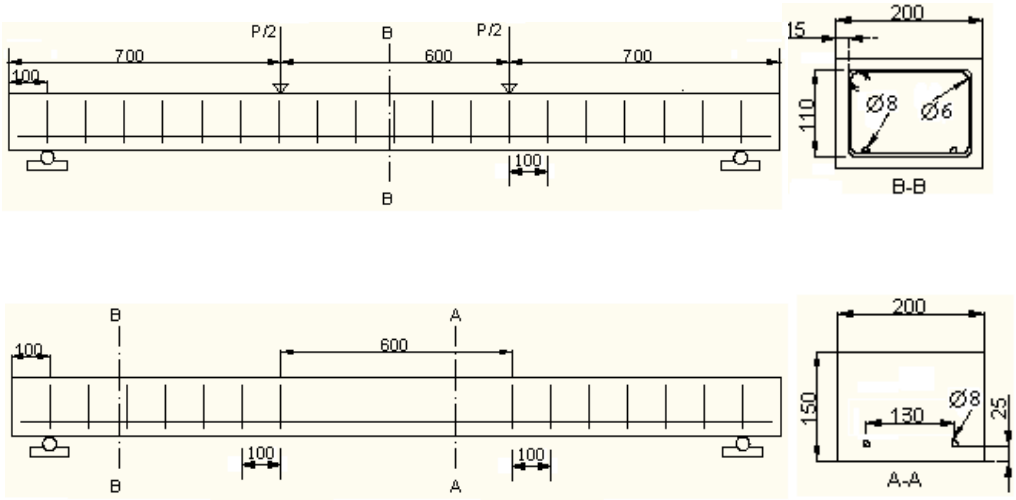

Figure 5.9a. Geometry of the specimens

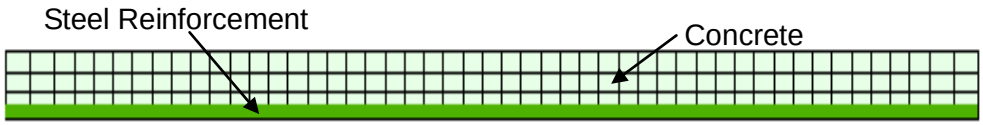

Figure 5.9b. Finite element mesh plot

Figure 5.10. Cracked Celsa Beam

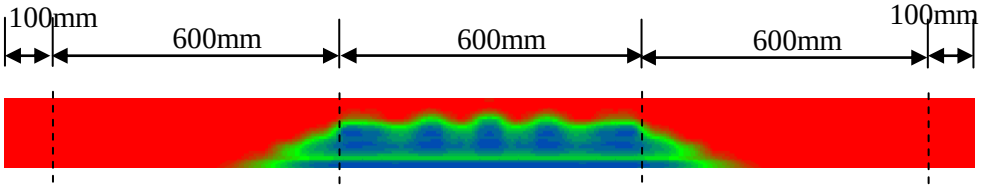

Figure 5.11a. Damage plot of specimen A at 2.6mm for non-local model

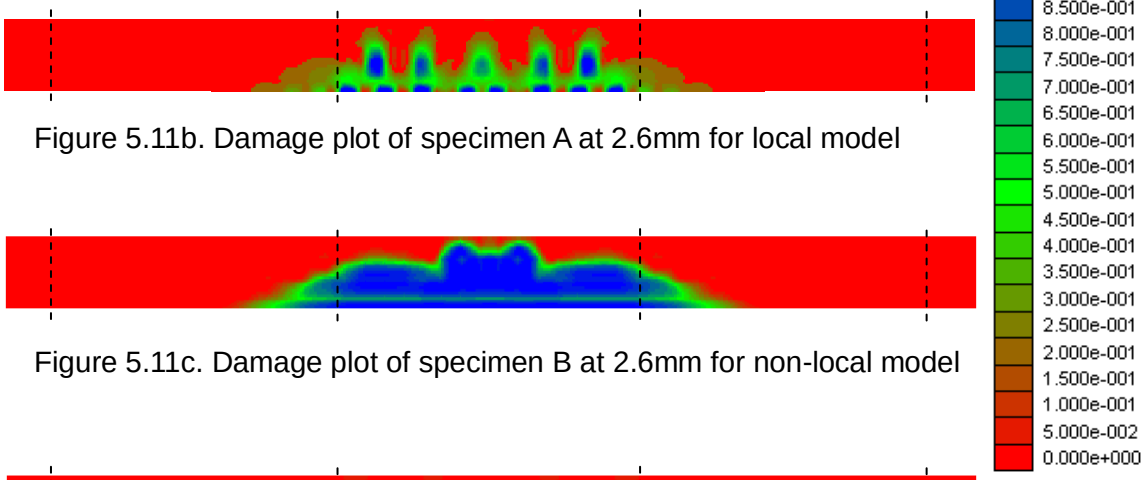

Figure 5.11b. Damage plot of specimen A at 2.6mm for local model

Figure 5.11c. Damage plot of specimen B at 2.6mm for non-local model

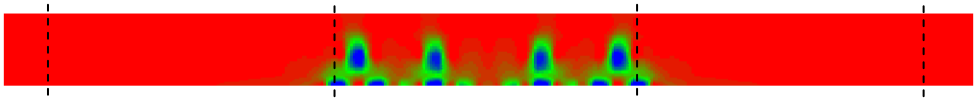

Figure 5.11d. Damage plot of specimen B at 2.6mm for local model

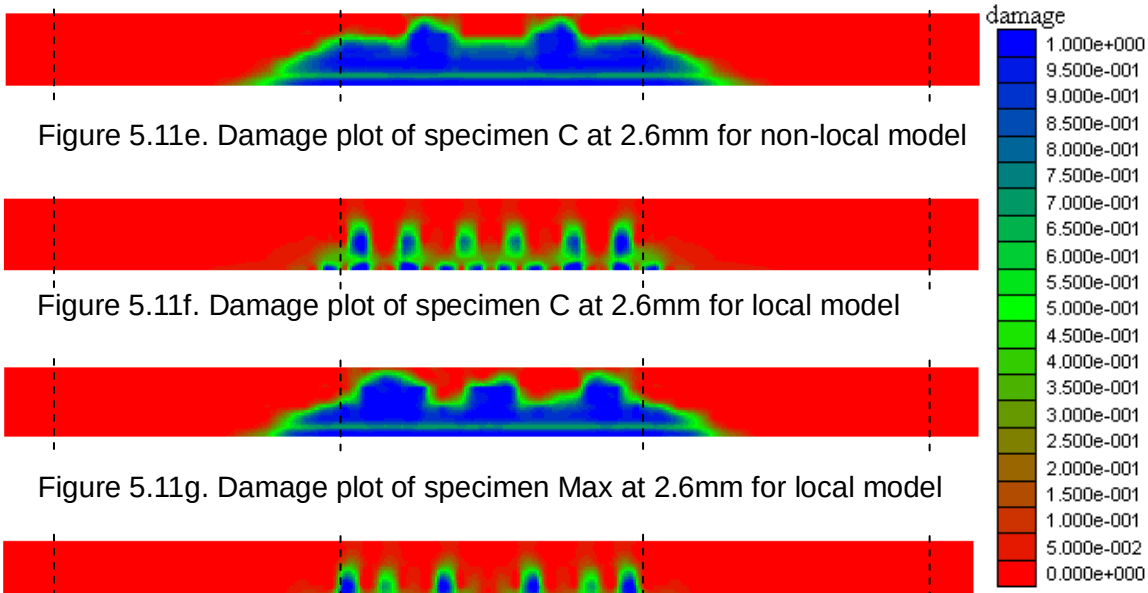

Figure 5.11e. Damage plot of specimen C at 2.6mm for non-local model

Figure 5.11f. Damage plot of specimen C at 2.6mm for local model

Figure 5.11g. Damage plot of specimen Max at 2.6mm for local model

Figure 5.11h. Damage plot of specimen Max at 2.6mm for local model

Load-deflection plots for each Celsa beams are shown in Figure 5.12a-d and strain profiles from analyses with the local and non-local models are presented in Figure 5.12e-h for the corresponding central displacements of 2.6mm.

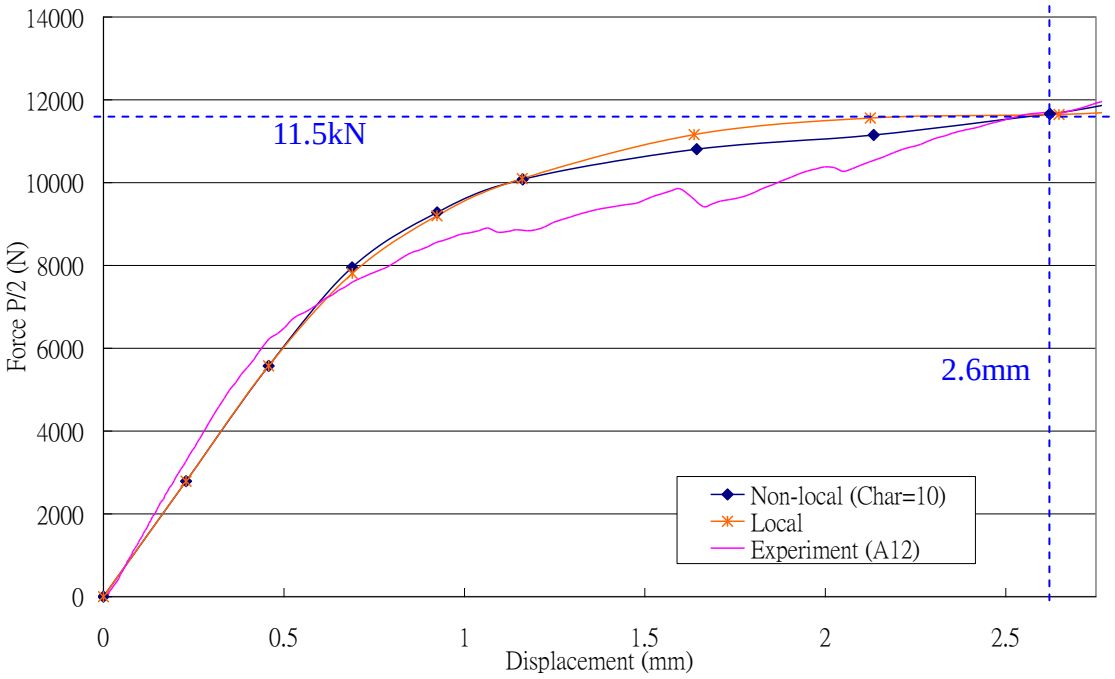

Figure 5.12a. Load – Central deflection Plot for Celsa beam A

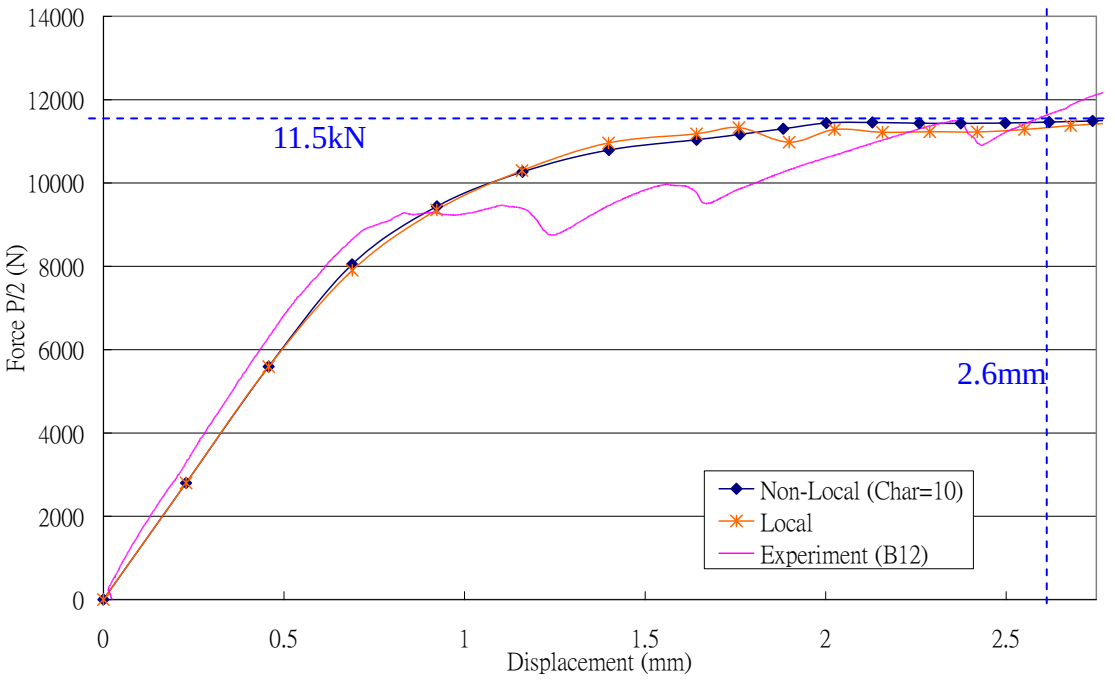

Figure 5.12b. Load – Central deflection Plot for Celsa beam B

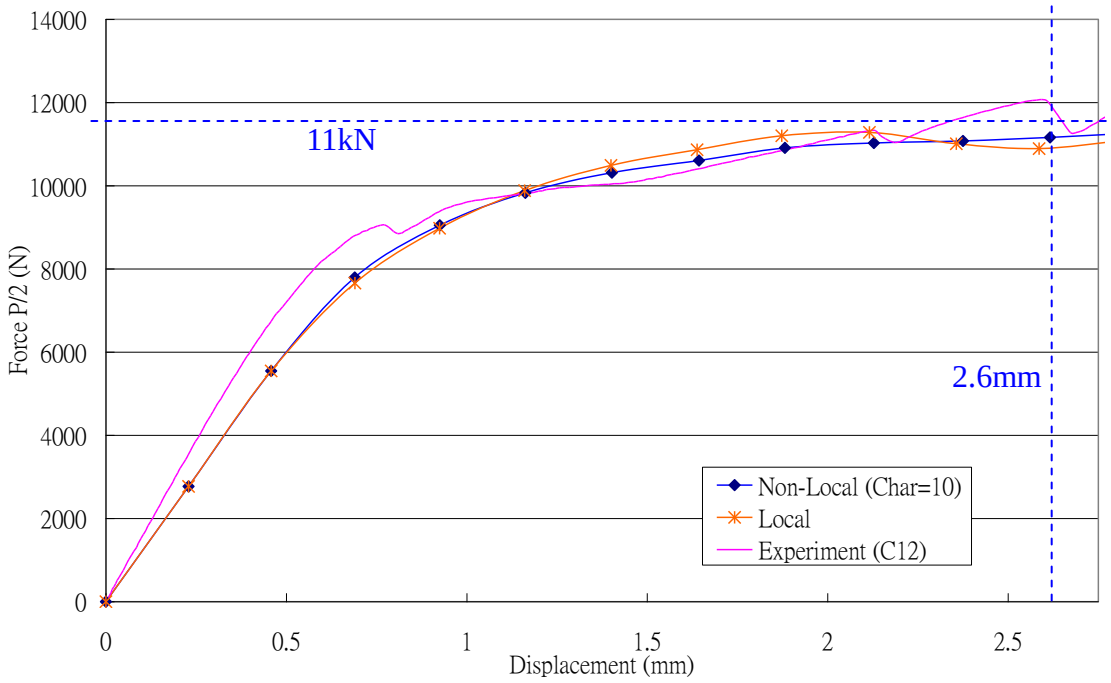

Figure 5.12c. Load – Central deflection Plot for Celsa beam C

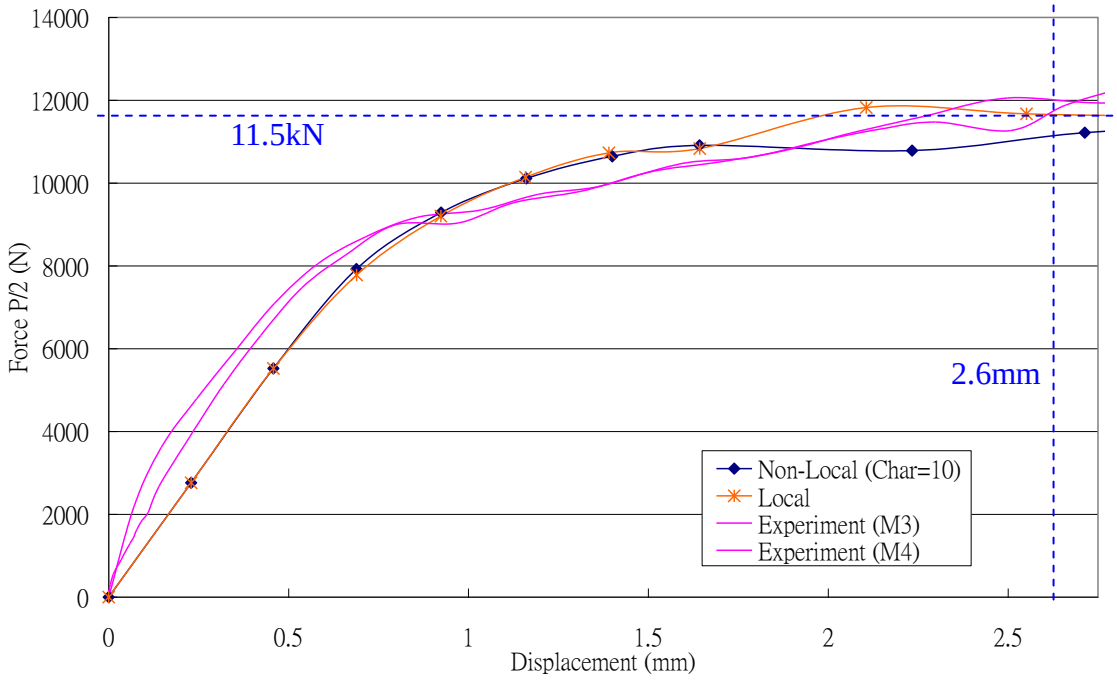

Figure 5.12d. Load – Central deflection Plot for Celsa beam Max

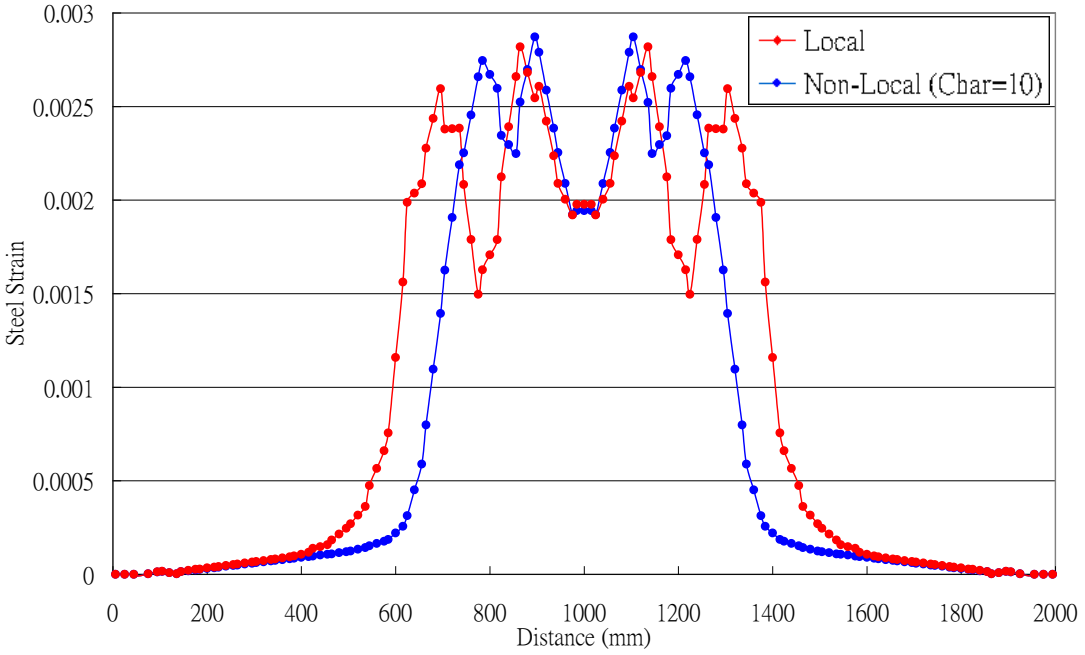

Figure 5.12e. Strain profile of both local and non-local approach for Celsa beam A at deflection level of 2.6mm

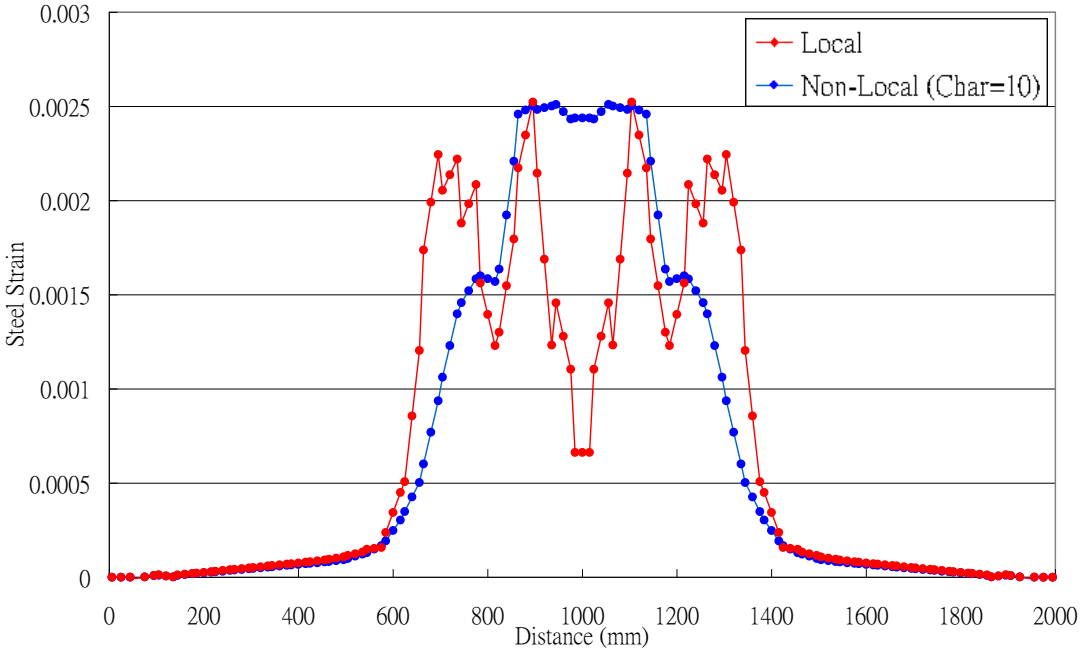

Figure 5.12f. Strain profile of both local and non-local approach for Celsa beam B at deflection level of 2.6mm

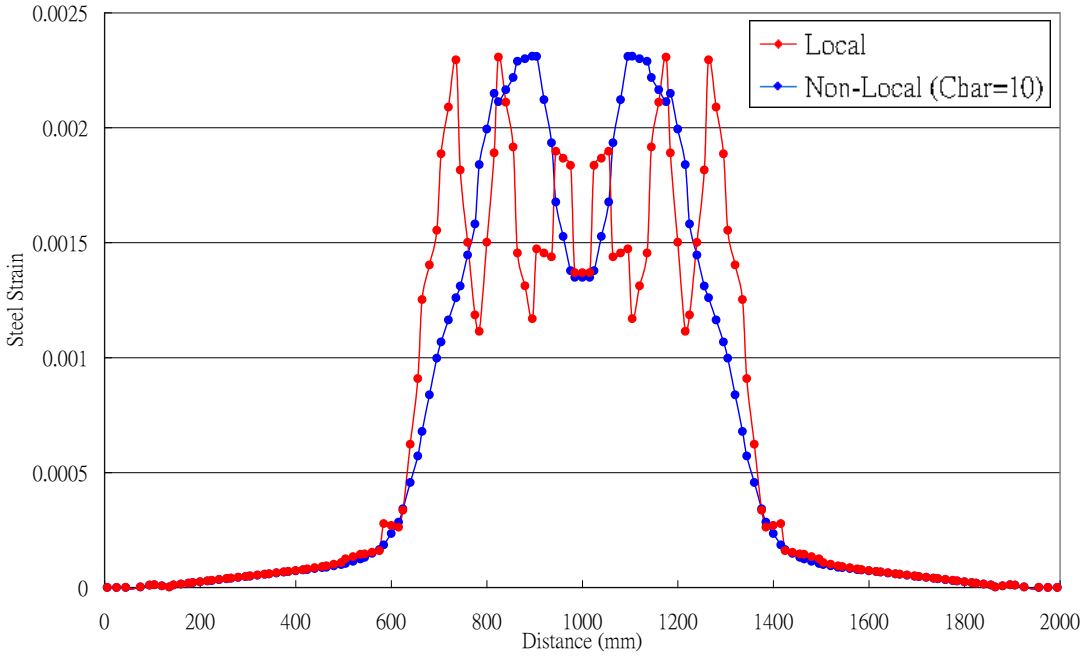

Figure 5.12g. Strain profile of both local and non-local approach for Celsa beam C at deflection level of 2.6mm

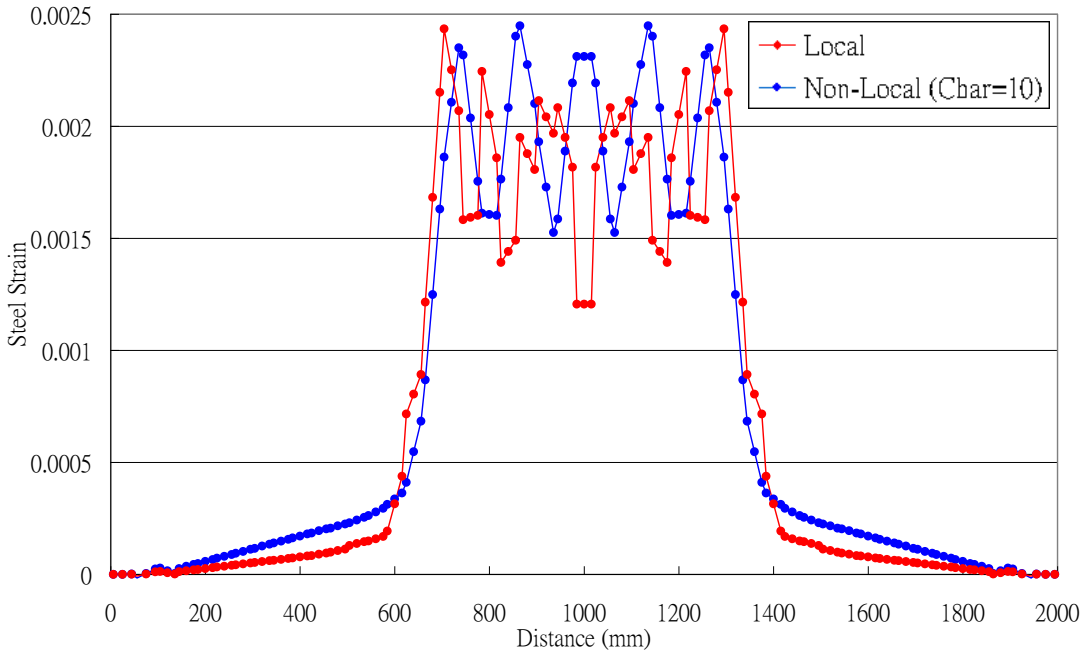

Figure 5.12h. Strain profile of both local and non-local approach for Celsa beam Max at deflection level of 2.6mm

The evolution of both strains development and damage with the local and non-local models are presented in Figure 5.13a-h below.

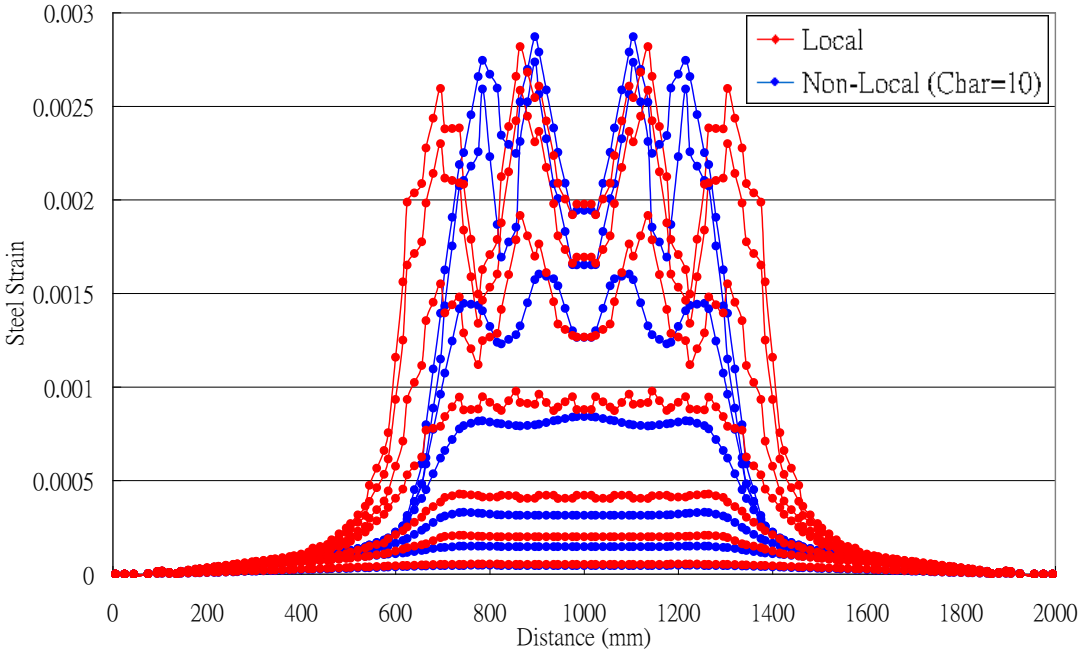

Figure 5.13a. Evolution of strain development of both local and non-local approach for Celsa beam A

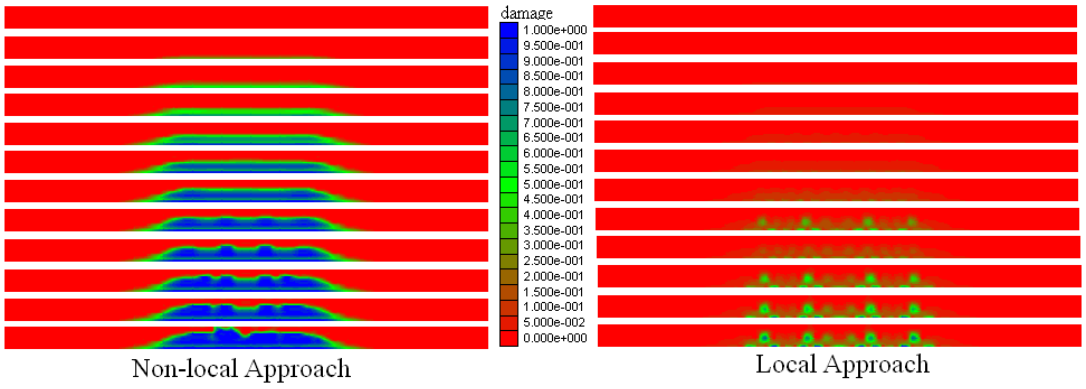

Figure 5.13b. Evolution of damage development of both local and non-local approach for Celsa beam A

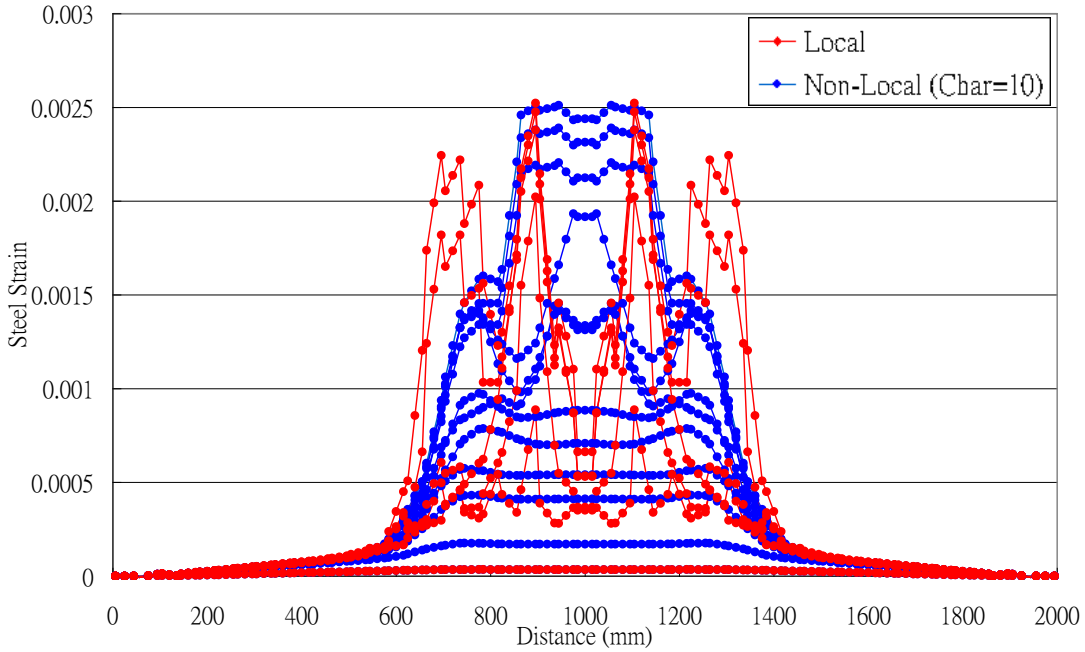

Figure 5.13c. Evolution of strain development of both local and non-local approach for Celsa beam B

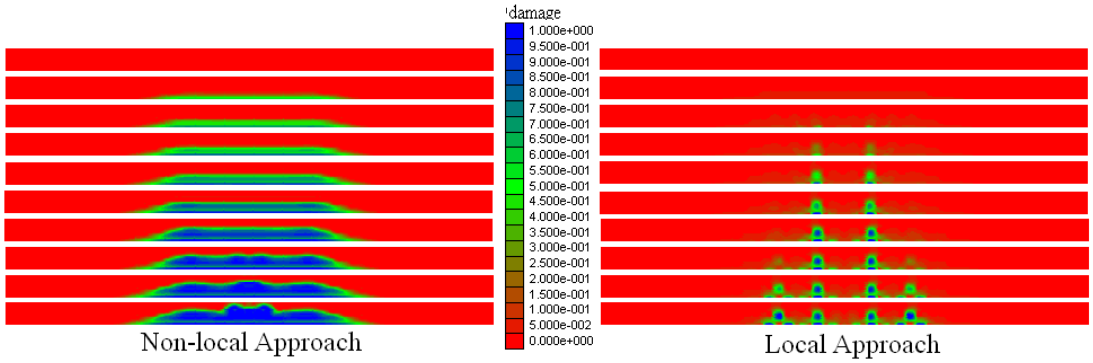

Figure 5.13d. Evolution of damage development of both local and non-local approach for Celsa beam B

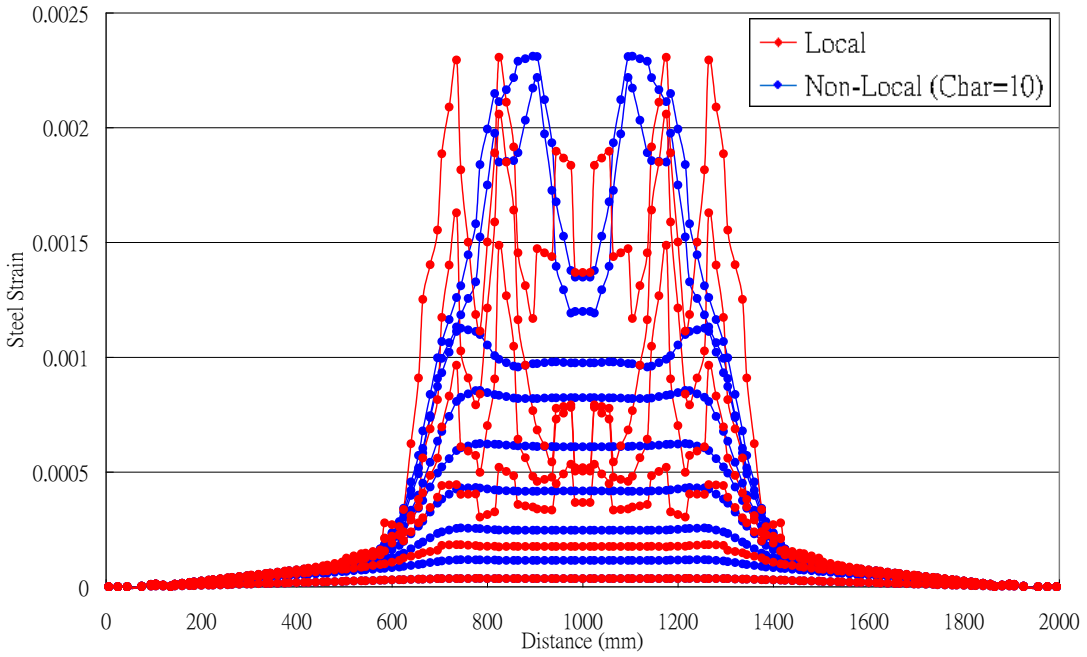

Figure 5.13e. Evolution of strain development of both local and non-local approach for Celsa beam C

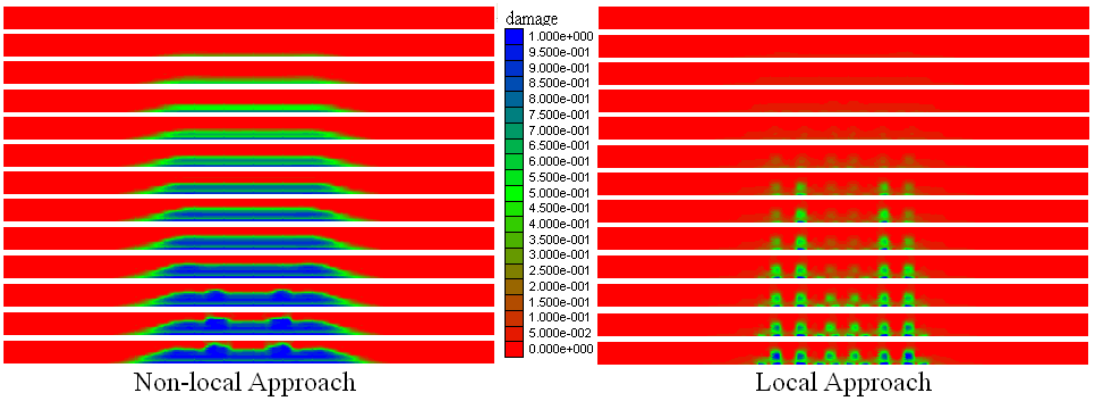

Figure 5.13f. Evolution of damage development of both local and non-local approach for Celsa beam C

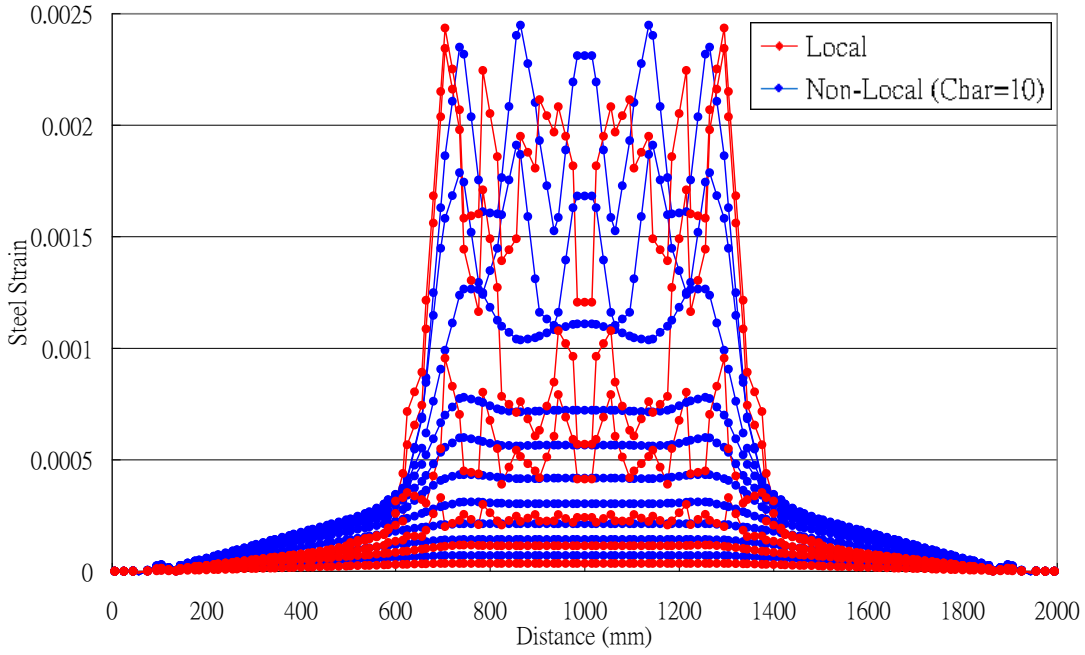

Figure 5.13g. Evolution of strain development of both local and non-local approach for Celsa beam Max

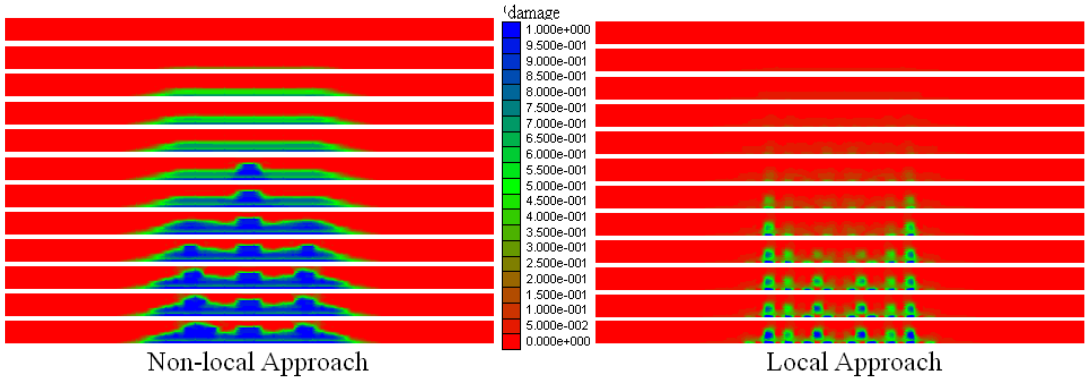

Figure 5.13h. Evolution of damage development of both local and non-local approach for Celsa beam Max

The results in terms of crack width and spacing, at a deflection of 2.6mm, are presented in Table 5.7.

Table 5.7. Results in terms of crack widths and spacings for the Cardiff Celsa Test

Specimens	Experiment			Numerical	Eurocode		
	$S_{r,m\,\exp}$ $S_{r,\max\,\exp}$ (mm)	$w_{k,m,\exp}$ $w_{k,\max,\exp}$ (mm)	Mean steel strain*	ε_{cmc}(Non-Local) ε_{cmc}(Local) $w_{k,m,num}$ ($S_{r,m\,\exp}$) $w_{k,\max,num}$ ($S_{r,\max,\exp}$)	Effective Strain ε_{eff}	$S_{r,m,code}$ $S_{r,\max,code}$ (mm)	$w_{k,m,code}$ $w_{k,\max,code}$ (mm)
A	128 233	0.40 0.66	0.0021	0.00235 0.00231 0.296 0.538	0.00175	118 200	0.206 0.351
B	115 252	0.32 0.50	N.A.	0.0018 0.00198 0.228 0.499	0.001735	118 200	0.204 0.347
C	119 274	0.29 0.39	0.00209	0.001786 0.00167 0.199 0.458	0.001801	118 200	0.212 0.360
Max	111 215	0.23 0.40	0.0018	0.0015 0.00172 0.191 0.370	0.00171	118 200	0.201 0.342

*Value based on mean concrete surface strain at bar level from DIC readings

For the Celsa beams, some localisation occurs at the selected working load level in both the local and non-local analyses although, as may be expected, the localisation is more pronounced in the local analysis. The overall response of the experimental beam is again well matched by the numerical responses.

The mean and maximum code crack spacings are close to the experimental values, as are the experimental and numerical mean strains, even though the latter were based on surface strain measurements.

The crack width calculated using the mean strain in the reinforcement and the mean experimental spacing is significantly below that measured in the experiments. This

suggests that in this case the finite element model underestimates the effective strain used for crack calculation.

5.6 Discussion

In order to aid discussion, three additional sets of comparisons are made in Tables 5.8a to 5.8h. These show differences between (Table 5.8a-5.8c) local analysis results and experimental, (Table 5.8d-5.8f) code (EC2) calculations and numerical results and (Table 5.8g-5.8h) code calculations and experimental results. In all cases, the differences between crack widths predicted with local and non-local analyses are inconsequential compared with the differences being discussed here; thus, only local results were used in the present comparison for clarity. Both the maximum and mean experimental crack spacings have been used in the calculations so that the differences due to the effective strains can be examined. The large natural variability of experimental crack spacings and major differences between values predicted by different codes of practice for this parameter have both been discussed earlier in the paper.

The experimental mean steel strains agree reasonably well with the numerical results with a difference of less than 20%, whilst the maximum difference between the experimental results and the code calculation is 41%. There is generally close agreement between the code predictions,, experimental results and numerical results for crack widths, as illustrated in Tables 5.8a-b, 5.8d-e and 5.8g-h. A similar comparison of the crack spacing is presented in Table 5.9.

Beeby and Scott (2005) compared 244 experimental values with crack widths from the CEB-FIP formulae and found the mean experimental/calculated width to be 0.81 with a standard deviation of 0.49. This provides a good indication of the level of variability of crack width data and suggests that the 40% discrepancy referred to above is consistent with the degree of variation generally found in experimental data.

Here no attempt has been made to evaluate the effects of creep, shrinkage or bond slip. Whilst crack width models use bond strength as a key parameter and (implicitly) assume that bond slip occurs, the fact that the mean reinforcement strains agree well with experimental values suggests that bond slip, at working load levels, may not be one of the dominating factors. The conclusion that cracking does not result from bond failure was reached by Beeby and Scott (2005), rather they suggest a model which represents the concrete in between inclined cracks which is illustrated in Figure 5.14.

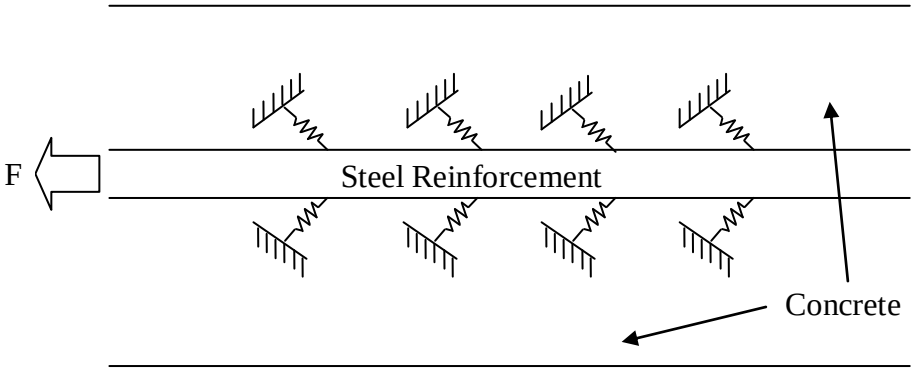

Figure 5.14. Schematic diagram of bar–concrete interaction proposed by Beeby and Scott (2005)

A conclusion from the present work is that, if common mean crack spacings are used, the numerical crack width results generally agree with code of practice predictions with

differences ranging from -42% to +59% and with the experimental results with differences ranging from -17% to +72%. If common max crack spacings are used these differences become -28% to +42% and -27% to +70% respectively. With respect to the reinforcement strains, it is concluded that, the numerical and experimental results match well match with differences ranging f from -20% to +10%. The differences between the numerical results and code of practice predictions for this parameter ranged from -27% to +41%.

Table 5.8a. Experimental & Local analysis of crack width with mean spacing

Example	$w_{k,m,\exp}$ (mm)	$w_{k,m,num}$ ($S_{r,m\exp}$) (mm)	$\left(\frac{Num-Exp}{Exp}\right)$ %
1	0.135	0.215	+59%
2 (3mm)	0.057	0.055	-4%
3(a)	0.40	0.296	-26%
3(b)	0.32	0.228	-29%
3(c)	0.29	0.199	-31%
3(max)	0.23	0.191	-17%

Table 5.8b. Experimental & Local analysis of crack width with max spacing

Example	$w_{k,\max,\exp}$ (mm)	$w_{k,\max,num}$ ($S_{r,\max,\exp}$) (mm)	$\left(\frac{Num-Exp}{Exp}\right)$ %
1	0.15	0.258	+72%
2 (3mm)	0.084	0.094	+12%
2 (4mm)	0.130	0.126	-3%
3(a)	0.66	0.538	-18%
3(b)	0.50	0.499	0%
3(c)	0.39	0.458	+17%
3(max)	0.40	0.370	-8%

Table 5.8c. Experimental & Local analysis of reinforcement strain

Example	Exp ε_{cmc}	Num ε_{cmc}	$\left(\frac{Num - Exp}{Exp}\right)$ %
1	0.00105	0.00104	-1%
2 (3mm)	0.00053	0.000531	0%
3(a)	0.0021*	0.00231	+10%
3(b)			
3(c)	0.00209*	0.00167	-20%
3(max)	0.0018*	0.00172	-4%

*Value at concrete surface, likely to be below value in centre of bar

Table 5.8d. Code (EC2) & Local analysis of crack width with mean spacing

Example	$w_{k,m,code}$ (mm)	$w_{k,m,num}$ ($S_{r,m,code}$) (mm)	$\left(\frac{Num - Code}{code}\right)$ %
1	0.217	0.308	+42%
2 (3mm)	0.039	0.028	-28%
3(a)	0.206	0.296	+44%
3(b)	0.204	0.228	+12%
3(c)	0.212	0.199	-6%
3(max)	0.201	0.191	-5%

Table 5.8e. Code (EC2) & Local analysis of crack width with max spacing

Example	$w_{k,\max,code}$ (mm)	$w_{k,\max,num}$ ($S_{r,m,code}$) (mm)	$\left(\frac{Num - Code}{code}\right)$ %
1	0.369	0.523	+42%
2 (3mm)	0.066	0.048	-27%
2 (4mm)	0.084	0.066	-21%
3(a)	0.351	0.538	+53%
3(b)	0.347	0.499	+44%
3(c)	0.360	0.458	+27%
3(max)	0.342	0.370	+8%

Table 5.8f. Code (EC2) & Local analysis of reinforcement strain

Example	Code ε_{cmc}	Num ε_{cmc}	$\left(\frac{Num - Code}{code}\right)$ %
1	0.000735	0.00104	+41%
2 (3mm)	0.00073	0.000531	-27%
2 (4mm)	0.00092	0.000734	-20%
3(a)	0.00175	0.00231	+32%
3(c)	0.001801	0.00167	-7%
3(max)	0.00171	0.00172	+1%

Table 5.8g. Code (EC2) & Experiments with mean spacing

Example	$w_{k,m,\exp}$ (mm)	$w_{k,m,code}$ ($S_{r,m\exp}$) (mm)	$\left(\frac{Code - Exp}{Exp}\right)$ %
1	0.135	0.152	+13%
2 (3mm)	0.057	0.076	+33%
2 (4mm)	0.090	0.0957	+6%
3(a)	0.40	0.224	-44%
3(b)	0.32	0.200	-38%
3(c)	0.29	0.214	-26%
3(max)	0.23	0.190	-18%

Table 5.8h. Code (EC2) & Experiments with max spacing

Example	$w_{k,\max,\exp}$ (mm)	$w_{k,\max,code}$ ($S_{r,\max,\exp}$) (mm)	$\left(\frac{Code - Exp}{Exp}\right)$ %
1	0.15	0.182	+21%
2 (3mm)	0.084	0.114	+36%
2 (4mm)	0.13	0.144	+10%
3(a)	0.66	0.408	-38%
3(b)	0.50	0.437	-13%
3(c)	0.39	0.493	+27%
3(max)	0.40	0.368	-8%

The final issue to be explored is the degree of agreement between the spacing of the localised strain bands in the numerical analyses and the experimental crack spacings. Numerical localisation occurred in all local analyses and, to some degree, in example 1 and some of example 3 in the non-local analyses. However, it may be seen from Table

5.9 that, generally, the spacings of the localised bands from local analyses are close to the corresponding experimental values as well as the code of practice values.

Table 5.9. Summary of crack spacing

Example	$S_{r,m\exp}$ (mm)	$S_{r,mFE}$ (mm)	$S_{r,m,code}$ (mm)	$S_{r,m,CEBFIP}$ (mm)
1	207	178	296	185
2 (3mm)	104	67	53	54
3A (Local)	128	110	118	125
3B (Local)	115	135	118	125
3C (Local)	119	108	118	125
3Max (Local)	111	116	118	125

5.7 Conclusions

- The overall responses of the beams in the numerical analyses agree well with those from the experiments.
- The mean steel strain computed in both local and non-local analyses are in good agreement with experimental data and the code of practice values.
- The predictions of mean crack widths show considerably variability: however, the differences between the predictions made with the method proposed here show slightly less overall discrepancy with the experimental values than with those from the EC2 formulae.
- A conclusion is that, if common mean crack spacings are used, the proposed method gives mean crack widths within ±59% of the EC2 formula and ±72% of experimental values; if common max crack spacings are used, the proposed method gives mean crack widths within ±42% of the EC2 formula and ±70% of experimental values.

- A conclusion regarding the values of reinforcement strain is that the numerical results match the experiment results well with differences ranging from ±20%, whilst the differences between the numerical results and code of practice predictions range from ±41%.
- Crack spacings calculated from the distance between the centres of localised bands in the finite element analyses showed good agreement with the experiments as well as with the EC2 code predictions and the CEB-FIP code predictions.

Chapter 6 – MODEL VALIDATION AND COMPARISON WITH EXPERIMENT

6.1 Introduction

In Chapter 4, experimental testing on bond and the surface cracking for concrete beams reinforced with different rib bars was described and presented. In Chapter 5, the smeared cracking approach is used to model the cracking behaviour of reinforced concrete beams under pure flexural bending.

In this chapter the numerical model described in Chapter 5 is used to simulate all of the reinforced beams tested experimentally. Here, comparisons will be made between experimental and numerical first cracking loads, ultimate loads and mean reinforcement strains.

The numerical procedures and meshes employed are the same as those described in Chapter 5 and thus this chapter concentrates solely on the results from the simulations and the comparisons.

6.2 Initial Cracking Load And Ultimate Load

In Chapter 4, the arrangement of the flexural beam tests was described and in these tests four different grades of steel reinforcing bar were used.

Six specimens were tested in Batch M and 12 specimens in Batches A, B and C. Comparisons of the results for initial cracking load and ultimate load from the finite element analyses, the experimental data and the code prediction are shown in Table 6.1. It is noted that in the ‘code predictions’ are based on EC2 assumptions with all partial factors removed and were calculated using mean material strengths. It is observed that the initial cracking load of the beam specimens increases slightly as the rebar bond

strength increases, whereas the ultimate load capacity of beam specimens increases significantly with bond strength.

Table 6.1 Initial cracking load capacity and ultimate load capacity of beam specimens

Beam Specimen	A1	A2	A3	A4	A5	A6	A7	A8	A9	A10	A11	A12	FEM	Code
Initial Cracking Load(kN)	8.2	8.2	7.5	8.8	8.6	9.3	9.1	9.0	8.6	9.5	8.8	8.9	7.8	-
Ultimate Load(kN)	24.3	22.7	23.1	22.4	23.5	24.3	23.4	24.1	23.4	24.4	23.6	23.8	23.2	21.0
Beam Specimen	B1	B2	B3	B4	B5	B6	B7	B8	B9	B10	B11	B12	FEM	Code
Initial Cracking Load(kN)	6.8	7.0	7.7	7.3	7.1	6.9	7.9	8.2	9.5	8.3	8.6	8.4	7.9	-
Ultimate Load(kN)	19.7	19.1	22.0	20.6	24.4	21.1	21.3	21.1	22.2	22.0	21.2	20.3	22.5	20.0
Beam Specimen	C1	C2	C3	C4	C5	C6	C7	C8	C9	C10	C11	C12	FEM	Code
Initial Cracking Load(kN)	11.1	10.0	8.3	9.1	9.9	7.6	9.1	9.5	9.8	9.6	8.6	9.1	7.66	-
Ultimate Load(kN)	29.4	28.2	27.8	27.5	23.4	23.0	23.0	22.9	22.6	23.5	22.7	23.0	22.6	20.5
Beam Specimen	-	-	-	-	-	-	M1	M2	M3	M4	M5	M6	FEM	Code
Initial Cracking Load(kN)	-	-	-	-	-	-	10.6	7.2	9.0	9.2	9.3	10.1	7.78	-
Ultimate Load(kN)	-	-	-	-	-	-	27.0	26.7	26.0	26.5	27.6	26.7	26.8	20.0

Table 6.2 Summary of initial cracking load capacity and ultimate load capacity of beam specimens

Beam Specimen		Minimum	Average	Maximum	Standard Derivation	FEM	Code
Batch A :	Initial Cracking Load	8.6	9.0	9.5	0.3	7.8	-
	Ultimate Load	22.4	23.6	24.4	0.6	23.2	21
Batch B :	Initial Cracking Load	7.9	8.5	9.5	0.5	7.9	-
	Ultimate Load	20.3	21.4	22.2	0.7	22.5	20.0
Batch C :	Initial Cracking Load	8.6	9.3	9.8	0.4	7.66	-
	Ultimate Load	22.6	23.0	23.5	0.3	22.6	20.5
Batch M :	Initial Cracking Load	7.2	9.3	10.6	1.2	7.78	-
	Ultimate Load	26.0	26.8	27.6	0.5	26.8	20.0

The results shown in Table 6.1 are summarized in Table 6.2, in which it can also be observed that both initial cracking loads and ultimate loads tend to increase with bond strength however, the degree of increase for initial cracking load capacity is small in comparison to that for the ultimate load capacity. Furthermore, the increase in ultimate load capacity is not proportional to the increase in bond strength. Theoretically there is little increase in overall flexural strength with bond strength, if the bond strength is sufficient to transfer the maximum force in the reinforcement to the concrete, with the maximum reinforcement force being that consistent with the theoretical ultimate flexural moment. There is not much difference between the performances of Batch A, Batch B, Batch C and Batch M for initial cracking loads, but Batch M has a noticeably higher ultimate load than the others.

There are some differences between the experimental and numerical results and this is believed to be mainly due to the fact that a non-slip model is used and de-bonding failure is not considered in numerical calculations, even although de-bonding failures did occur in the experimental beams. In the nonlinear range, the trends of the finite element and the experimental results are generally similar.

Furthermore, since de-bonding failure was not considered in the numerical calculations, no slip between the bars and concrete was simulated and therefore the rate of increase of tensile stresses in the concrete adjacent to a crack may have been greater in the model than in the experimental beams. As a consequence, the level of damage induced at the crack sections would be higher in the numerical calculations under the same applied load. It was therefore expected that the ultimate loads from the numerical simulations would be slightly lower than those obtained from the experiments. This was true for Batches A, C and M, but not for Batch B, for which the numerical peak load was slightly higher than the mean of the experimental results. It is observed that both the

standard deviations of the reinforcement ultimate strengths and compression concrete strengths in Batch B were significantly higher than in the other batches, which might due to variations in the manufacture of the steel reinforcement and the mixing/casting of concrete. It is therefore believed that the high numerical peak load in Batch B may be due to the variation in the strengths of the steel and concrete used for Batch B.

In addition, it is observed that the ultimate loads from the design code predictions are lower than experimental results and the numerical simulations. It is believed that this is due to the relatively conservative assumptions used in the design code predictions.

6.3 P–δ Curves

Comparisons of the curves of load versus deflection at the middle of the beam from the finite element analyses and the experimental data are made. The load-displacement curves in the linear range from beginning to initial concrete cracking can be seen in Figure 6.1.

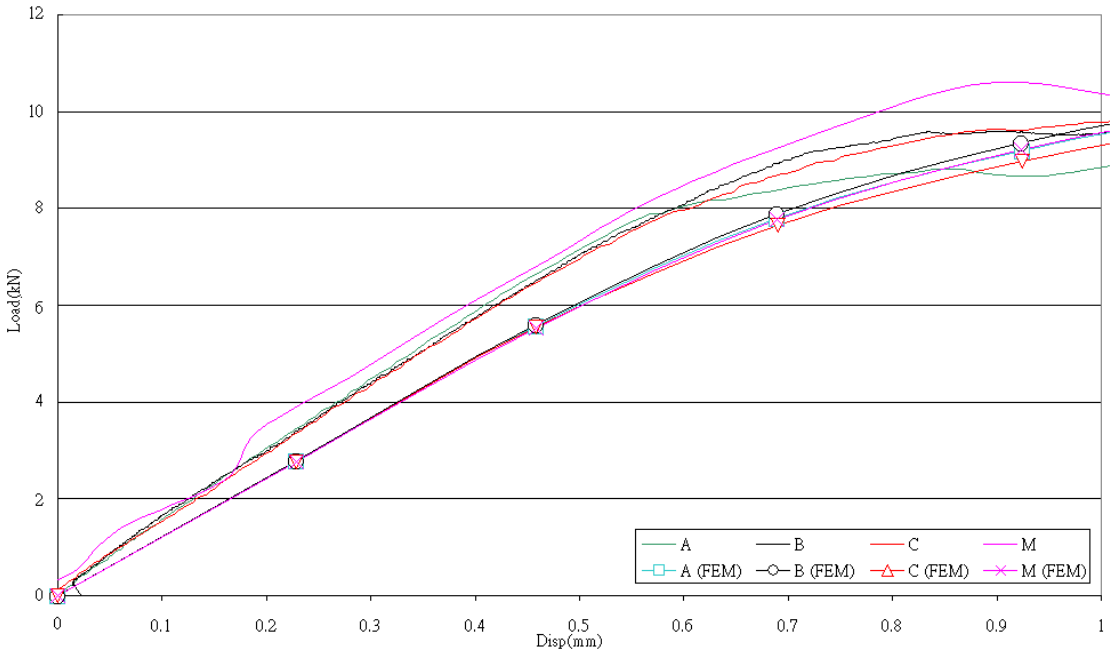

Figure 6.1. Comparisons of the curves of load versus deflection at the middle of the beam in linear and early non-linear range from the finite element analyses and the experimental data

In the elastic range, the numerical prediction is slightly higher than the experimental response, however the initial concrete cracking loads from the numerical simulation correlate well with those from the experiments. In general, the load-displacement plot above shows the results from numerical analysis agrees well with the results from the experimental data.

The load-displacement curves from initial concrete cracking to steel yield can be seen in Figure 6.2 below.

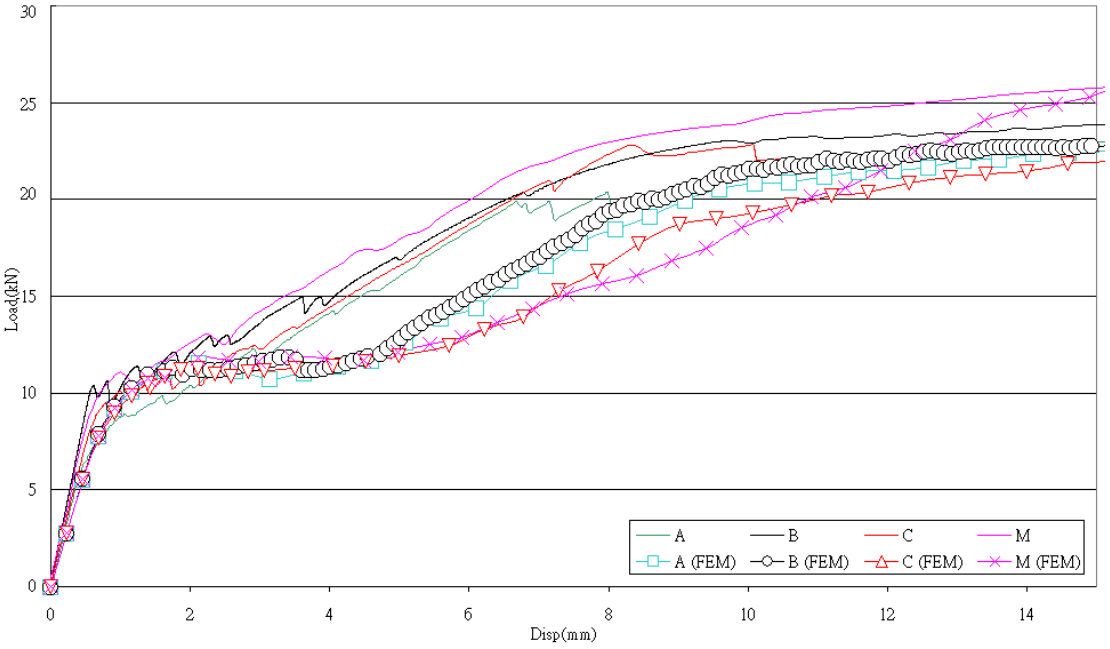

Figure 6.2. Comparisons of the curves of load versus deflection at the middle of the beam in non-linear range from the finite element analyses and the experimental data

Comparing the load-displacement curves from the numerical simulations and experimental results, it can be said that the simulation predicts well the load-displacement response of the flexural beam in the linear elastic stage, and reasonably well in the nonlinear range after the first cracking. However, the simulations

do underestimate the overall stiffness a little when compared with the experimental responses.

6.4 Average Tensile Strain in Main Steel Reinforcement

Comparisons of the load-average tensile strain plots from the finite element analyses and the experimental data for the main steel reinforced at mid-span are shown in Figure 6.3a-6.3c.

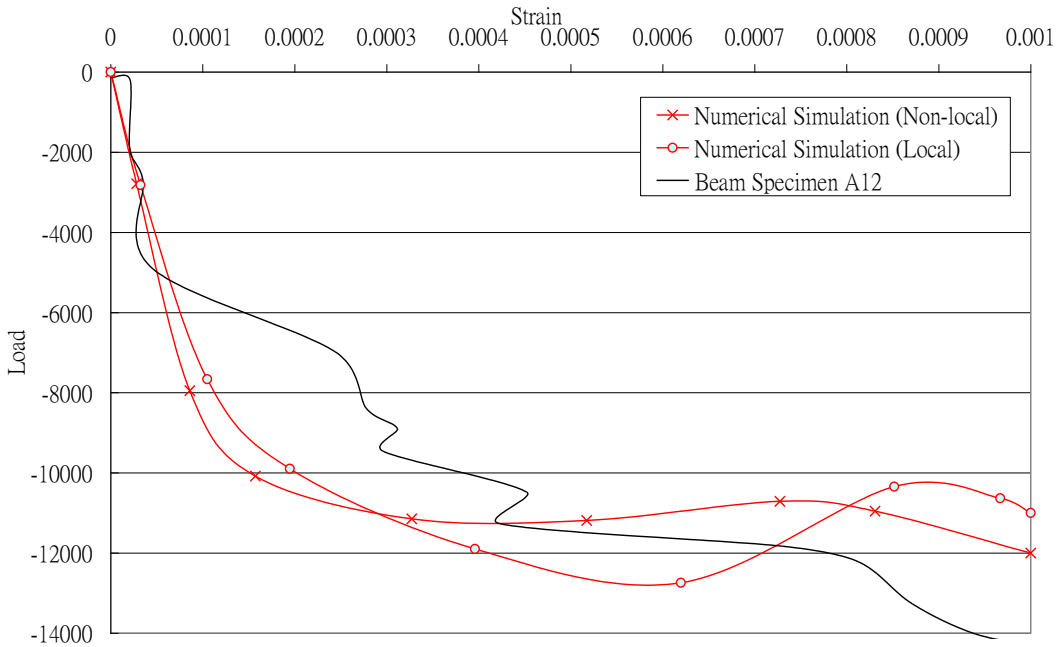

Figure 6.3a Comparisons of the load-tensile strain plots of Beam Specimen A12 between numerical analyses and the experimental result

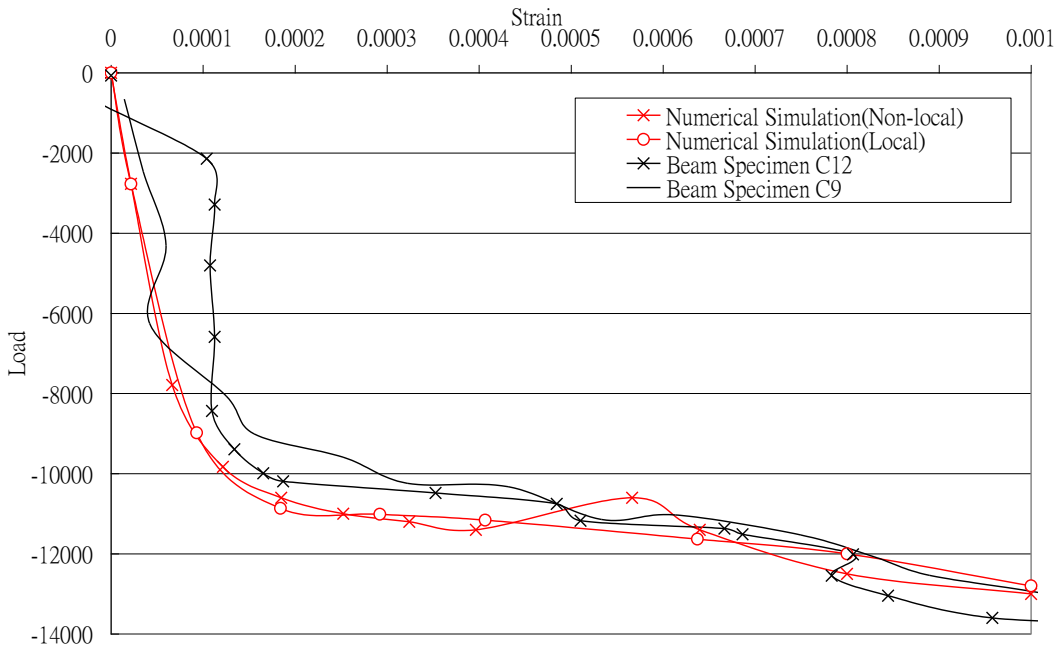

Figure 6.3b Comparisons of the load-tensile strain plots of Beam Specimen C9 between numerical analyses and the experimental result

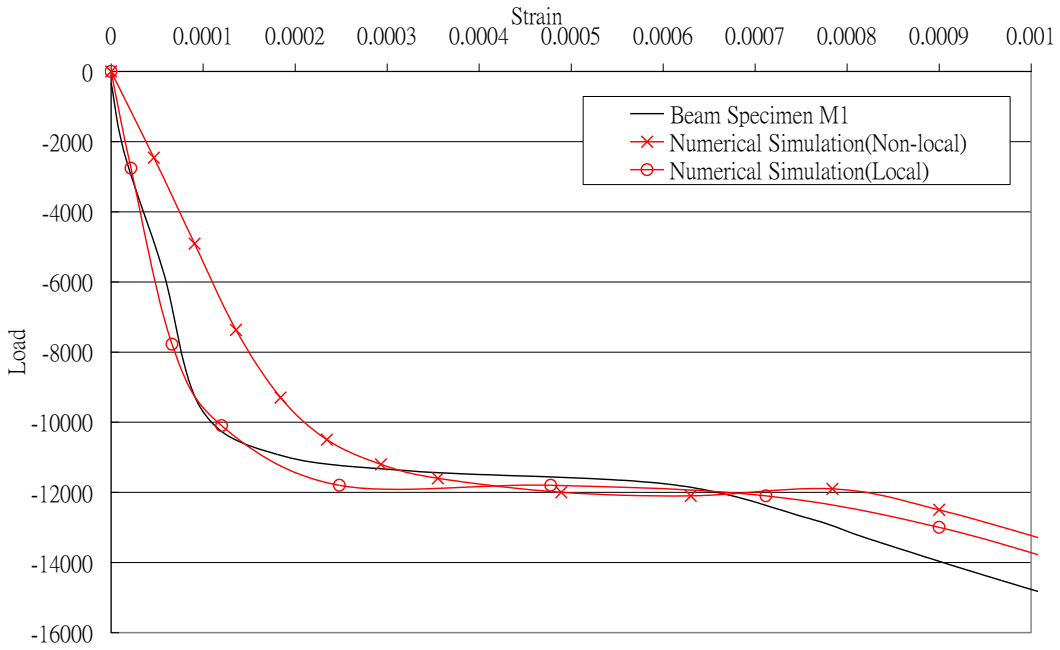

Figure 6.3c Comparisons of the load-tensile strain plots of Beam Specimen M1 between numerical analyses and the experimental result

For both the experimental and analytical responses in the linear elastic range, i.e. before concrete starts cracking, the strains from the finite element analysis correlate

well with those from the experimental data. In the nonlinear range, the trends of the finite element and the experimental results are also generally similar.

6.5 Evolution of Crack Development

In the flexural beam experiment, flexural cracks were found when the de-bonding failure happens at the middle of the beam. From experimental DIC measurements, it can be noted that the numbers of cracks were observed to increase with increasing load and the cracks then develop towards the top of the beam, as shown in Figure 4.11a-c.

Damage patterns at each applied load step from the numerical model are presented, in Figures 5.13a-h. The numerical crack patterns are assumed to be given by the areas of localised damage in Figures 5.13a-h. It is noted that the range of crack spacings (positions of localised damage) predicted by the numerical model (108mm-135mm) was similar to that measured in the experiments (111mm-128mm), and thus it may be stated that the crack patterns in numerical model and experimental beams agree well.

By comparing the crack evolution pattern from the numerical simulations and the experiment cracking evolution pattern, it can be observed that the cracks simulated by the numerical model (in general) have lower peak values and wider profiles, than in the experiments. The lower peak values and wider profiles may have resulted from the use of a large characteristic length in the non-local numerical model, however, the overall experimental crack evolution profiles agree reasonably well with those from the numerical model.

6.6 Discussion of Results

In order to calibrate the numerical model, the load-deflection response, the load-steel strain response, average crack widths and average crack spacings for each batch of flexural beams are compared with those generated from the numerical model.

Load-deflection responses of the beam specimens obtained from the experiments are compared to those from the numerical simulations, in Figure 6.1 and 6.2. These show good agreement in the elastic range and the predicted first cracking loads are promising. Once cracking occurs, the value of the peak loads tend to be slightly underestimated by the numerical model relative to those from the experiments. The yield loads from the experimental and numerical simulations are also in good agreement.

Comparisons of crack widths and crack spacings at a mid-deflection level of 2.6mm are shown for Beam Specimens A, B, C and M in Table 5.7, in which it is shown that the numerical responses in the elastic range, and in the range after first cracking but before yielding, agree well with both the code of practice calculations and the experimental results. Furthermore, in Table 5.7, and in Figure 6.3 above, the mean steel strain computed in both local and non-local analyses are also compared to the steel strains extracted from experimental data. Strain measurements were only considered up to the point of initial yielding and thus a comparison could not be obtained in the plastic range. However, the numerical model shows good agreement with the measured experimental structural response for both the elastic and inelastic ranges.

6.7 Comparison of Numerical Model and Experiment with Eurocode 2

An approach for crack control is presented in Eurocode 2 (EC2) and therefore the EC2 approach was applied to the present ‘Celsa’ beams. This allowed the comparison of this

code based method with the numerical predictions as well as with the experimental results to determine whether both the code formulae and proposed numerical model are applicable to crack prediction.

Allowing for the fact that the design approach of Eurocode 2 is conservative, it can be said that the agreement between the code calculations and experimental results, given in Table 5.8h, is reasonable.

The numerical predictions compare well with the code calculations, as illustrated in Table 5.8d-e, although it is noted that the numerical simulations slightly overestimated the crack widths when compared with the experimental results.

The steel strains from the numerical simulations, experiments, and code calculations are compared in Tables 5.8c and 5.8f. This comparison shows good agreement and confirms that the numerical model is able to predict the steel strains with good accuracy.

6.8 Conclusion

The above comparisons between code based formulae, experimental results and numerical simulations have considered a wide range of measured parameters which include concrete crack widths and crack spacings, reinforcement strains, load-displacement response, load-strain response, first cracking loads and yield loads. The comparisons show generally good agreement between the approaches. This gives confidence in the experimental data and validates the numerical (and calculation) approaches developed.

Chapter 7 – CONCLUSIONS AND THE WAY FORWARD

7.1 General

This chapter summarises the general conclusions that may be drawn from the present investigation and comments on the future outlook of the research. For specific conclusions, readers are directed to the conclusion sections at the end of each of the individual work chapters.

The research objectives, as outlined in the introduction to this thesis, were to:

1. Undertake bond tests to investigate and improve the understanding of the effect on bond stress of different reinforcement rib patterns and their relative rib area, f_R.
2. Undertake flexural beam experiments for concrete beams reinforced with different types of ribbed steel bar, in order to better understand the development of cracks and the effect on crack pattern of different rib patterns.
3. Simulate the crack development within reinforced concrete under tensile loading using a non-linear finite element model with a smeared crack approach.
4. Compare the results of a numerical simulation of the experimental works to validate the experimental results and to provide a worked example of how the numerical model could be used to predict the behaviour of steel reinforced concrete specimens.

In respect of each of these four objectives, the following research has been undertaken, which has led to the conclusions being made below.

7.2 Experimental Programme

7.2.1 Bond Tests

Bond experiments were designed and completed in which the bond performance of reinforcing steel bars with different rib patterns and so different f_R values were examined by pullout tests and bond beam tests. The main conclusions of these tests were:

- In both pullout tests and bond beam tests, a trend of higher bond stress, i.e. stronger bond, with steel bars with higher f_R value was observed.
- While the trend of higher f_R value implying stronger the bond is valid for both pullout tests and bond beam tests, it is noticed that this trend is more pronounced in the bond beam test. The presence of high confinement in the bond beam test is the main reason for this.

7.2.2 Flexural Beam Tests

In addition to the bond tests above, experiments using flexural beams were designed and completed, in which the SLS behavior, including the crack development of concrete beams reinforced with steel bars having different rib patterns and so different f_R values, was examined. The main conclusions were:

- The pattern of crack spacings and crack widths for different orientations of the reinforcing bar was largely random and therefore it is believed that the orientation of the steel bar does not affect the cracking behaviour.
- The average crack spacing of beams with stirrups in the middle zone was found to be about 100mm, which was the same as the spacing of the stirrups cast in the beam specimen, whereas the average crack spacing of beams with no stirrups in the middle zone was always greater than that. It is believed that the results for the beams with no stirrups in the middle zone are an appropriate representation of the

theoretical cracking behaviour of a simple reinforced concrete beam. However, in practice such a beam would always have stirrups throughout its length, the consequence of which is that the cracks will always tend to form at the location of the stirrups.

- There were more but smaller cracks formed in the concrete beams which were reinforced with steel bars with a greater f_R value, i.e. the maximum crack spacing and crack width decreased with an increasing f_R value.
- Bond strength is directly influenced by the f_R value in that bond strengths are greater the larger the f_R value, while on the other hand, crack width and crack spacing are likewise directly influenced by the f_R value in that crack width and crack spacing are smaller the greater the f_R value. As such the stronger the bond and the smaller the cracks when steel bar with a higher f_R value is used, although it should be recognized that the range of relative rib areas f_R considered was small.
- Adopting a DIC system to monitor the strain and displacement of the beam and to trace the evolution of crack development throughout the testing is a relatively accurate and reliable method for this size of specimen.

7.3 Numerical Simulation

In the numerical analyses, the concrete cracking is indicated by the damage in concrete. To capture the response of the concrete material behaviour, a damage constitutive concrete model has been presented and was used to simulate the reinforced concrete beam specimens for different types of simple loadings and structural test cases. The main findings of this research were:

- The overall response of the beams in the numerical analyses agrees well with that from the experiments.

- The mean steel strain computed in both local and non-local analyses are in good agreement with experimental data and the code of practice values.
- The predictions of mean crack widths show considerably variability, however the differences between the predictions made with the method proposed here show slightly less overall discrepancy with the experimental values than with those from the EC2 formulae.
- A conclusion is that, if common mean crack spacings are used, the proposed method gives mean crack widths within ±59% of the EC2 formula and ±72% of experimental values; if common maximum crack spacings are used, the proposed method gives mean crack widths within ±42% of the EC2 formula and ±70% of experimental values.
- A conclusion regarding the values of reinforcement strain is that, the numerical results match well with experiment results within ±20%, and the numerical results match with the code of practice predictions within ±41%.
- Crack spacings calculated from the distance between the centres of localised bands in the finite element analyses showed a good agreement with the experiments as well as the BS EN1992-1 (2004) predictions and the CEB-*fip* model code (1990) predictions.

7.4 Model Validation and Comparison with Experiments

In order to calibrate the numerical model, the load-deflection response, the load-steel strain response, average crack widths and average crack spacings for each batch of flexural beams were compared with those generated from the numerical model. The main findings of this research were:

- Load-deflection responses of the beam specimens obtained from the experiments were compared to those from the numerical simulations. These showed good agreement in the elastic range and the first cracking loads were promising. Once cracking occurs, the value of the peak loads tended to be slightly underestimated by the numerical model relative to those from the experiments. The yield loads from the experimental and numerical simulations were in good agreement
- Comparisons of crack widths and crack spacings at mid-span derived from the numerical responses in the elastic range, and in the range after first cracking but before yielding, agreed well with both the code of practice calculations and the experimental results.
- Comparisons of the mean steel strain computed in both local and non-local analyses with the values extracted from experimental data exhibited good agreement in both the elastic and inelastic ranges.
- When looking at crack widths, the numerical predictions compared well with the code calculations although the numerical simulations slightly overestimated the crack widths when compared with the experiment result.
- When looking at steel strains, the numerical simulations, experiments, and code calculations demonstrated good agreement and confirmed that the numerical model was able to predict the steel strains with good accuracy.

The above comparisons between code based formulae, experimental results and numerical simulations considering a wide range of measured parameters which included concrete crack widths and crack spacings, reinforcement strains, load-displacement response, load-strain response, first cracking loads and yield loads generally exhibited good agreement between the approaches considered. This gives

confidence in the experimental data and validates the numerical (and calculation) approaches developed.

7.5 Further Work

There are three main issues which need to be further investigated, before this numerical model can truly replicate the experimental work and move towards commercialisation. The first issue relates to the need to incorporate a bond model to appropriately predict the relationship between rib patterns and bond strength. The second issue relates to the need of further crack width and crack spacing flexural beam experiments with more rib patterns and a wider range of f_R values. The third issue relates to the need for further investigation of crack spacing in flexural beam experiments with various stirrup spacings.

The first issue requires an appropriate bond model to predict and model the bond strength of a particular design or layout of rib pattern. From the work of this thesis, it has been identified that the higher the f_R, the greater the bond strength, nevertheless the accuracy of the f_R value as derived by the formula provided in BS EN 15630 remains uncertain and the weighting of the contribution of each of the parameters to the f_R value might need further investigation.

The second issue requires more experimental testing of beams with different rib patterns having a wider range of f_R values to further investigate the corresponding effect on crack width and crack spacing formed under flexural bending. To provide a reliable set of experimental results for analysis, reinforcing bars with a wide range of f_R values have to be tested with sufficient number of specimens for each type of steel bar.

The third issue requires more flexural beam tests with various stirrup spacings, such as double or half of the current 100mm spacing, to further investigate the effect on crack spacing. To provide a reliable set of experimental results for analysis, a sufficient number of test samples with each stirrup spacing to minimize the effects of experimental error need to be tested.

REFERENCE

Abosrra L., Ashour A. F. and Youseffi M. (2011). Corrosion of steel reinforcement in concrete of different compressive strengths. Construction and Building Materials, 25:3915–3925.

Aifantis E. C. (1984). On the microstructural origin of certain inelastic models. Journal of Engineering Materials Technology (ASME), 106:326–330.

Al-Sulaimani G. J., Kaleemullah M., Basunbul I. A. and Rasheeduzzafar (1990). Influence of corrosion and cracking on bond behaviour and strength of reinforced concrete members. Proceedings of American Concrete Institute, Vol 87, No. 2, pp220-231.

Almusallam A. A., AL-Gahtani A. S. and Rasheeduzzafar A. R. A. (1996). Effect of reinforcement corrosion on bond strength. Construction and Building Materials, 10 (2), pp. 123–129

Alander C. (2002). The effect of rib geometry on crack widths and the service life of structures. 3rd International Symposium on Bond in Concrete: from Research to Standards. Budapest, Hungary, 343–350.

American Society of Civil Engineers. (1982). State-of-the-art report: Finite element analysis of reinforced concrete. Task Committee on Finite Element Analysis of Reinforced Concrete Structures.

Askes H. and Aifantis E. C. (2002). Numerical modeling of size effects with gradient elasticity: Formulation, meshless discretization and examples. International Journal of Fracture, 117, 347-358.

Askes H., Moratab I. and Aifantis E. C. (2008). Finite element analysis with staggered gradient elasticity. Computers & Structures, 86:1266-1279.

Bazant Z. P. (1984). Size effect in blunt fracture :Concrete, Rock, Metal. Journal of Structural Engineering, ASCE, V. 110, No.4, pp.518-535.

Bazant Z. P. (1991). Why continuum damage is nonlocal:Micromechanics arguments. Journal of Engineering Mechanics, 117(5), 1070-1087.

Bazant Z. P. and Jirásek M. (2002). Nonlocal integral formulations of plasticity and damage: Survey of progress. Journal of Engineering Mechanics ASCE, 128 1119-1149.

Bazant Z. P. and Pijaudier-Cabot G. (1988). Nonlocal continuum damage, localization instability and convergence. Journal of Applied Mechanics; 55:287-293.

Bažant Z. P. and Planas J. (1998). Fracture and Size Effect in Concrete and Other Quasibrittle Materials. CRC Press : Boca Raton and London.

Bazant Z. P. and Oh B. H. (1983). Crack band theory for fracture of concrete. Material and Structures; 16:155–177.

Bazant Z. P., Ožbolt J. and Eligehausen R. (1994). Fracture size effect : review of evidence for concrete structures. Journal of Engineering Mechanics, 120 (8), 2377-2398.

Bazant Z. P. and Sener S. (1998). Size effects in pullout tests. American Concrete Institute Material Journal 8, 347-351.

Beeby A. W. (2004). The influence of parameter φ/ρeff on crack widths. Structural Concrete, 5, No. 2, 71–83.

Beeby A. W. and Scott R. H. (2005). Cracking and deformation of axially reinforced members subjected to pure tension. Magazine of concrete research; 57(10):611-621.

Belytschko T. and Black T. (1999). Elastic crack growth in finite elements with minimal remeshing. Computational Methods in Applied Mechanics and Engineering; 45(5):601–620.

Belytschko T., Moës N., Usui S. and Parimi C. (2001). Arbitrary discontinuities in finite elements. International Journal for Numerical Methods in Engineering 50, 993-1013.

Beranek W. J. (1980). Experimental techniques for the analysis of deformation. Documentatoin-Page 119, Inst. TNO for building Material and Structural, Delft.

Bigaj A. J. (1995). Bond behaviour of deformed bars in NSC and HSC: experimental study. Delft University of Technology, Department of Civil Engineering, No. 25.5-95-II.

Borosnyoi A. and Balazs G. L. (2005). Models for flexural cracking in concrete : the state of the art. Journal of Structural Concrete; 6(2):53-62.

BS EN 197-1. (2000). Composition, specifications and conformity criteria for common cements. BSI London.

BS EN 1008. (2002). Mixing water for concrete. Specification for sampling, testing and assessing the suitability of water, including water recovered from processes in the concrete industry, as mixing water for concrete. BSI London.

BS EN 1992-1 (2004). Design of concrete structures — Part 1–1: General rules and rules for buildings. BSI London.

BS EN 10080. (2005). Steel for the reinforcement of concrete–Weldable reinforcing steel–General. BSI London.

BS EN 12620. (2008). Aggregates for Concrete. BSI London.

BS EN 12350-2. (2009). Testing fresh concrete, Part 2: Slump-test. BSI London.

Cabrera J. G. and Ghodussi P. (1992). Effect of reinforcement corrosion on the strength of steel concrete bond. Proceedings Proc International Conference On Bond in Concrete- from research to practice. Latvia. pp 10.11-10.24.

Carden E. P. and Fanning P. (2004). Vibration based condition monitoring: a review. Structural Health Monitoring, 3, 355–77.

Carmeliet J. (1999). Optimal estimation of gradient damage parameters from localization phenomena in quasi-brittle materials. Mechanics of cohesive-frictional materials, 4:1 - 16.

Carol I., Rizzi E and Willam K. (2002). An 'extended' volumetric/deviatoric formulation of anisotropic damage based on a pseudo-log rate. European Journal of Mechanics A-Solids 21(5) 747-772.

Carpinteri A., Chiaia B. and Ferro G. (1994). Multifractal scaling law for the nominal strength variation of concrete structures, Size Effect in Concrete Structures (eds. H. Mihashi, H. Okamura, Z.P. Bavzant), E.& F.N. Spon, London, pp. 193-206.

CEB-*fip* Model Code 1990. (1993). Comite Euro-International Du Beton. Thomas Telford, ISBN 0-7277-1696-4, Great Britain.

CEB Bulletin No. 151. (1982). Bond action and bond behaviour of reinforcement - State of the art report, Bulletin D'Information No.151, CEB.

Celsa Steel UK of Celsa Group. webpage : http://www.celsauk.com/

Chaboche J. L. (1979). Le concept de contrainte effective appliquee a l'elasticite ea a viscoplasticite en presence d'un endommagement anisotrope. Colloquium Euromech 115, Grenoble.

Chen A. C. T. and Chen W. F. (1975). Constitutive relations for concrete. Journal of Engineering Mechanics, ASCE, 101(8) 465-481.

Chi M. and Kirstein A. F. (1958). Flexural Cracks in Reinforced Concrete Beams. Journal of the American Concrete Institute, Vol. 54, No. 10, pp. 865-878.

Chinn J., Ferguson P. M. and Thompson J. N. (1955). Lapped Splices in R.C. Beam. Journal of the American Concrete Institute, Vol52, No.2, pp. 201-214.

Chou L., Niwa J. and Okamura H. (1983). Bond Model for Deformed Bars Embedded in Massive Concrete. Proceedings of 2nd Japan Concrete Institute Colloquium on Shear Analysis of RC Structures, Japan Concrete Institute, 45-52.

Cintron R. (2008). Strain Measurements with the Digital Image Correlation System: Vic-2D. Civil, Environmental, and Architectural Engineering, University of Colorado Boulder. Boulder.

Clark A. P. (1956). Crack in Reinforced Concrete Flexural Members. Journal of the American Concrete Institute; 52(8):851-862.

Comi C. and Perego U. (2001). Fracture energy based bi-dissipative damage model for concrete. International Journal of Solids and Structures; 38, 6427-6454.

Concrete Society. (1997). Guidance on radar testing of concrete structures, Technical Report No. 48.

Contrafatto L. and Cuomo M. (2006). A framework of elastic-plastic damaging model for concrete under multiaxial stress states. International Journal of Plasticity 22, 2272-2300.

Cox J. V. and Herrmann L. R. (1999). Validation of a plasticity bond model for steel reinforcement. Mechanics of Cohesive-frictional Materials 4(4): 361-389.

Darwin D., Zuo J., Tholen M. L., and Idun E. K. (1996). Development length criteria for conventional and high relative rib area reinforcing bars. American Concrete Institute Structural Journal, No. 3, 93 347-359.

de Borst R. (2001). Some recent issues in computational failure mechanics. International Journal for Numerical Methods in Engineering; 52:63–95.

de Borst R. and Guitierrez M. (1999). A unified framework for concrete damage and fracture models including size effects. International Journal of Fracture, 95(1-4), 583-599.

de Borst R. and Pamin J. (1996). Gradient plasticity in numerical simulation of concrete cracking, European Journal of Mechanics: A/Solids 15, 295–320.

de Borst R. and Mulhaus H. B. (1992). Gradient-dependent plasticity: formulation and algorithm aspect. International Journal for Numerical Methods in Engineering; 35:521–539.

Desmorat R., Gatuingta F. and Ragueneaua F. (2007). Nonlocal anisotropic damage model and related computational aspects for quasi-brittle materials. Engineering Fracture Mechanics. 74(10), 1539-1560.

Diederichs U. and SchneiderU. (1981). Bond Strength at High Temperature. Magazine of Concrete Research 33(115), 75–83.

Dufour F., Pijaudier-Cabot G., Choinska M. and Huerta A. (2008). Extraction of a crack opening from a continuous approach using regularized damage models. Journal of Computers and Concrete;5 (4) 375-388.

Edwards A. D. and Jannopoulos P. J. (1978). Local bond stress-slip relationship under repeated loading, Magazine of Concrete Research 30 (103), pp. 62–72.

Eligehausen R., Bertero V. V., and Popov E. P. (1983). Local Bond Stress-Slip Relationships of Deformed Bars Under Generalized Excitations: Tests and Analytical Model. Technical Report UCB/EERC-83. Earthquake Engineering Research Centre, University of California, Berkeley, California.

Elfgren L. and Noghabai K. (2002). Tension of reinforced concrete prisms. Bond properties of reinforcement bars embedded in concrete tie elements. Summary of a RILEM round-robin investigation arranged by TC 147-FMB Fracture mechanics to anchorage and bond. Material & Structures; 35:318–325.

Elfgren L. and Noghabai K. (2001). Tension of reinforced concrete prisms. Round robin analysis and tests on bond: a report from an investigation arranged by RILEM Technical Committee 147-FMB Fracture Mechanics to Anchorage and Bond. Research Report. Luleå University of Technology, Division of Structural Engineering.

Este G. and Willam K. (1994). Fracture energy formulation for inelastic behaviour of plain concrete. Journal of Engineering Mechanics, ASCE. 120(9): 1983–2011.

Fang C., Lundgren K., Chen L. and Zhu C. (2004). Corrosion influence on bond in reinforced concrete. Cement and Concrete Research, 34 11, 2159–2167.

Faria R., Oliver J. and Cervera M. (1998). A strain-based plastic viscous-damage model for massive concrete structures. International Journal of Solids and Structures 35(14), 1533-1558.

Farrar C. R., Doebling S. W. and Nix D. A. (2001). Vibration-Based Structural Damage Identification. Philosophical Transactions of the Royal Society: Mathematical, Physical & Engineering Sciences, 359(1778), 131 - 149.

Feenstra P. H. and de Borst R. (1995). A plasticity model and algorithm for mode-I cracking in concrete. International Journal for Numerical Methods in Engineering; 38: 2509-2529.

Ferguson P. M. (1996). Bond Stress: the state of art, Report by American Concrete Institute Committee 408, American Concrete Institute Journal 63(11),408.1-408.22.

Ferguson P. M., Turpin R. D. and Thompson J. N. (1955). Minimum bar spacing as a function of bond and shear strength, American Concrete Institute Journal 50(10), 869-888.

Ferrara L. and di Prisco M. (2001). Mode I fracture behaviour in concrete : non local damage modelling. ASCE Journal of Engineering Mechaniscs, 127(7):678-692

Ferrara L. and di Prisco M. (2002). A nonlocal approach with evolutionary internal length for the analysis of mode I fracture processes in concrete. In 15th ASCE Engineering Mechanics Conference, Columbia University, New York, NY.

Gambarova P. and Karakoc C. (1982). Shear confinement interaction at the bar to concrete interface. Proceedings of the Bond in Concrete International Conference, Peisley College of Technology, Scotland, pp 82-96. Applied Science Publishers (P. Bartos, editor).

Geers M. G. D., Borst R. D. and Peijs T. (1999). Mixed numerical experimental identification of nonlocal characteristics of random-fibre-reinforced composites. Composites Science and Technology, 59:1569-1578.

Gerstle W. H. and Ingraffea A. R. (1990). Does bond-slip exist? Micromechanics of Failure of Quasi-Brittle Materials, in Proceedings of the International Conference, Albuquerque,New Mexico (S.P. Shah, S.E. Swartz, and M.L. Wang, ed.).

Goto Y. (1971). Cracks formed in concrete around deformed tension bars. American Concrete Institute Journal, no. 4.

Goto Y. (1988). Computational modelling of concrete fracture, Ph.D. thesis, Department of Civil Engineering, Delft University of Technology, Delft, The Netherlands.

Giuriani E. and Plizzari G. A. (1985). Local Bond-Slip Law after Splitting of Concrete. Studie Ricerche, School for the Design of R.C. Structures, Milan University of Technology, 7:57-118.

Giuriani E., Plizzari G. A. and Schumm C. (1991). Role of stirrups and residual tensile strength of cracked concrete on bond, American Society of Civil Engineers, Journal of Structural Engineering 117(1), 1-18.

Grassl P. and Jirásek M. (2004). On mesh bias of local damage models for concrete Fracture Mechanics of Concrete Structures, Proceedings of FraMCoS-5, Vail, Colorado, pp. 255-262.

Guizani L. and Chaallal O. (2011). An experimental study on bond–slip in moderately confined concrete subjected to monotonic and cyclic loading using an experimental plan. Canadian Journal of Civil Engineering, 38(3): 272-282, 10.1139/L10-133

Guo L. P., Sun W., He X. Y. and Xu Z. B. (2008). Application of DSCM in prediction of potential fatigue crack path on concrete surface. Engineering Fracture Mechanics, 75 (3–4), pp. 643–651.

Han D. J. and Chen W. F. (1987). Constitutive modelling in the analysis of concrete structures. Journal of Engineering Mechanics, ASCE 113(4), 577-593.

Hanus J., Shield C. K. and French C. E. (2000). Development Length of GFRP Reinforcement in Concrete Bridge Decks. Technical Report MN/RC-2000-26 Minnesota Department of Transportation.

Harajli M. H., Hamad B. S. and Rteil A. A. (2004). Effect of Confinement on Bond Strength Between Steel Bars and Concrete. American Concrete Institute Structural Journal, V. 101, No. 5 (September–October): pp. 595–603.

Hillerborg A., Modeer M. and Peterson P. E. (1976). Analysis of crack formation and crack growth in concrete by means of F. M. and finite elements. Cement and Concrete Research, 6:773–782.

Hult J. (1977). Introduction and General Overview, in Continuum Damage Mechanics:Theory and Applications, D. Krajcinovic, J. Lemaitre Eds., CISM Springer-Verlag.

Jain A. K. (2000). Reinforced Concrete Limit State Design, Nem Chand and Bros. Roorkee.

Jefferson A. D. (2010). Finite element material models for concrete. Proceedings of The Tenth International Conference on Computational Structures Technology, Valencia, Review Paper.

Jirásek M. and Patzák B. (2002). Consistent tangent stiffness for nonlocal damage models. Computers & Structures; 80:1279-1293.

Jirasek M. and Zimmermann T. (1998). Rotating crack model with transition to scalar damage. Journal of Engineering Mechanics, ASCE, 124, 277-284.

Kachonov L. M. (1958). On the creep fracture time. Izvestiya Akademii Nauk USSR Otd. Tech. 8, 26–31.

Kaklauskas G., Gribniak V., Bacinskas D. and Vainiunas P. (2009). Shrinkage influence on tension stiffening in concrete members. Engineering Structures, Volume 31, Issue 6, Pages 1305–1312.

Małecki T., Marzec I., Bobinski J. and Tejchman J. (2007). Effect of a characteristic length on crack spacing in a reinforced concrete bar under tension. Mechanics Research Communications; 34: 460–465.

Karve S. R. and Shah V. L. (1994). Limit State Theory and Design of Reinforced Concrete Structures Publishers, Jal Tarang, 36 parvati, Pune-411009.

Mazars J. and Pijaudier-Cabot G. (1989). Continuum damage theory – application to concrete. Journal of Engineering Mechanics; 115(2): 345-365.

Krajcinovic D. and Fonseka G. U. (1981). The continuous damage theory of brittle materials. Part I: General theory. Journal of Applied Mechanics ASME 48, 809-815.

Le Bellego C., Dube J. F., Pijaudier–Cabot G. and Gerard B. (2003). Calibration of nonlocal damage model from size effect tests. European Journal of Mechanics. A/Solids, 22:33-46.

Lutz L. A. and Gergely P. (1967). Mechanics of bond and slip of deformed bars in concrete. Journal of the American Concrete Institute Proceedings, vol 64, no. 11, pp 711-721.

Macginley T. J. and Choo B. S. (1990). Reinforced Concrete – Design Theory and Examples, E. & F.N. Spon, London.

Mahnken R. and Kuhl E. (1999). Parameter identification of gradient enhanced damage models with the finite element method. European Journal of Mechanics. A/Solids, 18:819-835.

Maier T. (2004). Comparison of non-local and polar modelling of softening in hypoplasticity. International Journal for Numerical and Analytical Methods in Geomechanics, Volume 28, Issue 3, pages 251–268.

Małecki T., Marzec I., Bobinski J. and Tejchman J. (2007). Effect of a characteristic length on crack spacing in a reinforced concrete bar under tension. Mechanics Research Communications; 34: 460–465.

Malhotra V. M. (1976). Testing hardened concrete: non-destructive methods, monograph No. 9, American Concrete Institute, Detroit, MI, chapter 12.

Malvar L. J. (1992). Bond of Reinforcement under Controlled Confinement, American Concrete Institute Materials Journal, 89 (6), 593-601

Marchner T. and Vermeer P. A. (2000). Macromodelling of softening in noncohesive soils. In Proceeding of the International Symposium on Continuous and Discontinuous Modelling of Cohesive Frictional Materials, Stuttgart.

Marfia S., Rinaldi Z. and Sacco E. (2004). Softening behaviour of reinforced concrete beams under cyclic loading. International Journal of Solids and Structures 41, 3293-3316.

Mayer U. and Eligehausen R. (1998). Bond Behavior of Ribbed Bars at Inelastic Steel Strains. 2nd International Ph.D. Symposium in Civil Engineering, Budapest.

Mayer U. and Eligehausen R. (2002). Influence of the related rib area of reinforcement on the structural behaviour of RC members – does an optimal rib pattern exist? 3rd International Symposium on Bond in Concrete: from Research to Standards. Budapest, Hungary, 335–342.

Mazars J. (1986). A description of micro and macro scale damage of concrete structures. Engineering Fracture Mechanics 25(5/6).

Mazars J. and Pijaudier-Cabot G. (1989). Continuum damage theory – application to concrete. Journal of Engineering Mechanics, 115(2) 345-365.

McCabe S. L. and Pantazopoulou S. J. (1998). Evaluation of Bond Performance in Reinforced Concrete Structures, American Concrete Institute Special Publications, VOL 180, pages 1-22.

McCann D. M. and Forde M. C. (2001). Review of NDT methods in the assessment of concrete and masonry structures. Nondestructive Testing and Evaluation International 34, 71–84.

Mirmiran A. and Philip S. (2000). Comparison of acoustic emission activity in steel-reinforced and FRP-reinforced concrete beams. Construction and Building Materials, Vol. 14, pp.299-310.

Moës N., Dolbow J. and Belytschko T. (1999). A finite element method for crack growth without remeshing. International Journal for Numerical Methods in Engineering; 46:131–150.

Molina J. C., Calil Junior C. and Carreira M. R. (2009). Pullout strength of axially loaded steel rods bonded in glulam at a 45º angle to the grain. Materials Research. 2009; 12(4):427-432.

Morita S. and Fujii S. (1985). Bond-Slip Models in Finite Element Analysis, Proceedings of Japan-US Seminar on Finite Element Analysis of Reinforced Concrete Structures, Tokyo, American Society of Civil Engineers 348-363.

Morita S. and Kaku T. (1979). Splitting bond failures of large deformed reinforcing bars, American Concrete Institute Structural Journal, 76(1), pp. 93-110.

Mosalam K. M. and Paulino G. H. (1997). Evolutionary characteristic length method for smeared cracking finite element models. Finite Elements in Analysis and Design, 27:99-108.

Nagatomo K. and Kaku T. (1992). Bond behaviour of deformed bars under lateral compressive and tensile stresses. Proceedings of International Conference on Bond in Concrete, Riga.

Narayanan R. S. and Beeby A. W. (2005). Designers' Guide to EN1992-1-1 and EN1991-1-2. Eurocode 2: Design of concrete structures. General rules and rules for buildings and structural fire design. Thomas Telford, UK.

Neville A. and Aitkin P-C. (1998). High performance concrete-an overview. Materials and Structures, 31(206):111–7.

Ng P. L., Lam J. Y. K. and Kwan A. K. H. (2010). Tension Stiffening in concrete beams. Part1 FE Analysis. Structures and Buildings, Institution of Civil Engineers; 163(SB1):19-28.

Ngo D. and Scordelis A. C. (1967). Finite element analysis of reinforced concrete beams. American Concrete Institute Journal; 64(3):152–163.

Noghabai K. (1998). Effect of Tension Softening on the Performance of Concrete Structures. Doctoral Thesis:21. Luleå University of Technology, Division of Structural Engineering. pp. 150.

Oliver J. (1995). Continuum modeling of strong discontinuities in solid mechanics using damage models. Computational Mechanics 1995; 17:277–296.

Oliver J., Cervera M. and Manzoli O. (1999). Strong discontinuities and continuum plasticity models: the strong discontinuity approach. International Journal of Plasticity; 15:319–351.

Oliver J. and Huespe A. E. (2004a). Continuum approach to material failure in strong discontinuity settings. Computational Methods in Applied Mechanics and Engineering; 193:3195–3220.

Oliver J. and Huespe A. E. (2004b). Theoretical and computational issues in modelling material failure in strong discontinuity scenarios. Computational Methods in Applied Mechanics and Engineering; 193:2987–3014.

Oliver J., Huespe A. E. and Samaniego E. (2003). A study on finite elements for capturing strong discontinuities. International Journal for Numerical Methods in Engineering; 56:2135–2161.

Oliver J., Huespe A. E., Samaniego E. and Chaves W. V. (2004c). Continuum approach to the numerical simulation of material failure in concrete. International Journal for Numerical and Analytical Methods in Geomechanics; 28:609–632.

Oliver J., Huespe A. E., Pulido M. D. G. and Chaves E. (2002). From continuum mechanics to fracture mechanics: the strong discontinuity approach. Engineering Fracture Mechanics, 69: 113-136.

Orangun C. O. and Breen J. E. (1977). Revaluation of test data on development length and splices. American Concrete Institute Journal, Proceedings, No. 3, 74 114-122.

Orangun C. O. and Breen J. E. (1975). Strength of anchored bars: A re-evaluation of test data on development length and splices, Research Report No. 154-3F, Center for Highway Research, University of texas at Austin, Austin, Tex., 78.

Ožbolt J. (1993). General microplane model for concrete. In Wittmann, F., editor, 1st Bolomey Workshop numerical Models in Fracture Mechanics of Concrete, pages 173-187. A.A. Balkema, Rotterdam.

Pamin J. (1994). Gradient-dependent plasticity in numerical solution of localization phenomena, Ph.D. thesis, Delft University of Technology, The Netherlands.

Patzak B. and Jirasek M. (2004). Adaptive Resolution of Localized Damage in Quasi-brittle Materials. Journal of Engineering Mechanics, 130, 6.

Peerlings R. H. J., de Borst R., Brekelmans W. A. M. and de Vree J. H. P. (1996). Gradient enhanced damage for quasi-brittle materials. International Journal for Numerical Methods in Engineering 39(19), 3391 – 3403.

Peerlings R. H. J., de Borst R., Brekelmans W. A. M. and Geers M. G. D. (1998). Gradient-enhanced damage modelling of concrete failures. Mechanics of Cohesive-Frictional Materials; 4:339–359.

Peerlings R. H. J., Geers M. G. D., de Borst R. and Brekelmans W. A. M. (2001). International Journal of Solids and Structures 38, 7723-7746.

Pijaudier-Cabot G. and Bazant Z. P. (1987). Non-local damage theory. ASCE Journal of Engineering Mechanics; 113: 1512-1533.

Pijaudier-Cabot G., Haidar K. and Dube J. (2004). Non-local damage model with evolving internal length. International Journal of Numerical Analytical Methods in Geomechanics; 28:633–652

Pillai S. U. and Menon D. (1999). Reinforced Concrete Design, Tata McGraw-Hill Publishing Company Limited.

Plizzari G. A., Schumm C. and Giuriani E. (1987). The Effect of Residual Tensile Strength of Cracked Concrete on the Local Bond-Slip Law after Splitting. Studie Ricerche, School for the Design of R.C. Structures, Milan University of Technology, 9:129-155.

Rabczuk T. and Belytschko T. (2007). A three-dimensional large deformation meshfree method for arbitrary evolving cracks. Computer Methods in Applied Mechanics and Engineering; 196:2777–2799.

Rashid Y. R. (1968). Analysis of prestressed concrete pressure vessels. Nuclear Engineering and Design 7(4), 334-344.

Rehm G. (1961). On the basic behaviour of bond between steel and concrete. Deutscher Ausschuß für Stahlbeton, No. 138, Verlag W. Ernst & Sohn, Berlin.

Rehm G. (1969). Evaluation criteria for high-bond rebars. Festschrift Riisch.

Rehm G. and Eligehausen R. (1979). Bond of Ribbed Bars Under High-Cycle Repeated Loads. American Concrete Institute Journal, Vol.76, No.2, 297-309.

RILEM Technical Committee 90-FMA. (1987). Fracture mechanics of concrete/applications. Second Draft Report over the State of the Art, Division of Structural Engineering, Lulea University of Technology, S-951 87 Lulea, Sweden.

Reinhardt H. W. and Van der Veen C. (1990). Splitting Failure of a Strain-Softening material due to Bond Stresses. In Alberto Carpinteri, editor, Applications of Fracture Mechanics to Reinforced Concrete, pages 333-346, Turin. Elsevier Applied Science.

Robert M. and Benmokrane B. (2010). Effect of aging on bond of GFRP bars embedded in concrete. Cement and Concrete Composites. Volume 32, Issue 6, Pages 461–467.

Rots J. G. (1985). Bond-slip simulations using smeared cracks and/or interface elements. Research Report 85-01, Structural Mechanics Group, Department of Civil Engineering, Delft University of Technology, Delft, The Netherlands.

Ru C. Q. and Aifantis E. C. (1993). A simple approach to solve boundary-value problems in gradient elasticity. Acta Mechanica, 101, 59-68.

Salari M., Saeb S., Willam K. J., Patchet S. and Carrasco R. (2004). A coupled elastoplastic damage model for geomaterials. Computer Methods in Applied Mechanics and Engineering 193, 2625-2643.

Schneider U. (1985). Properties of materials at high temperatures – Concrete & RILEM-Committee 44-PHT Department of Civil Engineering, University of Kassel, Kassel.

Sfantos G. K. and Aliabadi M. H. (2007). Multi-scale boundary element modelling of material degradation and fracture. Computer Methods in Applied Mechanics and Engineering 196 (7), 1310–1329.

Shima H., Chou L. L. and Okamura H. (1987). Micro and macro models for bond in reinforced concrete, Journal of the Faculty of Engineering, University of Tokyo, 39(2), 133-194.

Simo J. C. and Ju J. W. (1987). Strain and stress based continuum damage models—I. Formulation. International Journal of Solids and Structure 23, 821–840.

Simo J. C., Oliver J and Armero F. (1993). An analysis of strong discontinuities induced by strain-softening in rate-independent inelastic solids. Computational Mechanics; 12:49–61.

Simone A., Wells G. N. and Slugs L. J. (2003). From continuous to discontinuous failure in a gradient-enhanced continuum damage model. Computer Methods in Applied Mechanics and Engineering, 192:4581-4607.

State of the Art Report: FRP Reinforcement, 440R-32, American Concrete Institute, Detroit, MI.

Sukumar N., Moës N., Moran B. and Belytschko T. (2000). Extended finite element method for three-dimensional crack modelling. International Journal for Numerical Methods in Engineering; 48:1549–1570.

Sutton M. A., Orteu J-J. and Schreier H. (2009). Image Correlation for Shape, Motion and Deformation Measurements, Springer.

Tammo K., Lundgren K. and Thelandersson S. (2009). Nonlinear analysis of crack widths in reinforced concrete. Magazine of Concrete Research;61(1): 23–34.

Tassios T. P. (1979). Properties of bond between concrete and steel under load cycles idealizing seismic actions. Paris : Comite Euro-International du Beton.

Tastani S. P. and Pantazopoulou S. J. (2002). Experimental evaluation of the direct tension pull-out bond tests. Proceedings-Bond in concrete-from research to standards. Budapest.

Tepfers R. (1973). A Theory of Bond applied to Overlapped Tensile Reinforcement Splices for Deformed Bars. PhD thesis, Chalmers University of Technology, Goteborg.

Tepfers R. (1979). Cracking of concrete cover along anchored deformed reinforcing bars. Magazine of Concrete Research 31(106), 3-12.

Tholen M. L. and Darwin D. (1998). Effect of reinforcing bar deformation pattern on flexural ductility. American Concrete Institute Structural Journal, 95(1):37-42.

Tijssens M. G. A., Sluys B. L. J. and van der Giessen E. (2000). Numerical simulation of quasi-brittle fracture and damaging cohesive surfaces. European Journal of Mechanics A/Solids;19:761–779.

Tong P. and Pian T. H. H. (1973). On the convergence of the finite element method for problems with singularity. International Journal of Solids and Structures; 9:313–321.

van der Veen C. (1992). Bond in Concrete: from Research to Practice. Cryogenic bond behaviour and tensions stiffening, Proceedings of International Conference. CEB-RTU (Riga Technical University), Riga (latvia), 10.1-10.10.

van Mier J. G. M. (1997). Fracture processes of concrete. CRC Press.

van Mier J. G. M. (2004). Reality behind fictitious cracks? In Li V. C., Leung C. K. Y., William K. J. and Billington S. L., editors. Fracture Mechanics of Concrete Structures, pages 11-30.

Weibull W. (1939). A Statistical Theory of the Strength of Materials. Proc. Royal Swedish Institute for Engineering Research. Stockholm, Sweden. 151:1.

Willam K. J. and Warnke E. P. (1975). Constitutive models for triaxial behaviour of concrete. Proceeding of International Association for Bridge and Structural Engineers, Report 19, Zurich, Switzerland, 1-30.

Wu H. Q. and Gilbert R. I. (2009). Modeling short-term tension stiffening in reinforced concrete prisms using a continuum-based finite element model. Engineering & Structures; 31(10):2380-2391.

Yamao H., Chou L. and Niwa J. (1984). Experimental Study on Bond Stress-Slip Relationship, Proceedings of Japan Society of Civil Engineers, No. 343, 219-228.

Zuo J. and Darwin D. (2000). Splice strength of conventional and high relative rib area bars and high strength concrete, American Concrete Institute Structural Journal, No. 4, 97, 630-641.

APPENDIX I – EVOLUTION AND DEVELOPMENT OF CRACKS IN FLEXURAL BEAM SPECIMENS

This appendix contains the evolution and development of cracks for all flexural beam specimens in Batch A, C and Max without stirrups in the central 600mm zone, of which typical figures in each batch have been reported in Chapter 4.

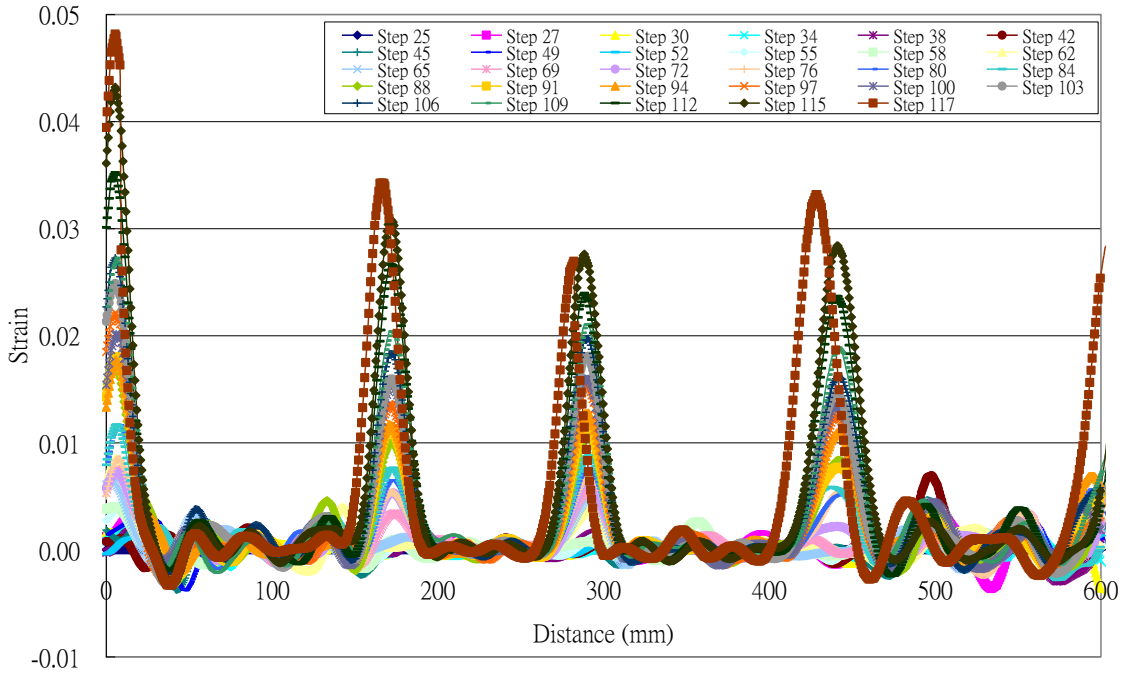

The evolution and development of cracks in Beam specimen A7

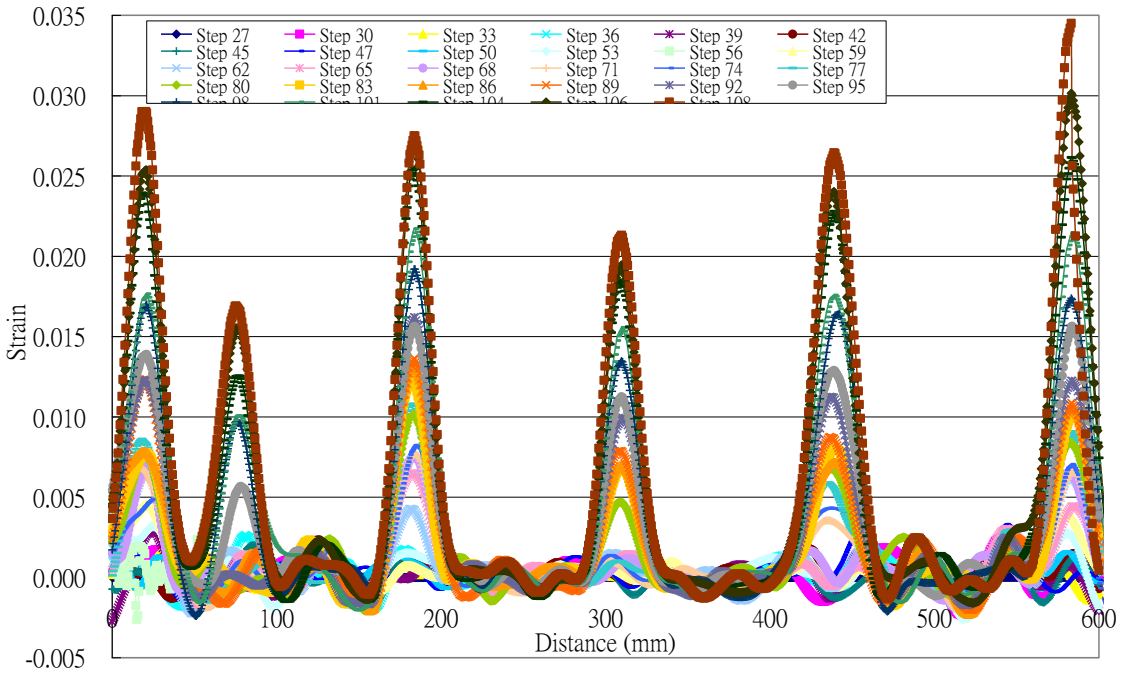

The evolution and development of cracks in Beam specimen A8

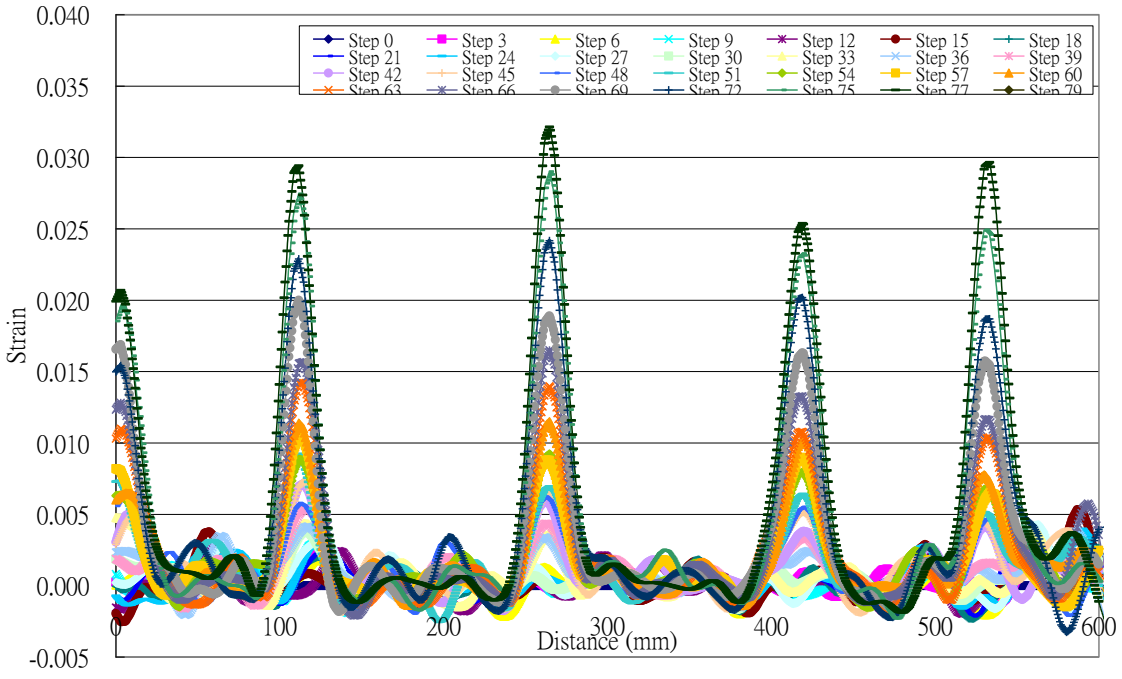

The evolution and development of cracks in Beam specimen A9

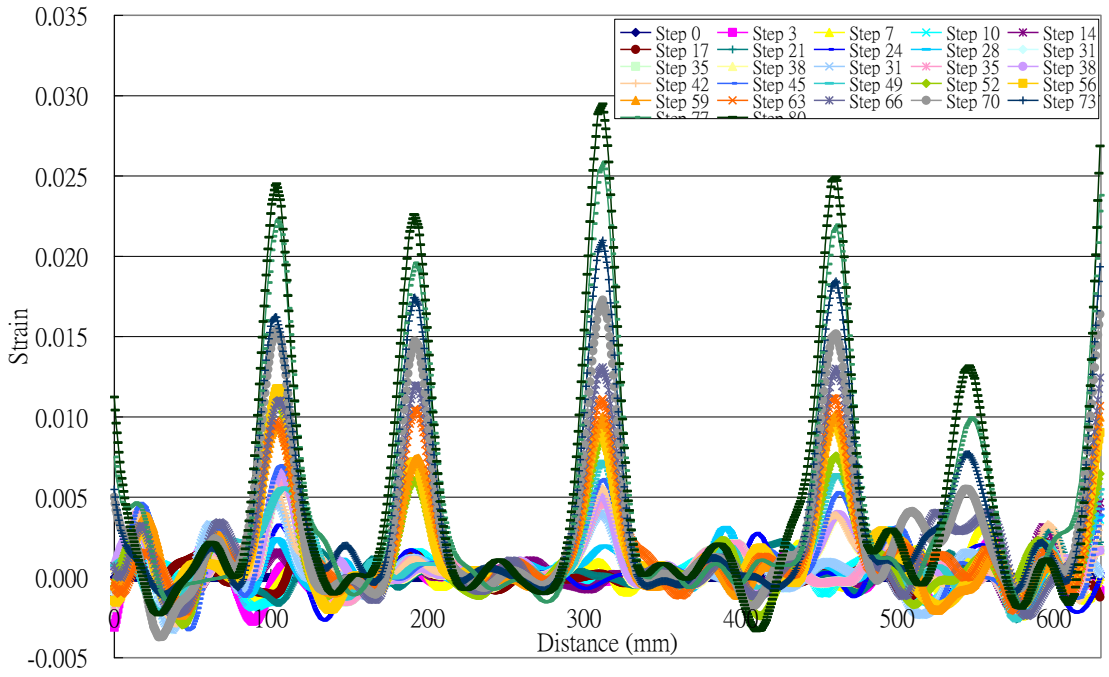

The evolution and development of cracks in Beam specimen A10

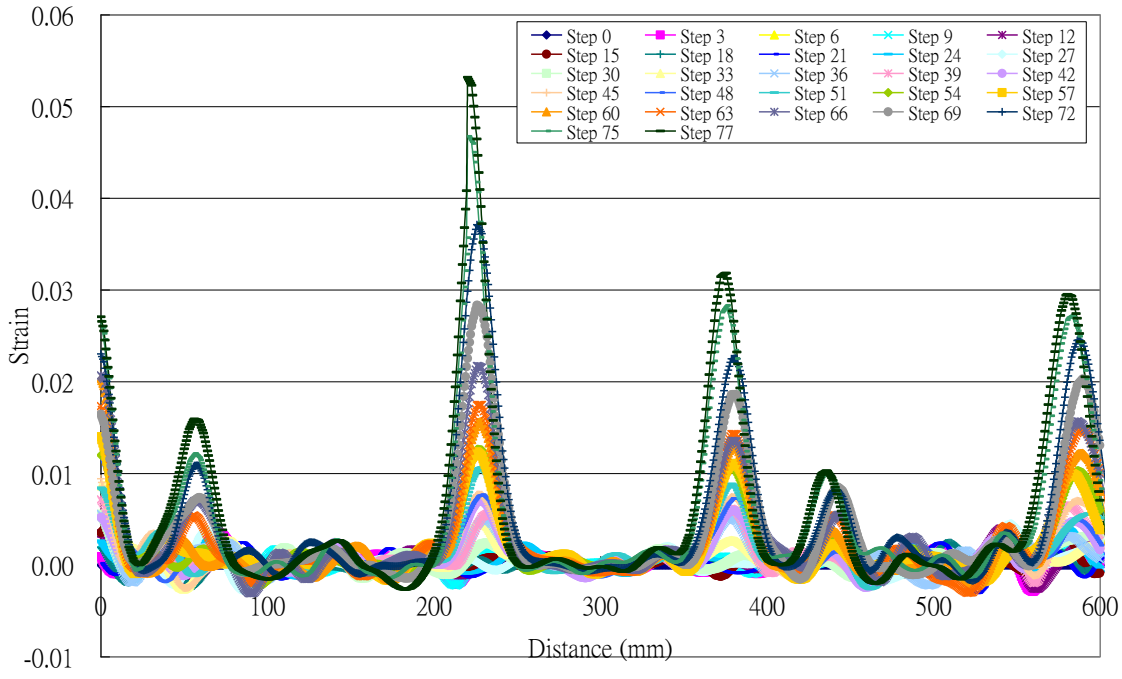

The evolution and development of cracks in Beam specimen A11

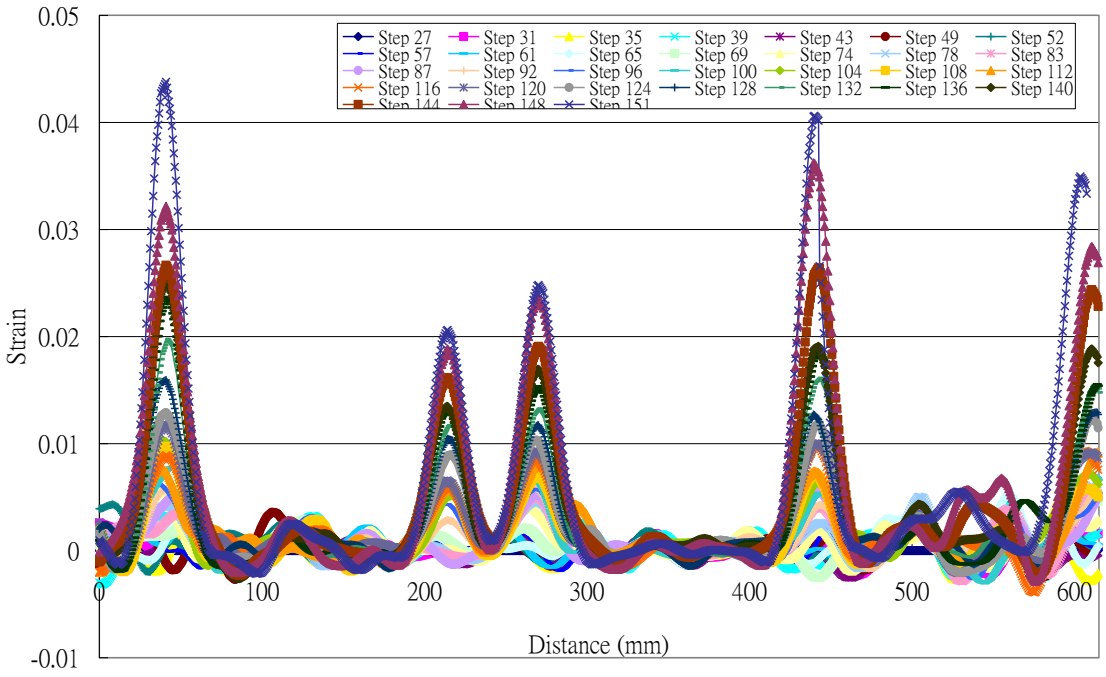

The evolution and development of cracks in Beam specimen A12

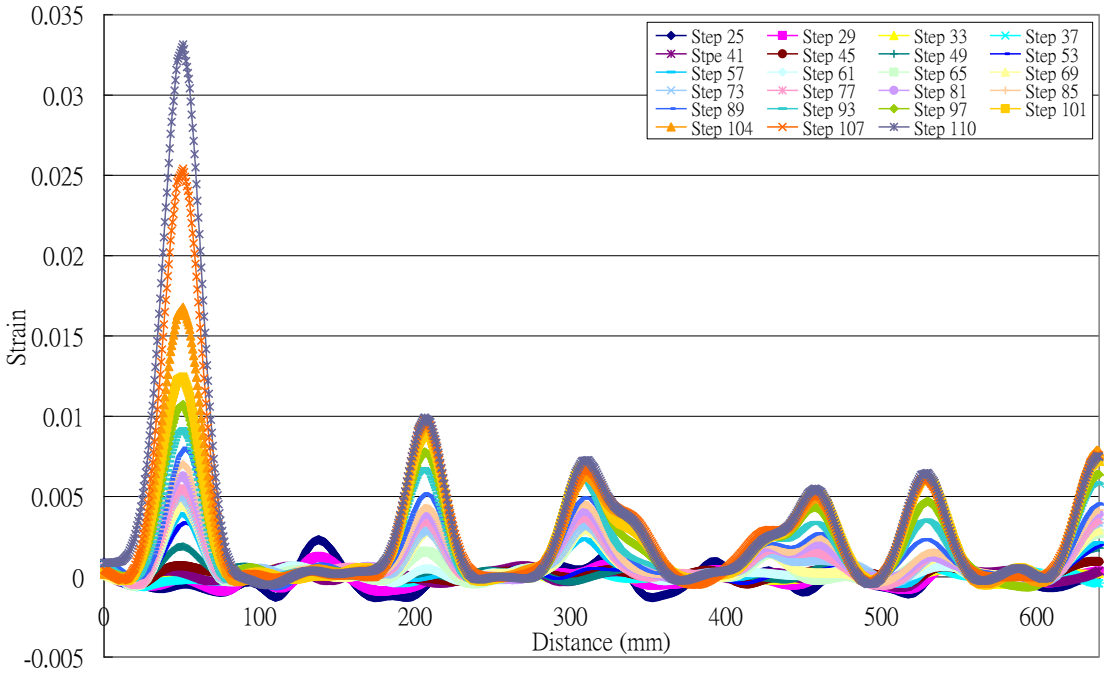

The evolution and development of cracks in Beam specimen C7

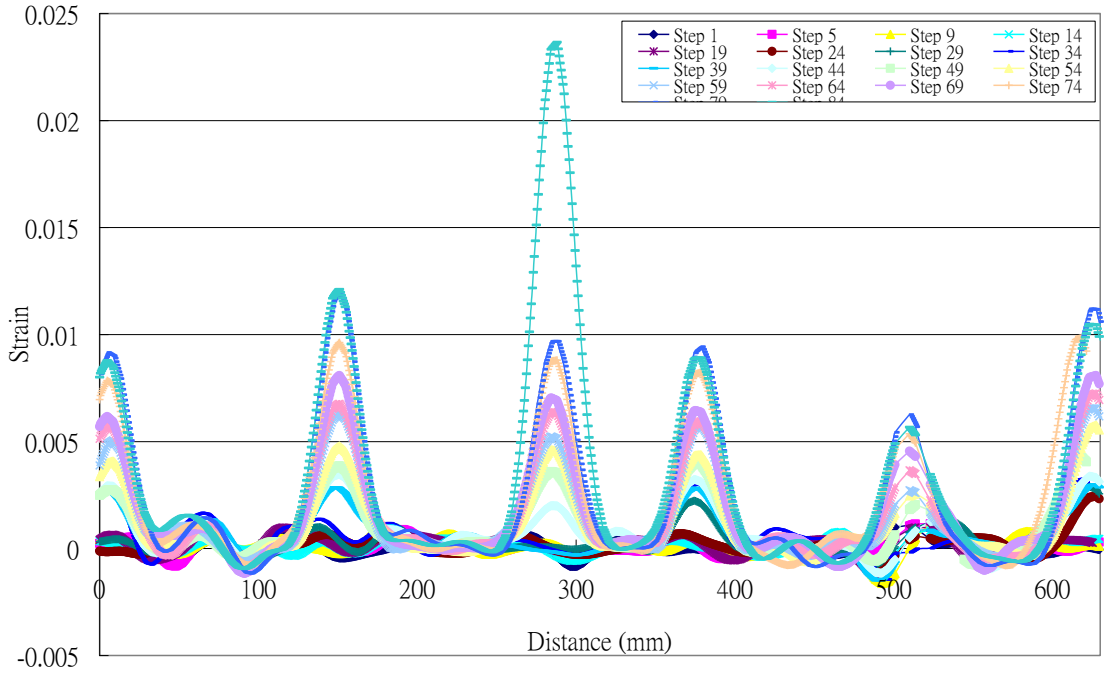

The evolution and development of cracks in Beam specimen C8

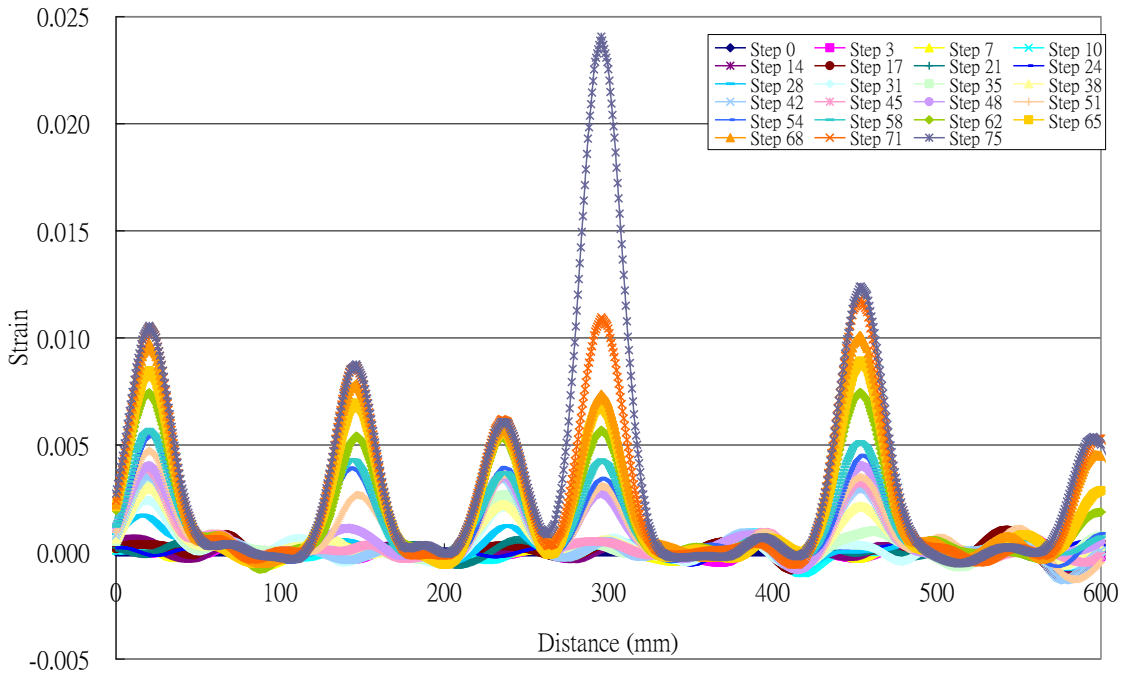

The evolution and development of cracks in Beam specimen C9

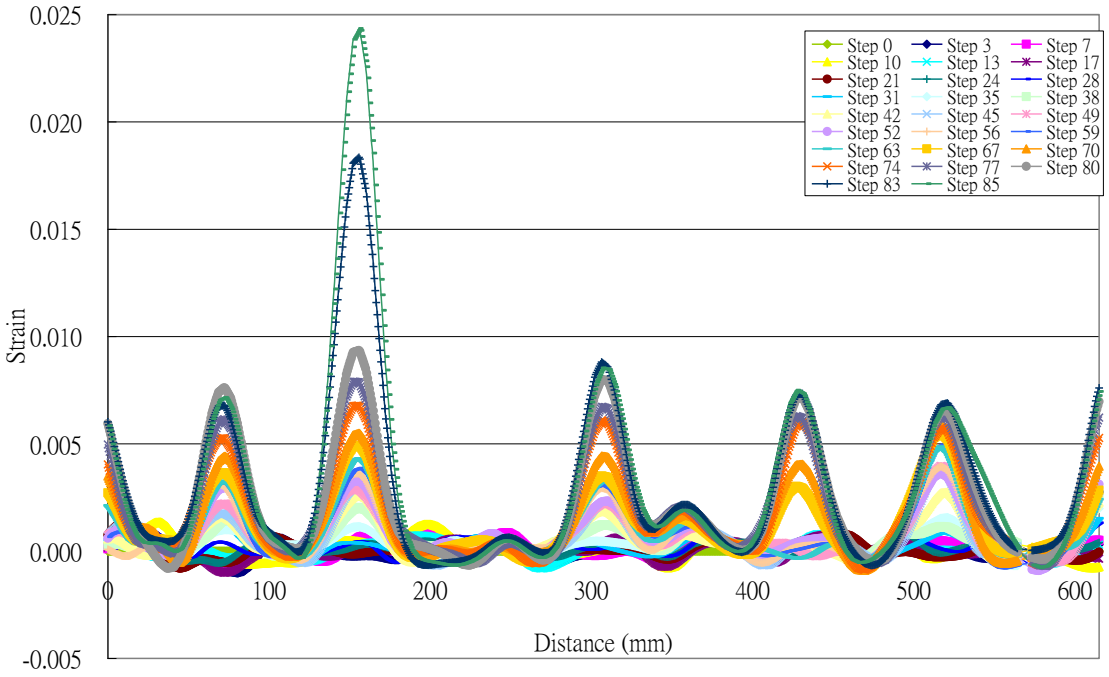

The evolution and development of cracks in Beam specimen C10

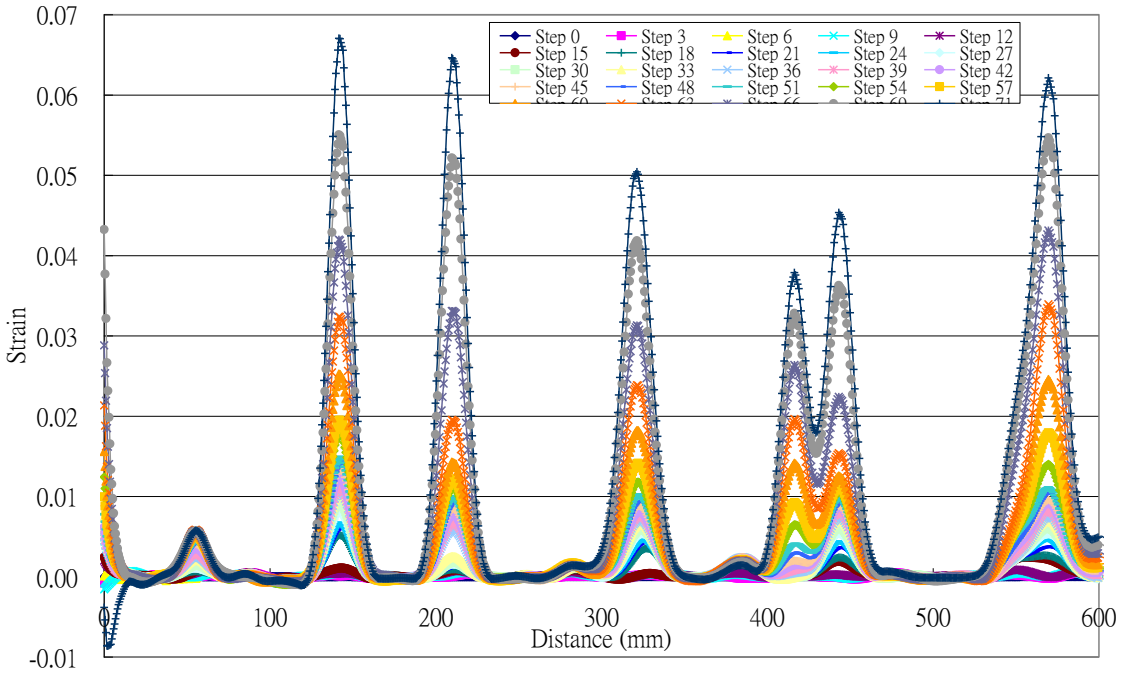

The evolution and development of cracks in Beam specimen M1

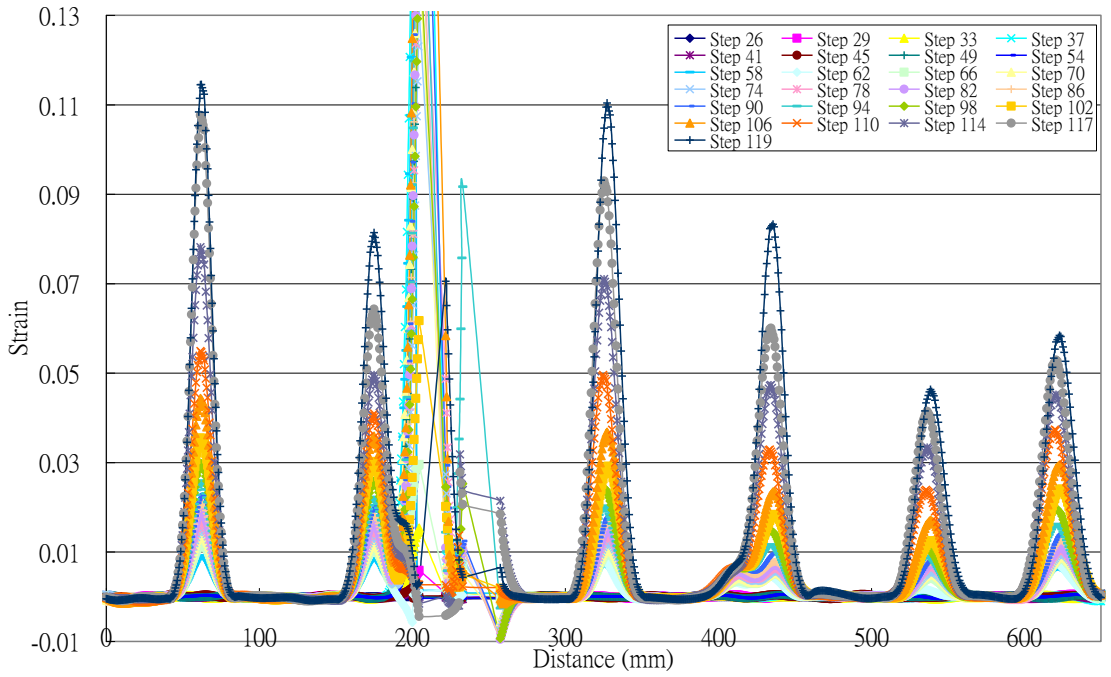

The evolution and development of cracks in Beam specimen M2

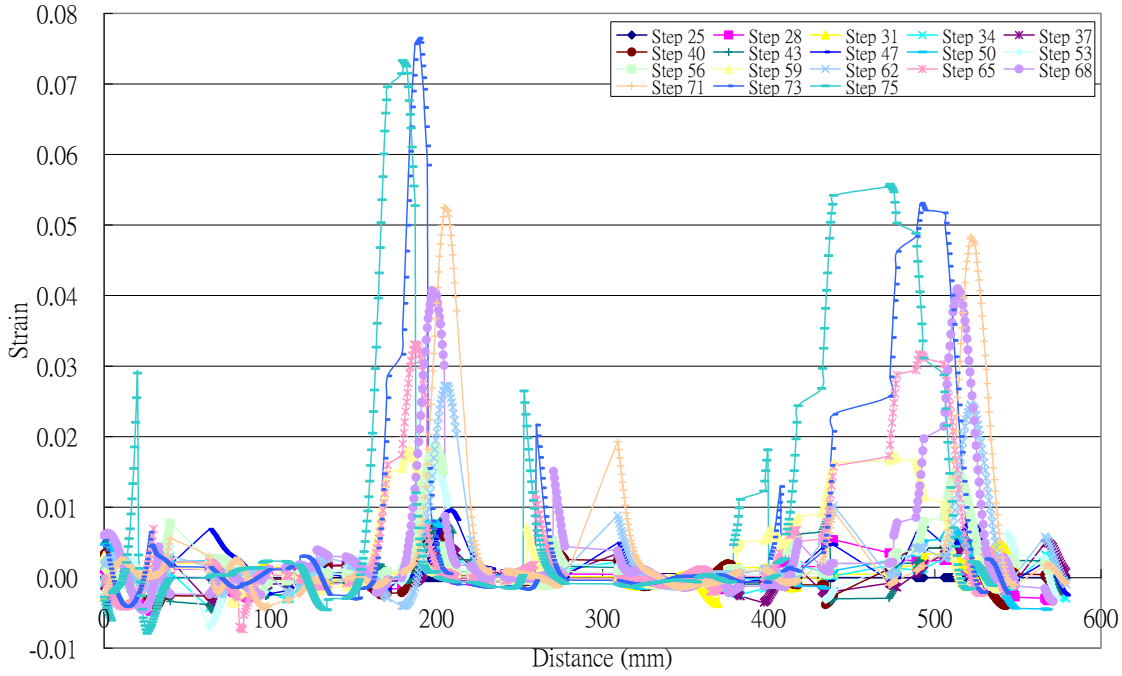

The evolution and development of cracks in Beam specimen M4

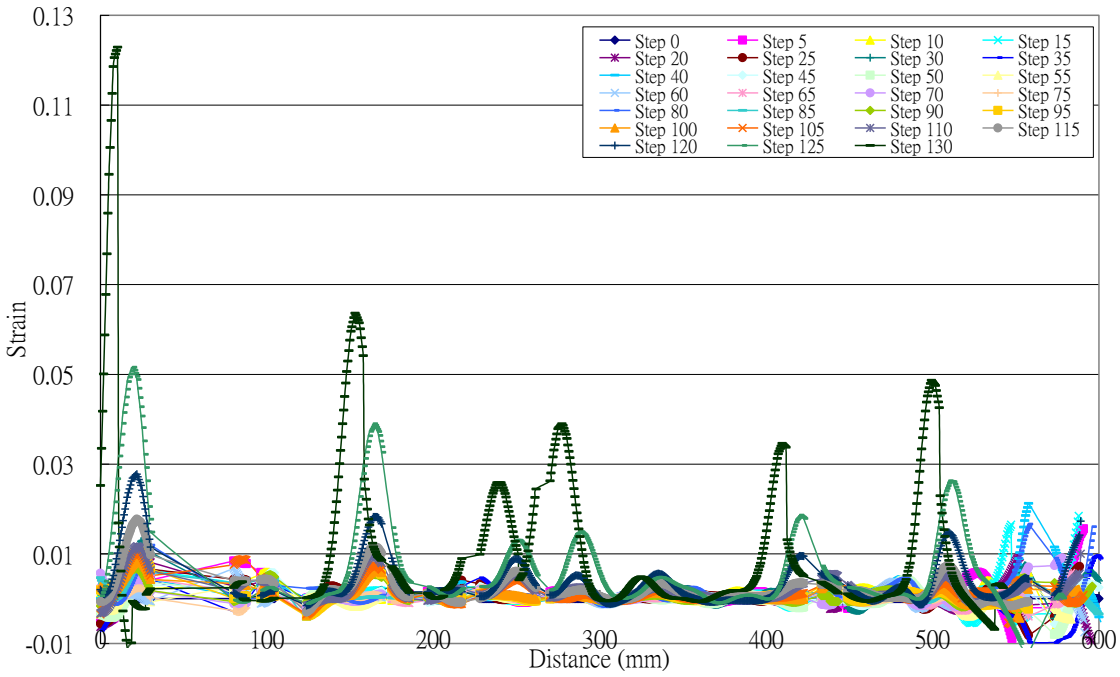

The evolution and development of cracks in Beam specimen M5

APPENDIX II – EVOLUTION AND DEVELOPMENT OF CRACKS IN FLEXURAL BEAM SPECIMENS

This appendix contains the videos and animations showing the evolution and development of cracks for all flexural beam specimens in Batch A, C and Max without stirrups in the central 600mm zone. The files are stored in the CD enclosed with this thesis.